UNIVERSITY OF CALIFORNIA

SANTA CRUZ

PACIFIC OCEAN PLEISTOCENE AND HOLOCENE SURFACE TEMPERATURE VARIABILITY AND IMPLICATIONS FOR CLIMATE CHANGE

A dissertation submitted in partial satisfaction
of the requirements for the degree of

DOCTOR OF PHILOSOPHY

in

EARTH AND PLANETARY SCIENCES

by

Kelsey A. Dyez

September 2012

The Dissertation of Kelsey A. Dyez
is approved:

_____
Professor Paul L. Koch, Chair

_____
Professor A. Christina Ravelo

_____
Research Scientist Adina Paytan

_____
Tyrus Miller
Vice Provost and Dean of Graduate Studies

Contents

Figures

Tables

Abstract

PACIFIC OCEAN PLEISTOCENE AND HOLOCENE SURFACE TEMPERATURE VARIABILITY AND IMPLICATIONS FOR CLIMATE CHANGE

KELSEY A. DYEZ

As humanity embarks on a global experiment in climate warming associated with increased levels of atmospheric greenhouse gases, we require a thorough understanding of the mechanisms, dynamics, and spatial extent of current and past environmental change on a range of timescales. In the past 1.5 million years (Pleistocene and Holocene), glacial-interglacial cycles emerge as the dominant pattern of orbital-scale global temperature change with millennial-scale oscillations superimposed. The ~100-ka glacial cycles are especially well recognized in the oceanographic and geologic records, though the climate-ocean dynamics and feedback mechanisms responsible for these glacial cycles are often a source of debate. Past sea-surface temperature (SST) is an especially useful indicator of past environmental conditions and a multitude of paleotemperature indicators exist. I make use of a number of geochemical signals for SST including the magnesium-calcium ratio of biogenic calcite, oxygen isotopes, and the alkenone unsaturation index from lipid ketones in order to better understand the mechanisms and dynamics of the current and past climate system.

The California Current and the tropical Pacific are two of the major features that influence climate in California, the tropics, and across the globe through direct effects (*e.g.*, upwelling, sea surface temperature changes) and atmospheric teleconnections. This dissertation examines past oceanic and atmospheric change in these two critical regions and linkages with high-latitude climate, insolation, and radiative greenhouse gas forcing. The coastal California chapter addresses questions regarding the regional and local strength of the California Current, upwelling intensity, and precipitation variability in the Holocene. Tropical Pacific chapters deal with the spatial distribution of tropical Pacific sea-surface temperatures as a reflection of oceanographic change and a driver of global climate. Each of these regions offers lessons for understanding climate variability from the late Pleistocene to the present and future climates.

Acknowledgements

I feel a debt of gratitude to Christina Ravelo and Paul Koch for advising me in these projects at UC Santa Cruz. I feel incredibly lucky to have had the opportunity to work with such knowledgeable, skilled, and helpful researchers. Both have inspired me to think deeply, question assumptions, and find balance in my work. Thank you for your generous support; I could not have asked for better mentors. I am also grateful to Adina Paytan for serving on my reading committee and contributing her time, energy, and ideas to the progress of this work.

I would also like to acknowledge the many fine researchers who have generously contributed their expertise to my projects. I would like to especially thank my collaborators on this journey. Stephen Schellenberg (San Diego State University) provided critical and helpful sampling, analysis, and editing advice and allowed me to use his lab to learn to micromill fossil mussel shells. Heather Ford proved an invaluable source of instruction in the use of the micromill and in measuring minor element ratios using the ICP-OES in the UC Santa Cruz Marine Analytical Lab. Alan Mix (Oregon State University) helped by analyzing the benthic isotope data from ODP Site 1239 that formed the age model from that site. Mark Hylkema (California State Parks) provided samples and guidance regarding the anthropological middens at

Pt Año Nuevo and Sand Hill Bluff. Seth Newsome and Tom Guilderson analyzed the radiocarbon samples that date these middens.

Special thanks as well go to Linda Anderson, Jon LaRiviere, Dyke Andreasen, Rob Franks, and Sora Kim who contributed support in the laboratories at UC Santa Cruz. The ideas presented are also the result of many helpful conversations with Yair Rosenthal, Chris Edwards, Deborah Jones, Julie Fergusen, Diane Gifford-Gonzalez, Katie Snell, and many others at various stages in the of the development of this endeavor. I owe a debt of gratitude to Jessica Macias, Victor Castro, and Joey Hermosillo for their careful assistance with sediment processing and picking out foraminifera in the microscopes.

Lastly, I would also like to thank my parents, Marie Yoder and Rodney Dyck, and my wife, Alejandra Dyez, none of whom have flagged in their loving-kindness and support, and for whom I am very tremendously grateful.

1. INTRODUCTION

Although variations in incoming solar radiation have been linked to long-term changes in Earth's climate over the past 1.5 million years, the climate mechanisms that translate these subtle changes in solar radiation received at the top of the atmosphere to the global glacial-interglacial cycles have been debated for decades. Internal climate feedbacks amplify certain frequencies of the insolation records. The climate feedbacks I focus on most closely are the building and melting of ice sheets and sea ice (e.g. Clark et al., 2006; Gildor and Tziperman, 2001), stratification and mixing of the world's oceans (e.g. Kemp et al., 2010), changes in atmospheric and oceanic circulation, and variations in atmospheric greenhouse gas concentrations (e.g. Hansen and Sato, 2012). Part of the difficulty in parsing the relative influence of these internal components of the climate system stems from an incomplete record of past climate. Therefore, in this dissertation I present new records of climate variability from the tropical and subtropical Pacific, use timeseries analysis to better understand the periodic nature and timing of the records, synthesize the current understanding of each potential mechanism of Pleistocene tropical Pacific SST change, and offer new insights into the climate variability of the tropical and subtropical Pacific Ocean.

A number of unanswered questions about Pleistocene and Holocene climate can inform our approach to understanding the past climate system. This dissertation

includes explorations of the following questions. How did environmental conditions affect early human populations and resource use? What was the late and middle Holocene like on the central California coast? How did the cold tongue develop over the Pleistocene and through the mid-Pleistocene transition? How does the Intertropical Convergence Zone respond to glacial-interglacial changes? How sensitive are tropical SST records to radiative greenhouse gas forcing? How are the tropics and high-latitudes related? These questions and others are explored in the context of new and existing records of tropical and North Pacific Pleistocene climate change.

Surface temperature can be used as a climate signal to address these questions in the field of past climate change and climate variability and temperature reconstructions also have implications for biological organisms, precipitation, winds, heat transport, atmospheric and oceanic circulation. However, detailed reconstructions of surface temperature patterns cannot be inferred from only a few isolated records of temperature change. In this sense, the production of the SST data is the first contribution from this work. A second, but equally important, contribution is the lens through which such data is viewed. As more climate records are produced, an ever-evolving and refined framework of mechanisms of past climate change is created.

The causes of the Pleistocene glacial/interglacial cycles have been studied for over 170 years, beginning with proposals from Joseph Adhémar in the mid-1800s, James Croll in the late 1800's, and Milutan Milankovitch in the first half of the 20th century. More recently, careful dating of evidence for the ice ages cycles led to the idea that glacial intervals are paced by orbitally-derived changes in top-of-the atmosphere insolation (e.g. Hays et al., 1976; Tziperman et al., 2006). The Pleistocene epoch (Fig. 1.1) has been recently divided into times when the primary pacing between warm and cold intervals occurred on 41-ky periodicity (early Pleistocene) and on 100-ky periodicity (late Pleistocene). The most recent warm interval in the oscillation of climate cycles represents the Holocene (12.5 kya to present).

The projects in this study focus on atmospheric and oceanic circulation in the North Pacific subtropical gyre, the California current, and the equatorial Pacific. In the North Pacific, large-scale wind-driven circulation is clockwise and incorporates the strong Kuroshio western boundary current, the broad, diffuse California eastern boundary current, and westward equatorial currents (Hickey, 1979; Huyer, 1983). Along the equator and just to the north of it, strong easterly trade winds bound the Intertropical Convergence Zone (ITCZ), move warm surface water westward, and drive surface divergence and upwelling. Warm tropical surface water fills the western Pacific warm pool off the coast of New Guinea (Fig. 1.2) with some of the warmest surface seawater on Earth. The warm pool often drives intense atmospheric

convection, transfers water vapor to the atmosphere (de Garidel-Thoron et al., 2005), and promotes the Walker circulation (rising air in the western Pacific, eastward travel aloft, and sinking dry air in the eastern Pacific). Coastal upwelling along the Peru margin and surface-water divergence along the equator create a cold tongue (Fig. 1.2) of upwelling water that extends westward from the coast of South America.

The chapters of this dissertation each explore an aspect of Pleistocene and Holocene climate variability; each chapter can be approached independently. Anthropologists and those who study coastal California or Holocene climate of the western states may be most interested in Chapter 2 while the climate modeling and paleoceanographic communities may be most interested in the Chapters 3-5. Those concerned with the Earth-system response to greenhouse gas forcing and new methods for calibrating the Mg/Ca paleothermometer should see Chapter 4 and the detailed methods in the supplemental material for that chapter. Each chapter is briefly described below.

Chapter 2, "Mollusk geochemical records of Holocene climate and the California Current" establishes the geochronology of anthropogenic shell middens on the central coast of California and works to constrain environmental parameters near Point Año Nuevo, CA, and Davenport, CA. This chapter uses geochemical records (primarily ^{14}C, Mg/Ca ratios, and $\delta^{18}O$ of shell calcite) to estimate upwelling, coastal SST, and precipitation for coastal California. These records of past upwelling, SST, and

precipitation variability had the potential to provide high-resolution windows of environmental change, though I show that this species *Mytilus californianus*, may not be the most faithful recorder of interannual-scale variability. Rather we show that on longer timescales portions of the mid-Holocene may have been warmer and drier than late Holocene conditions, while records from later portions of the mid-Holocene and the late Holocene indicate that upwelling, temperature, and precipitation rates have been relatively stable over the past ~3500 years on the central California coast.

In Chapter 3, "Evaluating drivers of Pleistocene eastern tropical Pacific sea-surface temperature," I systematically evaluate existing theories regarding the factors that cause tropical SST to change and present a new synthesis. A wide variety of mechanisms have been proposed for controlling Pleistocene sea-surface temperature variability in the eastern tropical Pacific, from high-latitude climate to local insolation, to ocean dynamics. This chapter presents a new compilation of an alkenone-based SST records from the southern margin of the eastern Pacific warm pool, at ODP Site 1239, and published records tropical Pacific and extratropical climate change to evaluate proposed theories of tropical Pacific SST variability. The high-resolution spatial SST record from Site 1239 includes glacial-interglacial cycles from the early and late Pleistocene and allows for an additional examination of the mid-Pleistocene climate transition from 41-kyr to 100-kyr cycles alongside a transition to colder, more intense, glacial periods. The results of this work show that

for the entirety of the Pleistocene, eastern equatorial SST changes may have been modulated by insolation changes in the precession bandwidth, ice-sheet changes in the obliquity bandwidth, and are closely tied to atmospheric CO_2 concentrations and the global carbon cycle at the eccentricity bandwidth. The initial 'pacing' of climate cycles, though, is likely derived from changes in orbital insolation forcing and then translated from extratropical latitudes to the tropics.

Chapter 4, "Late Pleistocene tropical Pacific temperature sensitivity to radiative greenhouse gas forcing," presents a new temperature record from the western Pacific and estimates the past tropical climate sensitivity to changes in greenhouse gas concentrations. Climate sensitivity is here defined as the sensitivity of surface temperatures to atmospheric CO_2 levels once feedbacks propagate through the climate system. The new record of SST is from ODP Site 871 in the western Pacific warm pool, a broad region of the tropics which is thought to be primarily controlled by direct radiative forcing. A variety of techniques are used to compare this high-resolution SST record with records of atmospheric CO_2 and CH_4 from the past 500 kyr. I show that the past tropical climate sensitivity to radiative greenhouse gas forcing is ~0.94 – 1.06 ^{o}C $(W\ m^{-2})^{-1}$, which is higher than has been predicted by most climate models. The difference may be due to the fact that models are not yet able to capture the full range of climate feedbacks that occur in the natural system. However, this past tropical sensitivity attempts to bridge the gap between models and other SST

records, which may appear to be more sensitive due to local ocean dynamics, thermocline changes, or sharp SST gradient changes.

This chapter also presents a new SST calibration for Mg/Ca-based temperatures derived from planktic foraminifera. Using published Holocene core-top Mg/Ca values, a new depth-based correction is calculated for calcium carbonate dissolution in the tropical Pacific. While yet preliminary, this type of calibration has the potential to quickly and more accurately estimate the range of SST that a given location may have experienced and represents a crucial step forward in paleo-SST reconstructions and estimations of past climate sensitivity.

Chapter 5, "Pleistocene sea-surface temperature patterns in the western warm pool and tropical Pacific," presents a much longer (1.5 Ma to present) temperature record from ODP Site 871 and compares this SST signal to other long records from the tropical Pacific. In the modern system, some of the warmest open-ocean surface water is found at equatorial ODP Site 806, which is often considered to be representative of the center of the western Pacific warm pool (Medina-Elizalde and Lea, 2005). However, equatorial upwelling is shown to be stronger at Site 806 than elsewhere in the warm pool, especially just off the equator. Since the thermocline is deep in the western Pacific, upwelling has little effect on SST, though during glacial periods the western Pacific thermocline may have been shallower, cooling the equator more than

the off-equatorial warm pool; a similar SST pattern is found in the eastern equatorial Pacific today. The final chapter presents a long SST record from the western Pacific Site 871 at ~5°N and makes comparisons with other tropical SST records from both the eastern and western Pacific surrounding the mid-Pleistocene transition.

In this project I show that during glacial intervals SST is colder at Site 806 on the equator than elsewhere in the warm pool. This result suggests that cooler upwelling at Site 806 may have driven larger glacial-interglacial oscillations in equatorial warm-pool SST. Comparisons with other tropical Pacific SST records show that while eastern tropical Pacific cooled over the course of the Pleistocene, western tropical Pacific records remained relatively warm, a result which supports an increase in the zonal SST gradient in the tropical Pacific through the past 1.5 Ma.

Taken together, these projects offer new observations that lend insight to the mechanisms and theories of past climate change. They show that new climate records are necessary to fully explain the limited observations of Pleistocene and Holocene climate available. These studies will benefit a diverse array of researchers, from anthropologists to climate modelers and paleoceanographers. These studies further emphasize the variety of paleoclimate inferences that can be made by measuring past ocean temperatures, from oceanic circulation changes to coastal resource availability and climate sensitivity.

REFERENCES

Clark, P.U., Archer, D., Pollard, D., Blum, J.D., Rial, J.A., Brovkin, V., Mix, A.C., Pisias, N.G., and Roy, M., 2006, The middle Pleistocene transition: characteristics, mechanisms, and implications for long-term changes in atmospheric pCO2: Quaternary Science Reviews, v. 25, no. 23-24, p. 3150–3184, doi: 10.1016/j.quascirev.2006.07.008.

de Garidel-Thoron, T., Rosenthal, Y., Bassinot, F., and Beaufort, L., 2005, Stable sea surface temperatures in the western Pacific warm pool over the past 1.75 million years: Nature, v. 433, no. 7023, p. 294–298.

Gildor, H., and Tziperman, E., 2001, A sea ice climate switch mechanism for the 100-kyr glacial cycles: Journal of Geophysical Research, v. 106, no. C5, p. 9117–9133.

Hansen, J., and Sato, M., 2012, Paleoclimate Implications for Human-Made Climate Change, *in* Berger, A., Mesinger, F., and Šijači, D. eds., Climate Change at the Eve of the Second Decade of the Century: Inferences from Paleoclimate and Regional Aspects: Proceedings of the Milutin Milankovitch 130th Anniversary Symposium, Springer, New York, p. 1–32.

Hays, J., Imbrie, J., and Shackleton, N., 1976, Variations in the earth's orbit: pacemaker of the ice ages: Science, v. 194, no. 4270, p. 1121–1132.

Hickey, B., 1979, The California current system--hypotheses and facts: Progress in Oceanography, v. 8, no. 4, p. 191–279.

Huyer, A., 1983, Coastal upwelling in the California Current system: Progress in Oceanography, v. 12, no. 3, p. 259–284.

Kemp, A.E.S., Grigorov, I., Pearce, R.B., and Garabato, A.C.N., 2010, Migration of the Antarctic Polar Front through the mid-Pleistocene transition: evidence and climatic implications: Quaternary Science Reviews, v. 29, no. 17-18, p. 1993–2009, doi: 10.1016/j.quascirev.2010.04.027.

Medina-Elizalde, M., and Lea, D., 2005, The mid-Pleistocene transition in the Tropical Pacific: Science, v. 310, no. 5750, p. 1009.

Tziperman, E., Raymo, M.E., Huybers, P., and Wunsch, C., 2006, Consequences of pacing the Pleistocene 100 kyr ice ages by nonlinear phase locking to Milankovitch forcing: Paleoceanography, v. 21, no. 4, p. PA4206, doi: 10.1029/2005PA001241.

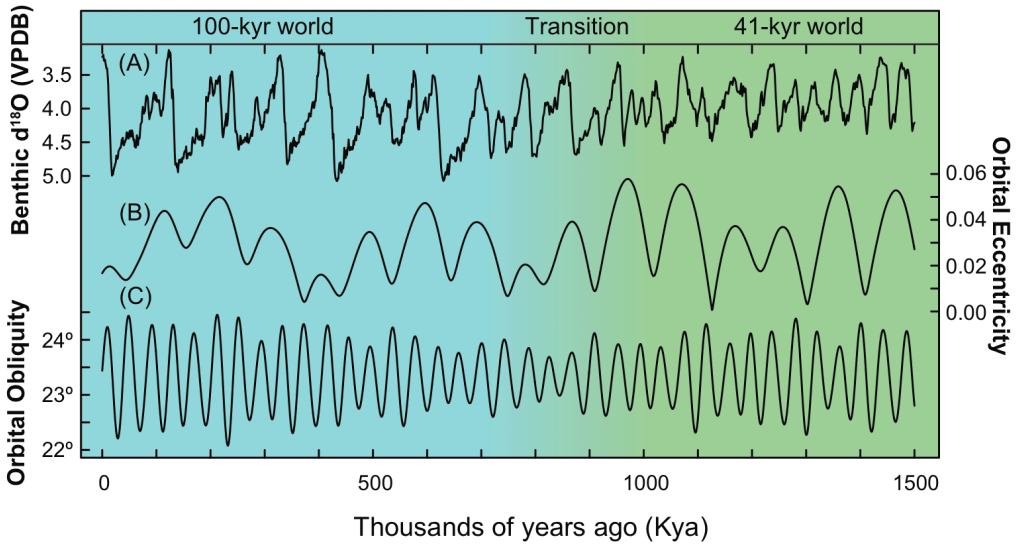

Figure 1.1 Evolution of selected records of climate and orbital parameters: (A) global benthic $\delta^{18}O$ stack, which is considered a proxy for global ice volume and high-latitude temperature, (B) orbital eccentricity (where 0 is a perfect circle), and (C) obliquity angle. The early Pleistocene is dominated by 41-kyr climate cycles (green) while the late Pleistocene varies on longer, more intense ~100-kyr cycles (blue).

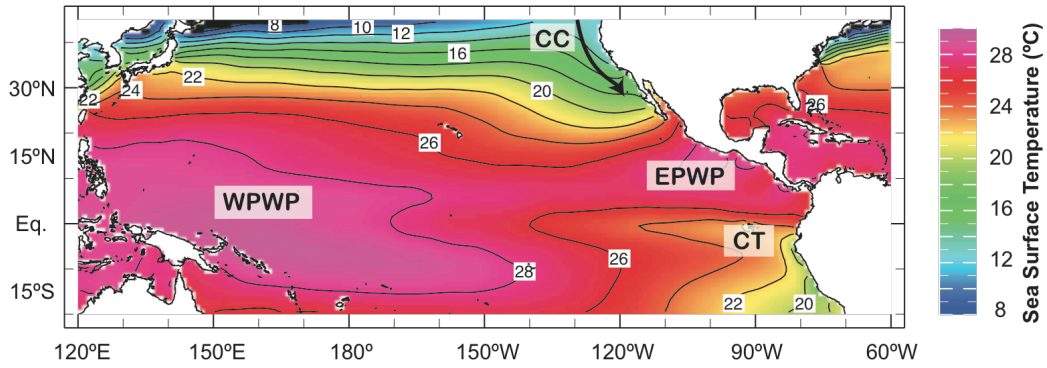

Figure 1.2 Asymmetric pattern of SST across the tropical and northern subtropical Pacific. The western Pacific warm pool (WPWP) covers causes broad atmospheric heating and represents upward atmospheric convection. The eastern Pacific warm pool (EPWP) is located just north of the eastern equatorial Pacific cold tongue (CT). The cold California Current (CC) accommodates regional upwelling and productivity along the coast of North America. Locations of individual records are within each chapter.

2. MOLLUSK GEOCHEMICAL RECORDS OF HOLOCENE CLIMATE AND THE CALIFORNIA CURRENT

Abstract

Precipitation and sea-surface temperature (SST) along the California coast is thought to have changed substantially from the middle to late Holocene, though few records derive from the coastal zone itself. Offshore records from the California Current suggest cooler temperatures for the mid-Holocene though inland California was warmer and drier than today. In the nearshore region, variations in SST, upwelling intensity, and precipitation rate may have influenced coastal and terrestrial productivity, which in turn impacted cultural shifts, territory movement, and resource use in ancient Californians. This study investigates nearshore marine temperature and precipitation using the Mg/Ca ratio and $\delta^{18}O$ value of mollusk calcite and radiocarbon data from midden deposits in coastal San Mateo and Santa Cruz counties. We use these geochemical parameters to infer past SST, and the $\delta^{18}O$ value of coastal seawater ($\delta^{18}O_{sw}$), and to estimate regional precipitation and upwelling effects. Our results suggest slightly warmer waters and drier conditions in the some parts of the mid-Holocene (6 – 3 kya), mean annual SST ~ 15.1°C and $\delta^{18}O_{sw}$ ~ +0.5‰ VSMOW for one time period) while late Holocene SST and $\delta^{18}O_{sw}$ were cooler and wetter than modern conditions (3 kya – present, mean annual SST ~9.1°C and $\delta^{18}O_{sw}$

~ -1.0‰ VSMOW) in the coastal zone of central California. However, variability in seasonal and inter-annual temperature and $\delta^{18}O_{sw}$ remain constant over the entire timescale with no evidence of major changes in the impacts of El Niño/Southern Oscillation in this region from the mid-Holocene to present.

Introduction

Climate records from the coastal system in California have the potential to answer key questions about the past coastal system and population changes and have implications for future change (Jones and Kennett, 1999; Barron and Anderson, 2011). The first open question that these records address is how coastal conditions are reflected in and driven by shifts in both offshore oceanic and atmospheric conditions and inland terrestrial conditions (e.g. Barron et al., 2003). The land-sea interface, which influences physical oceanography and meteorology, undermines extrapolations from the open ocean to the coastal zone and necessitates proxy records of oceanographic conditions within the coastal zone itself. Such coastal climate shifts may also have affected early human resource availability (Milliken et al., 2007; Jones et al., 2007) and potentially influenced Holocene human migration patterns in California.

Though past sea-surface temperatures (SSTs) have been estimated for the California Current (Barron and Anderson, 2011; Barron et al., 2003; Mix et al., 1999; Ostertag-

Henning and Stax, 2000; Sabin and Pisias, 1996), within San Francisco Bay (Schweikhardt et al., 2010; McGann, 2008; Ingram et al., 1996b), and inland California (Starratt, 2009; Benson et al., 2002; Stine, 1990) (Fig. 2.1), new records of mean annual SST and relative salinity are needed from materials that directly sample coastal waters. Coastal conditions are driven by a combination of broad offshore upwelling of cool, salty, nutrient-rich waters in the California Current, warmer, fresher water from San Francisco Bay, and the interaction of North Pacific and inland atmospheric systems with additional intense nearshore upwelling is driven by cyclonic wind stress curl and Ekman divergence (e.g. Bakun and Nelson, 1991). Environmental conditions (coastal SST, rainfall, and productivity) constrained the potential resource base available to early human populations. Warmer, less-productive water may have resulted in the more temporally and geographically transient human populations in the mid-Holocene while cooler, more productive coastal waters in the late Holocene likely supported larger, more consistent settlements at that time period (Jones and Kennett, 1999; Jones et al., 2008).

Regional Setting

Surface wind stress and the strength of the California Current interact with atmospheric pressure systems to influence precipitation, coastal runoff, and productivity in western North America (Gardner et al., 1997; Barron et al., 2003;

Chelton et al., 2007). From May to September, a North Pacific high-pressure system tends to divert precipitation from the central California coast; in November-March this high-pressure system is weaker and moves southward, which allows for rainy winters in the region (Huyer, 1983; Hickey, 1998; Pennington and Chavez, 2000). Maximum wind-stress curl and upwelling occur from late spring to summer in the modern system (Bakun and Nelson, 1991) and are associated with southward coastal currents (Breaker, 2006). Based on modern records from the past 50 years at Santa Cruz, the SST is ~13±2°C (Breaker, 2005), though SST within Monterey Bay, from Terrace Point (Long Marine Lab) to Pacific Grove is often warmer than SST outside Monterey Bay, for example, north of the bay at Año Nuevo (Rosenfeld et al., 1994) or south of the bay at Granite Canyon (Breaker, 2005).

Relatively cool summer surface waters and warmer air temperatures also combine to form fog—a significant source of summer moisture for this region (Filonczuk et al., 1995; Johnstone and Dawson, 2010). Modern summers on the central coast are often mild and foggy while nearshore waters are cooler, with associated high primary productivity that supports abundant of fish, mollusks, and marine mammal populations (Hood et al., 1990). Upwelling is suppressed in the winter by the seasonal northward Davison Current, when the climate is cooler and wet (Huyer, 1983; Barron and Anderson, 2011), resulting in periods of higher terrestrial productivity for

vegetable resources (acorns, small seeds) and terrestrial animal stocks (Erlandson, 1994; Kennett et al., 2007).

Climate conditions are recorded in the minor element and stable isotope values of marine fossils (e.g. Andrus, 2011; Klein et al., 1996a; Ford et al., 2010). In the coastal zone, however, upwelling patterns and freshwater from rivers and estuaries may also influence isotopic and elemental tracers. Our samples come from Pt. Año Nuevo, CA, and Sand Hill Bluff near Davenport, CA, on rocky coastal headlands ~20 km from one another. Satellite imagery and surface measurements confirm that modern average annual SST does not vary between the two locations (13°C annual average, (Locarnini et al., 2010; *JPL*, 2012)). Temperature is strongly influenced by an upwelling cell which advects cool water to Monterey Bay; here, upwelling may occur regardless of the regional extent or strength of upwelling in the California Current (e.g. Pennington and Chavez, 2000). During very wet periods, San Francisco Bay outflow also has the potential to contribute water with a low $\delta^{18}O_{sw}$ value to the coastal zone (Fox et al., 1990; Ingram et al., 1996b; Ingram et al., 1996a). However, since Pt. Año Nuevo is far from river mouths, its location may attenuate intense fluctuations in the amount of freshwater (with low-$\delta^{18}O$ water) entering the local system.

Holocene climate

Both continental and marine records of climate change are available for the middle to late Holocene (e.g. Barron et al., 2003; Pisias et al., 2001). Lake records (Pyramid Lake, NV, Lake Tahoe, Mono Lake; Fig. 2.1) indicate higher mean annual temperatures (3-5^{o}C warmer) and >30% less inland precipitation from 8 – 3 kya (Benson et al., 2002). At Lake Tahoe submerged tree evidence further supports a drier mid-Holocene from ~ 8 – 3 ka (e.g. Barron et al., 2003; Mensing et al., 2004). Microfossil assemblages from Stella Lake, NV, demonstrate a warm middle Holocene and cooler late Holocene (Reinemann et al., 2009) while submerged stump and deltaic evidence from Mono Lake also point to extreme droughts (~150-300 yrs) in the middle Holocene (Stine, 1990). Records from the San Francisco Bay estuary also seem to indicate climate was warmer and drier in the mid-Holocene, and became cooler and wetter in the late Holocene (Malamud-Roam et al., 2006).

However, alkenone-derived Holocene SSTs at ODP Site 1019 (on the edge of the continental shelf, 65 km off coast of the California/Oregon border; Fig. 2.1) suggest surface temperatures were 1-2^{o}C cooler than modern SST in the mid-Holocene (Barron et al., 2003; Mix et al., 1999; Ostertag-Henning and Stax, 2000; Sabin and Pisias, 1996) with a weak Aleutian Low and stronger North Pacific High pressure zone (Barron and Anderson, 2011). Higher foraminifera Cd/Ca ratios (Van Geen et al., 1992) and higher biogenic opal and organic calcium carbonate accumulation rates (Gardner et al., 1997) also suggest increased upwelling intensity and biological

productivity in the mid-Holocene. Modeling studies support decreased seasonality (Bartlein et al., 1998), a longer though less-vigorous upwelling season (Diffenbaugh, 2003), and source-water changes (Diffenbaugh and Ashfaq, 2007) as possible causes of cooler offshore SST 8 – 3 kya. The combination of cooler offshore SST and warmer inland temperatures may have produced more summer fog and supported the Holocene expansion of the coastal redwood ecosystems (Filonczuk et al., 1995; Johnstone and Dawson, 2010).

Human migration

Evidence for human populations on the central California coast begins to appear shortly after the Younger Dryas cold interval (12.9-11.5 kya, Alley, 2000). Jones (1992) finds evidence of human occupation 11–10 kya in coastal Mendocino County, 10 kya at Laguna Seca (Sonoma County), and 8-9 kya at Bodega Bay. Direct evidence for complex hunter-gatherer societies at coastal sites in central California appears at ~7 kya (Newsome et al., 2004), near Watsonville, CA. The prevailing climate affected resource distribution and in turn may have influenced the movement or density of these early societies, possibly contributing to the fact that middle Holocene middens are more rare on the central coast (Jones et al., 2007; Louderback et al., 2010). In the late Holocene (3–0 kya) more favorable conditions may have lead humans to expoit the open-ocean sites at Año Nuevo and Sand Hill Bluff (Fig. 2.1) for the rich late Holocene mollusk, seabird, and terrestrial vertebrate food resources (Hylkema, 1991).

Reconstructing Environmental Conditions

Here we use geochemical evidence from Holocene mollusks to evaluate hypotheses of climate change and early human resource use. The oxygen isotope value of calcium carbonate fossils ($\delta^{18}O_c$) is often used as an indicator of marine conditions and varies with temperature and the $\delta^{18}O$ value of sea water ($\delta^{18}O_{sw}$) from which the calcite precipitates (e.g. Klein et al., 1996a). In order to reconstruct sea-surface temperature using only oxygen isotope data from calcite, many studies assume the $\delta^{18}O_{sw}$ value to be constant. However, in coastal settings, seasonal inputs of low-$\delta^{18}O$ freshwater invalidate this assumption, so a reliable temperature reconstruction cannot always be made (e.g. Surge et al., 2003). Minor element ratios have also been used to estimate marine temperatures, and appear to be only weakly sensitive to variations in salinity (Lea et al., 1999; Klein et al., 1996a). Terrestrial and marine samples are dated using radiocarbon (^{14}C) analysis and, taken together, can be used to calculate the reservoir age of seawater (Ingram and Southon, 1996).

Fossil mollusk $\delta^{18}O_c$ values (e.g. Jones and Kennett, 1999), Mg/Ca ratios (Takesue and Van Geen, 2004; Carré et al., 2006), and coupled records of $\delta^{18}O$ and Mg/Ca ratios (Klein et al., 1996a) of shell calcite have been used to reconstruct SST on high-resolution (monthly to inter-annual) timescales. The Sr/Ca ratio in biogenic calcite

may be influenced by growth rate, salinity, or other factors and is not yet fully constrained (Putten et al., 2000; Klein et al., 1996b). A species-specific calibration for Mg/Ca content to temperature is necessary (Fig. 2.2A) since each species' calibration is different (Fig. 2.2A). Recent calibrations (Ford et al., 2010; Forcino, 2009) show that while environmental signals are not purely translated into the minor element and isotopic records, shell geochemistry in *Mytilus californianus* reflects changes in temperature and the $\delta^{18}O$ value of seawater. Here we use the geochemical ($\delta^{18}O_c$ and Mg/Ca) signature of radiocarbon-dated mollusk shells to show that coastal SST was warmer and $\delta^{18}O_{sw}$ of coastal water was higher in the mid-Holocene than the late Holocene.

Materials, Analytical Methods, and Approach

Materials

Our samples come from the surface of anthropogenic middens near Pt. Año Nuevo (SMa-17, -18, -19, -218, and -222) and from Sand Hill Bluff, ~20 km to the south (SCr-7). The Año Nuevo sites are on terraced Holocene sand dunes; each consists of a bioturbated stratum of mollusk shells, shell fragments, charcoal, flaked stone tools, and chipped stone from the Middle and Late Periods of coastal culture (Schlagheck, 2011; Hylkema, 1991). The Sand Hill Bluff site has been divided into three loci

(Schlagheck, 2011), though here we focus on the largest, Locus 1, with two strata, identified as 'Upper' and 'Lower'. Microsamples were taken from whole shells at all middens except the lower stratum of SCr-7, where only one available shell was large enough to warrant microsampling and additional data was collected from small shell fragments, both on the surface and from an excavation of the SCr-7 Lower stratum (Schlagheck, 2011). None of the shell samples have a record long enough to inform our understanding of ENSO variability.

Analytical Methods

Radiocarbon analyses were conducted at the Center for Accelerator Mass Spectrometry at Lawrence Livermore National Laboratory (Livermore, CA). Shell samples were embedded in epoxy, sectioned, polished, etched by chemical leaching in hydrochloric acid (HCl) and then carbonate was sampled from the polished and etched surface. Approximately 10 mg of shell carbonate was then evacuated in a 10-mL vacutainer and reacted with 0.5 mL of 85% phosphoric acid at 90°C to produce CO_2. Charcoal samples (1–2 mg) were soaked sequentially in acid (1N HCl) and base (1N NaOH), and given two acid rinses to remove CO_2 that may have been absorbed during the alkaline bath. This rinse sequence removed adhering humic and fulvic acids, as well as secondary carbonates. The samples were subsequently given a series of deionized water baths and dried. Samples were then loaded into quartz tubes with

copper oxide (CuO_2) and silver (Ag) powder, sealed, and combusted at 900 °C. Both charcoal and shell CO_2 were reduced to graphite using an iron catalyst and H_2 gas (Vogel et al., 1987). The resulting graphitized samples were pressed into individual aluminum target holders and measured for ^{14}C content by accelerator mass spectrometry (AMS). Results include a matrix-specific ^{14}C-free background subtraction and $\delta^{13}C$ correction. Radiocarbon ages were calibrated to calendar years using CALIB 6.0 and the IntCal09 calibration dataset (Stuiver and Reimer, 2009; Reimer et al., 2009).

To prepare for minor element and stable isotope analyses, shells were lightly scrubbed, rinsed with deionized water and then dried in a warm oven (~30°C). Complete valves (half-shells) were embedded in epoxy under vacuum, sectioned (~250 μm thick) along the maximum growth axis, mounted on glass slides, polished using a lap wheel, washed with deionized water, and dried in the warm oven. Samples were taken along growth bands from the calcite portion of the shell from the umbo to the commissure, transecting the life of the organism. The prismatic calcite layer of the shells was microsampled using a New Wave Micromill with Brasseler dental bits to drill paths along bands of darker or lighter color, avoiding the rough exterior of the shell and inner nacreous layer. Samples of ~150-400 μg of carbonate powder were then homogenized and split for minor element (100-300 μg) and stable isotope (50-100 μg) analysis.

Samples collected for minor element ratios were analyzed at San Diego State University using a Perkin-Elmer 4300 Dual View Inductively Coupled Plasma-Optical Emission Spectrometer (ICP-OES). Sample analytical procedures included calibration standards that spanned the predicted minor element concentration ranges, blanks to verify the absence of background effects, and liquid consistency standards made from *M. californianus* calcite (Ford et al., 2010). Fifty replicate measurements of a standard solution were analyzed within and among sample batches for an overall average Mg/Ca = 4.88 ±0.07 mmol/mol and Sr/Ca = 1.01 ±0.02 mmol/mol. Uncertainties represent standard deviation, except where noted. One out of every ten samples was split for duplicate minor element analyses: average standard deviation of duplicate samples was 0.09 mmol/mol (Mg/Ca) and 0.01 mmol/mol (Sr/Ca).

Samples collected for stable isotope analysis were analyzed at the University of California Santa Cruz Stable Isotope Laboratory using Fisons PRISM and OPTIMA mass spectrometers with common acid bath carbonate preparation systems. Carbonate analytical reproducibility was ±0.09‰ for $\delta^{18}O$ values and ±0.05‰ for $\delta^{13}C$ values, the standard deviation of individual analyses of an internal carbonate standard (CM05) within and among analytical runs (N=230 among all runs). Carbon isotope measurements were used for radiocarbon calibration (Stuiver and Reimer, 2009) and are reported for completeness, but are not discussed further in this work.

Approach

We determined midden and reservoir ages by AMS ^{14}C analysis of charcoal and shell materials. We dated a total of 46 shells and 16 charcoal samples (Tables 2.1, 2.2, and 2.3) with the goal of dating a minimum of five shells per midden to assess the level of time averaging. A midden was assumed to be more than a single component if a chi-squared test of shell ^{14}C ages at the sites was significant ($p<0.05$, n=4-6). Where available, we measured two charcoal samples to determine midden age and reservoir age between the mean ^{14}C age for mussels and the calibrated age for charcoal. Radiocarbon from terrestrial material was not available to calculate a reservoir age for SCr-7. We determined the $\delta^{18}O_c$ and $\delta^{13}C$ values and minor element ratios (Mg/Ca, Sr/Ca) by microsampling from growth bands in 13 mussel shells from 5 middens of late Holocene age, chosen to yield the maximum span of ages, and 18 shells and shell fragments from one middle Holocene midden. With the exception of specimen SCr-7 Lower A, shells used for isotopic and minor element analysis were not directly dated, but were collected from dated midden layers.

Temperature Estimation

We determined SST using the Mg/Ca ratio of mollusk calcite, which correlates positively with water temperature and is insensitive to changes in the isotopic composition of waters (Klein et al., 1996a). Though each species requires a species-specific calibration (Fig. 2.2A) and some studies show a weak relationship between temperature and shell Mg/Ca values (e.g. *P. maximus* and *M. edulis* (Freitas et al., 2006; Freitas et al., 2008)). Here the compiled (n=818) paired *M. californianus* Mg/Ca-temperature data (Fig. 2.2B) from along the California coast (Ford et al., 2010; Forcino, 2009) further refine the linear *M. californianus* Mg/Ca temperature relationship:

$$T\ (^{o}C) = 3.65\ (\pm\ 0.11)\ *\ Mg/Ca\ (\text{mmol/mol}) + 0.33\ (\pm\ 0.47), \qquad \textit{Equation 1}$$

where T is sea-surface temperature. The slope of the linear *M. californianus* Mg/Ca-temperature relationship is similar to that estimated for other bivalves (Fig. 2.2A). Though a compilation of data sets, Equation 1 is also within the 95% confidence intervals of both previous sets of *M. californianus* Mg/Ca-temperature data (Ford et al., 2010; Forcino, 2009). By combining data from a larger temperature range the r^2 value ($r^2 = 0.27$), while still low, improves relative to either previous study ($r^2 = 0.058$ or $r^2 = 0.18$). The 95% CI for temperature associated with Equation 1 for the range of temperatures in this study is ± 1.4–1.8°C (uncertainty varies linearly with temperature; at 8°C 95% uncertainty is ±1.4 °C; at 16 °C it is ±1.8 °C). The data

compilation represented by Equation 1 is the most applicable relation yet produced for *M. californianus* calcite Mg/Ca ratio because a range of a range of intertidal positions, specimen sizes, and site locations were included in the calibration. Since shells from archaeological middens also potentially represent a range of sizes and intertidal positions, this effort represents the most appropriate calibration available.

Sr/Ca ratios were monitored alongside Mg/Ca values. Some studies suggest a correlation between biogenic calcite Sr/Ca and growth rate, temperature, salinity (Klein et al., 1996b; Putten et al., 2000) or seawater Sr/Ca changes (Lear et al., 2003). We report Sr/Ca ratios for completeness, though Sr/Ca does not co-vary with any measured environmental parameters in modern *M. californianus* (Ford et al., 2010).

$\delta^{18}O_{sw}$ Estimation

Once temperature is estimated independently from seawater isotopic composition temperature, $\delta^{18}O_c$ is used to calculate $\delta^{18}O_{sw}$ from the compiled species-specific *M. californianus* paleotemperature equation, in Equation 2:

$$1000 \ln \alpha \text{ (calcite-}H_2O) = 18.47 \pm 0.42 \ (10^3 \ T^{-1}) - 32.9 \pm 1.5, \quad \textit{Equation 2}$$

where T is temperature in Kelvin, α is the fractionation factor, and $\delta^{18}O_c$ and $\delta^{18}O_{sw}$ are both measured on the VSMOW scale. This equation is within error of the previous calibration (Ford et al., 2010) and extends it to cooler temperatures (Fig. 2.3). To represent calcite oxygen isotope values on the VSMOW scale, a simple conversion from VPDB is necessary, updated to reflect a value of NBS-19 on the VPDB scale to be exactly -2.2‰ rather than the earlier -2.19‰ (Coplen et al., 1983; Coplen, 1996) and presented in Equation 3:

$$\delta^{18}O_{VPDB} = 0.97001 * \delta^{18}O_{VSMOW} - 29.99, \qquad \textit{Equation 3}$$

where $\delta^{18}O_{VPDB}$ and $\delta^{18}O_{VSMOW}$ are plotted on the respective scales.

Reservoir Age Estimation

Radiocarbon activity was measured in shells and charcoal from the same midden component to assess the difference between the atmospheric ^{14}C composition and the local ^{14}C signature of ocean water, the radiocarbon 'reservoir age' (e.g. Stuiver et al., 1986). For surface ocean water, the reservoir age tends to increase with the strength of vertical mixing of ^{14}C-depleted deep water (Robinson and Thompson, 1981). Since terrestrial organic carbon incorporates atmospheric ^{14}C and marine organic carbon incorporates marine ^{14}C, the difference can be measured where charcoal and mussel

samples are deposited concurrently, using an average reservoir age of northern hemisphere surface water calculated via a 1-D atmosphere-ocean box-model forced with the atmospheric ^{14}C time-series (Stuiver et al., 1986); reservoir ages are reported as the difference (ΔR) from this modeled average (Fig. 2.4).

Results

Our results are from two time periods: the middle Holocene (6 to 3 kya) and the late Holocene (3 kya to present). Middens are estimated to be between 3.3 and 5.9 kya (cal BP) at Sand Hill Bluff and 0 and 2.4 kya (cal BP) near Point Año Nuevo (Tables 2.1 and 2.2). At Sand Hill Bluff the upper stratum dates to 3200-3680 cal BP while the lower stratum covers a larger time span. One shell, SCr-7 Lower A, was dated directly (5430-5620 cal BP), while shells from a recent excavation are associated with dates spanning 5430-5900 cal BP (Schlagheck, 2011) and surface fragments can only be associated more broadly with the full range of dates collected from the surface of the lower stratum (4530-5890 cal BP). Charcoal dates from the late Holocene middens range from 300 to 2360 cal BP and suggest that each midden represents a spread of less than ~300 years. While $\delta^{18}O_c$ values do not change (t-test, $p>0.5$, null not rejected) from the middle Holocene to the late Holocene (average 1.2 ± 0.4‰ VPDB); SST and $\delta^{18}O_{sw}$ do change and are treated below.

Reservoir Age

Six out of the eight late Holocene middens yield charcoal dates are within ±100 years of one another, which meets our criteria for estimating reservoir ages (Table 2.1). Average Δ*R* is 210 ± 90 years; all late Holocene reservoir ages fall within the uncertainty of this average. The Δ*R* we calculate for the late Holocene from each midden at Año Nuevo is within the uncertainty of this modern value (246 ± 21 ^{14}C years, Fig. 2.3); a Kruskal-Wallis test verifies that all late Holocene reservoir ages are similar ($p>0.4$, null not rejected).

Middle Holocene (6 – 3 kya) at Sand Hill Bluff

Mid-Holocene upper-stratum material (SCr-7 Upper, 3200-3680 cal BP) yielded 118 samples from 2 specimens. Average $\delta^{18}O_c$ was 1.1‰ ± 0.3‰ VPDB and average Mg/Ca was 2.5 ± 0.5 mmol/mol (Fig. 2.5 and Table 2.4). These values translate via the above equations to an average SST of 9.3°C ± 2.0 °C and $\delta^{18}O_{sw}$ value of -1.0‰ ± 3.2‰ VSMOW. From the lower-stratum one shell shows higher average Mg/Ca values, warmer SST, and higher resulting $\delta^{18}O_{sw}$ values (4.1 ± 0.5 mmol/mol, 15.1 ± 2.0 °C, 0.5 ± 3.4 VSMOW, respectively). This SST is ~5±2°C warmer than temperatures inferred for the upper stratum and the difference is significant (U-test, $p<0.001$). Additional shell fragments from the surface of the lower stratum yield an

average Mg/Ca value of 3.5 ± 0.9 mmol/mol and SST of 13.0 ± 3.1 °C. Seven of these fragments (B, C, E, F, H, K, L) confirm temperatures higher than the late Holocene population (individual U-tests, $p<0.05$) though one other (J) does not ($p>0.1$, null not rejected). Potentially older excavated material from the lower stratum yields Mg/Ca values and SST values (2.0 ± 0.3 mmol/mol, 7.7 ± 1.1 °C) that are more similar to the cooler temperatures represented in the upper stratum.

Late Holocene (3 kya to present) at Año Nuevo

Geochemistry of mollusk calcite less than 2500 years old (n=13 specimens, 685 samples) is not different from the shell calcite from the upper stratum of the Sand Hill Bluff site (U-test, null not rejected, $p>0.4$). The average $\delta^{18}O_c$ is 1.2 ± 0.4‰ VPDB, the average Mg/Ca ratio is 2.4 ± 0.6 mmol/mol, SST is 9.2 ± 2.2°C, and $\delta^{18}O_{sw}$ of -0.1 ± 0.5‰ VSMOW (Fig. 2.5 and Table 2.4). The Mg/Ca values of the late Holocene are lower than modern and resulting SST is cooler than modern specimens near Santa Cruz, CA. Individual shell averages are presented in Table 2.4.

Environmental Change

Environmental change was tested between time periods with the middle and late Holocene treated as separate populations. Variance in $\delta^{18}O_c$ between the two

populations was not significantly different (F-test, $p>0.1$); however, variance is greater for mid-Holocene Mg/Ca, temperature, and $\delta^{18}O_{sw}$ than late Holocene values (F-test, $p<0.01$). Since variance changed, Mann-Whitney U-tests were used to resolve average value changes. Average Mg/Ca values and SST are higher in the middle Holocene (U-test, $p<0.01$) and $\delta^{18}O_{sw}$ is lower (U-test, $p<0.01$, Fig. 2.6). Within the late Holocene populations, Kruskal-Wallis tests suggest that no parameter is constant through the late Holocene (at $\alpha=0.05$ level, Fig. 2.7); post-hoc pairwise testing revealed small inter-midden differences, though differences were not the same for each parameter.

Discussion

Our results indicate the past ~4 ky may have represented relative climatic and oceanic stability, while California SST and precipitation were significantly warmer and drier in portions of the middle Holocene. Late Holocene reservoir ages (ΔR), though younger than previous estimates (Ingram, 1998), do not change (within error) through the late Holocene, which suggests the strength of local upwelling at the site has been roughly constant. Reservoir age estimates from San Francisco Bay, the nearest other Holocene record of ^{14}C ages, represent older water than on the coast (Fig. 2.4) and may reflect a higher fraction of ^{14}C-depleted freshwater input (Ingram, 1998) for San Francisco Bay from snowpack, rivers, or groundwater, which do not apply directly to coastal water.

High-resolution sampling within mollusk shells was intended to provide seasonal information since some mollusk species have clear growth bands either in color or shell thickness due to seasonal changes in shell growth rate or water composition and, when viewed in cross-section, can be used to infer shell age, annual cycles, or season of death (Shackleton, 1973; Jones et al., 2008). However, color bands in *M. californianus* specimens from the central California coast do not seem to vary on a regular seasonal cycle, with the possible exception of sample SMa-19C (Fig. 2.8). The lack of a regular seasonal cycle is probably not due to the low amplitude of SST change on the central coast, since modern nearshore water mean annual temperatures range up to 4°C (monthly averages) between warm and cool seasons (Breaker, 2005), while the average standard deviation in temperature for a single month spans 0.9 – 1.3°C (National Data Buoy Center buoy 46012). Instead sample averaging using paths (Fig may obscure seasonal cycles (Fig. 2.9) if paths do not represent contemporaneous material. The lack of information about sample intertidal position further obscures SST variability since we are not able to correct for possible subaerial exposure. For these reasons inter-shell samples are treated as a common shell average, except where noted below.

In situ measurements of $\delta^{18}O_{sw}$ in modern nearshore waters on the central California coast vary with an annual cycle from ~-0.8‰ in the winter to ~0.0‰ during the

summer (Forcino, 2009), consistent with an increase in freshwater run-off intensity during the winter. While the average $\delta^{18}O_{sw}$ values of the late Holocene, as reconstructed from fossil carbonate, are slightly lower, the associated uncertainties are relatively large (Fig. 2.10). Despite these uncertainties, the mid-Holocene results in approximately similar average $\delta^{18}O_{sw}$ values, suggesting more saline surface water and less precipitation in the mid-Holocene. Another possibility for the apparent shift in surface $\delta^{18}O_{sw}$ values is a change in the meteoric composition of local or large-scale precipitation (Dansgaard, 1964; Craig and Gordon, 1965; Bowen, 2010) or a change in the $\delta^{18}O$ of the source water through changed ocean mixing. Here we consider the $\delta^{18}O$ value of meteoric water unlikely to have varied greatly at this location since the atmospheric patterns that bring moisture to central coast originate in the north Pacific where currents or large-scale atmospheric patterns are unlikely to have changed greatly from the mid-to-late Holocene.

Low $\delta^{18}O_{sw}$ values, where associated with high SST, might signal conditions that are consistent with individual El Niño events and indicate high precipitation events that flooded the coastal zone with a freshwater $\delta^{18}O$ signal. The records of four individual shells (SMa-19A, -18A, -18C, and -218A) show evidence of transiently low $\delta^{18}O_{sw}$ and warmer temperature within a single shell microsample (highlighted in Fig. 2.5). Each of these short-lived, low-$\delta^{18}O_{sw}$ peaks and high temperatures are consistent with brief El Niño-like conditions on the central coast. Since El Niño events are defined by SST

anomalies in the tropical Pacific and these records only examine small windows into the climate state, we cannot precisely determine the character or timing of El Niño events from this dataset.

During the mid-Holocene higher Mg/Ca values in mollusk calcite indicate ~5±2°C warmer coastal SST than the late Holocene while higher average $\delta^{18}O_{sw}$ values indicate less precipitation ~5500 years ago, similar to reconstructions of inland California temperature and precipitation (up to 5°C warmer and >30% less precipitation (Benson et al., 2002)). However, abnormally warm coastal temperatures are at odds with alkenone-based SST from Site 1019 and W8709a-PC8 (CA-OR border), which suggest 1 C° cooler or unchanged temperatures (Barron et al., 2003; Sabin and Pisias, 1996) in the mid-Holocene with respect to present values. Today nearshore temperatures are ~1°C cooler than the offshore heart of the California Current; our coastal temperatures suggest that the coastal temperatures were instead ~4°C cooler than the California Current in the late-Holocene, though up to 2°C of this difference could be due to uncertainties in the Mg/Ca estimate and up to 1°C could be due to the alkenone temperature estimates.

These interpretations assume that *M. californianus* shell Mg/Ca values are directly related to local nearshore temperature. Several factors may cast doubt on this assumption. The Mg/Ca values may be influenced by growth rate, which in turn may

be related to seasonality, since some mollusks show metabolic slow-down or even halt growth under cooler temperatures (Gillikin et al., 2007; Freitas et al., 2008). Thus, fossil and/or modern sampling may be biased toward higher temperatures if *M. californianus* grow more rapidly in warmer waters. However, temperatures on the California coast in any portion of the record do not exceed the range of normal growth for *M. californianus* (Coe and Fox, 1944), which reduces the likelihood of metabolic slowdown due to temperature extremes. Shell size and intertidal position may also be confounding the response of *M. californianus* Mg/Ca values to temperature and Mg/Ca values may be higher than expected (yielding higher temperature estimates) in smaller, faster-growing specimens and that these individuals are often subaerially exposed at the upper limit of the intertidal zone (Ford et al., 2010). However, this growth rate effect is likely to be most noticeable in the first ~1.5 years of growth in *M. californianus* (Coe and Fox, 1942) and our samples are all biased toward larger, more robust specimens that integrate a longer time span. These larger specimens are less likely to have lived in the upper intertidal zone and to be biased due to growth rate effects or subaerial exposure.

In some species, shell Mg/Ca formation includes an age bias in older samples since the slower growth of older specimens allows the organism more control over elemental differentiation in the extrapallial fluid from which the shell precipitates, thereby decreasing the sensitivity of shell elemental ratios to environmental

temperatures (Berner, 1975; Carré et al., 2006; Wheeler, 1992). While an age bias may affect the absolute temperatures, any species-specific effects are constant for the specimens sampled, and cannot account for the SST change between the late Holocene and mid-Holocene. Additionally, the temperature calibration curve used was constructed using samples from all size ranges, which, while contributing to the noise in the calibration, conservatively ensures that the calibration incorporates Mg/Ca-temperature effects at all ontogenetic growth rates.

Shell Mg/Ca values may also simply reflect changes in the temperature of the microenvironment in which the specimens grew. Could mid-Holocene organisms have lived in isolated warmer tidal pools or have been transported from a region of warmer SST? Today steep cliffs with minimal tide pools dominate Sand Hill Bluff, whereas the coast at Año Nuevo is less steep with more area for tide pools (*i.e.*, the geomorphic pattern opposite from the one needed to explain the difference in temperature). As stated above, we can find no inter-annual SST gradient between the two when we examine modern gridded data sets sites (Locarnini et al., 2010), or high-resolution satellite data for the nearshore (JPL, 2012). While we cannot discount the possibility that native populations transported these shells great distances along the coast from another locality with warmer or cooler SST, maximum transportation distances that seem likely for mussel shells are <10km. The only warmer or cooler water within 100 km of Sand Hill Bluff is the interior of Monterey Bay, though the

continuous sandy coastline is not ideal for supporting mussel populations. Thus, samples are likely to record temperature from the nearby coastal ocean at Sand Hill Bluff and Año Nuevo within a reasonable degree of error (~2°), leaving coastal SST warmer during intervals of the mid-Holocene than late Holocene SST.

Warmer coastal waters and higher $\delta^{18}O_{sw}$ values in mid-Holocene intervals than the late Holocene imply periods when regional temperature gradients, nearshore coastal upwelling strength, or mid-Holocene coastal precipitation changed. Though reservoir ages are not available, warmer temperatures in central California could reflect suppressed upwelling in the mid-Holocene. These results are consistent with a boundary eddy that may have re-circulated the warmer waters from Monterey Bay in the mid-Holocene to insulate this zone from cooler upwelling before the establishment of the modern Davenport upwelling plume that extends south from Pt. Año Nuevo. Perhaps regional-scale heterogeneities in upwelling, ocean currents, and SST were not always organized identically to the late Holocene and modern system. Since we do observe values similar to the late Holocene for the upper stratum and excavated fragments of SCr-7, we infer the SST and $\delta^{18}O_{sw}$ difference to be temporal rather than spatial between the Año Nuevo and Sand Hill Bluff middens.

The calculated $\delta^{18}O_{sw}$ value from warmer time periods is ~1.0‰ greater than in the late Holocene, suggesting an increase in the evaporation-precipitation difference and

less precipitation. Higher seawater $\delta^{18}O$ could be due to greater evaporation of coastal surface waters or decreased precipitation runoff to the coastal zone. The latter cause would imply that mid-Holocene drought in other parts of California, as indicated by lower lake levels and sedimentary $\delta^{18}O$ evidence (Benson et al., 2002), may have extended to the coastal region in the mid-Holocene. Less precipitation on the central coast may also be one reason why so few archaeological middens are found from the mid-Holocene. Early humans may have subsisted elsewhere if the coast was too dry or not productive enough for large, lasting populations. However, another possibility is that sea level rise 1-2 m (Milne et al., 2005) and ~750 m of cliff retreat over the past 5 ky (Jones and Hildebrandt, 1990) may have removed evidence of mid-Holocene coastal middens.

The record of lower SST in the late Holocene is anomalous with respect to records from the California Current with suggest late Holocene SSTs only ~1°C cooler than modern. Cooler nearshore SST in the late Holocene could represent the upwelling of cooler water at Pt. Año Nuevo than today. Since we observe that reservoir ages do not seem to have changed over the past 2.3 kyr, only the temperature of upwelling may have changed, rather than the relative strength of upwelling. This change may have been facilitated by a weakened Davidson current (Breaker, 2006) in the late Holocene that allowed cooler upwelling to occur in the winter.

These interpretations rely on the fact that the shell mineralogy is original and that diagenesis did not alter these samples. The outer layer of *M. californianus* is calcite and we were not able to test for recrystallization via XRD. However, since the original growth bands were present in all shells and since freshwater does not normally flow near the sites where middens were deposited, we assume that diagenesis may not be a factor controlling shell geochemistry.

Conclusion

Over the past ~4 ky, central California coastal mean annual SST was cooler than modern average SST, which may reflect cooler upwelling waters, though $\delta^{18}O_{sw}$ has and the rate of upwelling remained similar to the present in the late Holocene. Sufficient marine resources were available to support substantial human populations. Intervals within the middle Holocene represent times when SST was similar to modern, though $\delta^{18}O_{sw}$ was greater. The mid-Holocene temperature is anomalous from an oceanographic perspective; offshore records point to cooler California Current SST at this time. The greater $\delta^{18}O_{sw}$ values may represent a period of less precipitation than the late Holocene; the drier climate is consistent with inland terrestrial records for this time period. Lower precipitation rates and/or warm temperatures that have been documented at inland sites may have stretched to coastal

regions and limited the resources that were available to early humans in the region in the mid-Holocene.

Acknowledgements

We gratefully acknowledge the assistance of Dustin McKenzie for providing for additional specimens from the Cabrillo College collection, Diane Gifford-Gonzalez for bone identification, and Julie Fergusen for thoughtful comments and discussions.

References

JPL (2012). Global 1-km Sea Surface Temperature (G1SST). *JPL OurOcean Portal.* http://sst.jpl.nasa.gov/SST/ge_index.jsp

Alley, R., 2000, The Younger Dryas cold interval as viewed from central Greenland: Quaternary Science Reviews, v. 19, no. 1-5, p. 213–226.

Andrus, C.F.T., 2011, Shell midden sclerochronology: Quaternary Science Reviews.

Bakun, A., and Nelson, C., 1991, The seasonal cycle of wind-stress curl in subtropical eastern boundary current regions: Journal of Physical Oceanography, v. 21, no. 12, p. 1815–1834.

Barron, J.A., and Anderson, L., 2011, Enhanced Late Holocene ENSO/PDO expression along the margins of the eastern North Pacific: Quaternary International, v. 235, no. 1-2, p. 3–12, doi: 10.1016/j.quaint.2010.02.026.

Barron, J.A., Heusser, L., Herbert, T., and Lyle, M., 2003, High-resolution climatic evolution of coastal northern California during the past 16,000 years: Paleoceanography, v. 18, no. 1, p. 1020.

Bartlein, P., Anderson, K., Anderson, P., Edwards, M., Mock, C., Thompson, R., Webb, R., Webb, T., III, and Whitlock, C., 1998, Paleoclimate simulations for North America over the past 21,000 years features of the simulated climate and comparisons with paleoenvironmental data: Quaternary Science Reviews, v. 17, no. 6-7, p. 549–585.

Benson, L., Kashgarian, M., Rye, R., Lund, S., Paillet, F., Smoot, J., Kester, C., Mensing, S., Meko, D., and Lindström, S., 2002, Holocene multidecadal and multicentennial droughts affecting Northern California and Nevada: Quaternary Science Reviews, v. 21, no. 4-6, p. 659–682.

Berner, R., 1975, The role of magnesium in the crystal growth of calcite and aragonite from sea water: Geochimica et Cosmochimica Acta, v. 39, no. 4, p. 489–494, IN3, 495–504.

Bowen, G.J., 2010, Isoscapes: Spatial Pattern in Isotopic Biogeochemistry: Annual Review of Earth and Planetary Sciences, v. 38, no. 1, p. 161–187, doi: 10.1146/annurev-earth-040809-152429.

Breaker, L.C., 2006, Nonlinear aspects of sea surface temperature in Monterey Bay: Progress in Oceanography, v. 69, no. 1, p. 61–89, doi: 10.1016/j.pocean.2006.02.015.

Breaker, L.C., 2005, What's happening in Monterey Bay on seasonal to interdecadal time scales: Continental Shelf Research, v. 25, no. 10, p. 1159–1193, doi: 10.1016/j.csr.2005.01.003.

Carré, M., Bentaleb, I., Bruguier, O., Ordinola, E., Barrett, N., and Fontugne, M., 2006, Calcification rate influence on trace element concentrations in aragonitic bivalve shells: Evidences and mechanisms: Geochimica et Cosmochimica Acta, v. 70, no. 19, p. 4906–4920.

Chelton, D.B., Schlax, M.G., and Samelson, R.M., 2007, Summertime Coupling between Sea Surface Temperature and Wind Stress in the California Current System: Journal of Physical Oceanography, v. 37, no. 3, p. 495–517, doi: 10.1175/JPO3025.1.

Coe, W., and Fox, D., 1942, Biology of the California sea-mussel (Mytilus Californianus). I. Influence of temperature, food supply, sex and age on the rate of growth: Journal of Experimental Zoology, v. 90, no. 1, p. 1–30.

Coe, W., and Fox, D., 1944, Biology of the California sea-mussel (Mytilus californianus). III. Environmental conditions and rate of growth: The Biological Bulletin, v. 87, no. 1, p. 59.

Coplen, T., 1996, New guidelines for reporting stable hydrogen, carbon, and oxygen isotope-ratio data: Geochimica et Cosmochimica Acta, v. 60, p. 3359–3360.

Coplen, T., Kendall, C., and Hopple, J., 1983, Comparison of stable isotope reference samples:.

Craig, H., and Gordon, L., 1965, Isotopic oceanography: deuterium and O 18 variations in the ocean and the marine atmosphere, *in* Tongiogi, E. ed., Stable Isotopes in Oceanographic Studies and Paleotemperatures, Consiglio Nazionale delle Richerche, Pisa, Italy, p. 9–130.

Dansgaard, W., 1964, Stable isotopes in precipitation: Tellus, v. 16, no. 4, p. 436–468.

Diffenbaugh, N.S., 2003, Orbital suppression of wind-driven upwelling in the California Current at 6 ka: Paleoceanography, v. 18, no. 2, p. 1051, doi: 10.1029/2002PA000865.

Diffenbaugh, N.S., and Ashfaq, M., 2007, Response of California Current forcing to mid-Holocene insolation and sea surface temperatures: Paleoceanography, v. 22, no. 3, p. PA3101, doi: 10.1029/2006PA001382.

Erlandson, J., 1994, Early Hunter-Gatherers of the California Coast: Plenum Press,

New York, NY.

Filonczuk, M., Cayan, D., and Riddle, L., 1995, Variability of marine fog along the California coast:.

Forcino, F., 2009, *Mytilus californianus* as an environmental monitor: A case study from central California:.

Ford, H.L., Schellenberg, S.A., Becker, B.J., Deutschman, D.L., Dyck, K.A., and Koch, P.L., 2010, Evaluating the skeletal chemistry of Mytilus californianus as a temperature proxy: Effects of microenvironment and ontogeny: Paleoceanography, v. 25, doi: 10.1029/2008PA001677.

Fox, J., Mongan, T., and Miller, W., 1990, Trends in freshwater inflow to San Francisco Bay from the Sacramento-San Joaquin delta: Water Resources Bulletin,, no. 1, p. 101–116.

Freitas, P., Clarke, L., Kennedy, H., and Richardson, C., 2008, Inter- and intra-specimen variability masks reliable temperature control on shell Mg/Ca ratios in laboratory- and field-cultured *Mytilus edulis* and *Pecten maximus* (bivalvia): Biogeosciences Discussions, v. 5, no. 1, p. 531–572.

Freitas, P., Clarke, L., Kennedy, H., Richardson, C., and Abrantes, F., 2006, Environmental and biological controls on elemental (Mg/Ca, Sr/Ca and Mn/Ca) ratios in shells of the king scallop Pecten maximus: Geochimica et Cosmochimica Acta, v. 70, no. 20, p. 5119–5133.

Gardner, J., Dean, W., and Dartnell, P., 1997, Biogenic sedimentation beneath the California Current system for the past 30 kyr and its paleoceanographic significance: Paleoceanography, v. 12, no. 2, p. 207–225.

Gillikin, D., Lorrain, A., Meng, L., and Dehairs, F., 2007, A large metabolic carbon contribution to the $\delta^{13}C$ record in marine aragonitic bivalve shells: Geochimica et Cosmochimica Acta, v. 71, no. 12, p. 2936–2946.

Hickey, B., 1998, Coastal oceanography of western North America from the tip of Baja California to Vancouver Island, *in* Robinson, A. and Brink, K. eds., The Sea, Wiley, New York, NY.

Hood, R., Abbott, M., Huyer, A., and Kosro, P., 1990, Surface patterns in temperature, flow, phytoplankton biomass, and species composition in the coastal transition zone off Northern California: Journal of Geophysical Research, v. 95, no. C10, p. 18081–18094.

Huyer, A., 1983, Coastal upwelling in the California Current system: Progress in Oceanography, v. 12, no. 3, p. 259–284.

Hylkema, M., 1991, Prehistoric Native American adaptations along the central California coast of San Mateo and Santa Cruz counties: San Jose State University.

Ingram, B., 1998, Differences in radiocarbon age between shell and charcoal from a Holocene shellmound in Northern California: Quaternary Research, v. 49, no. 1, p. 102–110.

Ingram, B., and Southon, J., 1996, Reservoir ages in eastern Pacific coastal and estuarine waters: Radiocarbon, v. 38, no. 3, p. 573–582.

Ingram, B., Conrad, M., and Ingle, J., 1996a, Stable isotope and salinity systematics in estuarine waters and carbonates: San Francisco Bay: Geochim Cosmochim Ac, v. 60, no. 3, p. 455–467.

Ingram, B., Ingle, J., and Conrad, M., 1996b, A 2000 yr record of Sacramento-San Joaquin river inflow to San Francisco Bay estuary, California: Geology, v. 24, no. 4, p. 331.

Johnstone, J.A., and Dawson, T.E., 2010, Climatic context and ecological implications of summer fog decline in the coast redwood region: Proceedings of the National Academy of Sciences, v. 107, no. 10, p. 4533–4538, doi: 10.1073/pnas.0915062107.

Jones, D.A., and Hildebrandt, W.R., 1990, Archaeological Excavation at Sand Hill Bluff: Portions of Prehistoric Site CA-SCR-7, Santa Cruz, CA: Far Western Anthropological Group, 1–8 p.

Jones, T., 1992, Settlement trends along the California Coast, *in* Jones, T. ed., Essays on the Prehistory of Maritime California, Regents of the University of California, Davis, CA.

Jones, T., and Kennett, D., 1999, Late Holocene sea temperatures along the central California coast: Quaternary Research, v. 51, no. 1, p. 74–82.

Jones, T., Kennett, D., Kennett, J., and Codding, B., 2008, Seasonal stability in Late Holocene shellfish harvesting on the central California coast: Journal of archaeological science, v. 35, no. 8, p. 2286–2294.

Jones, T., Stevens, N., Jones, D., Fitzgerald, R., and Hylkema, M., 2007, The Central Coast: A Midlatitude Milieu, *in* Jones, T. and Klar, K. eds., California Prehistory: Colonization, Culture, and Complexity, Altamira Press, Lanham, MD.

Global 1-km Sea Surface Temperature (G1SST), 2012, Global 1-km Sea Surface Temperature (G1SST): JPL OurOcean Portal.

Kennett, D., Kennett, J.P., Erlandson, J.M., and Cannariato, K.G., 2007, Human responses to Middle Holocene climate change on California's Channel Islands: Quaternary Science Reviews, v. 26, no. 3-4, p. 351–367, doi: 10.1016/j.quascirev.2006.07.019.

Klein, R., Lohmann, K., and Thayer, C., 1996a, Bivalve skeletons record sea-surface temperature and δ18O via Mg/Ca and 18O/16O ratios: Geology, v. 24, no. 5, p. 415.

Klein, R., Lohmann, K., and Thayer, C., 1996b, Sr/Ca and 13C/12C ratios in skeletal calcite of Mytilus trossulus: Covariation with metabolic rate, salinity, and carbon isotopic composition of seawater: Geochimica et Cosmochimica Acta, v. 60, no. 21, p. 4207–4221.

Lea, D., Mashiotta, T., and Spero, H., 1999, Controls on magnesium and strontium uptake in planktonic foraminifera determined by live culturing: Geochimica et Cosmochimica Acta, v. 63, no. 16, p. 2369–2379.

Lear, C.H., Elderfield, H., and Wilson, P.A., 2003, A Cenozoic seawater Sr/Ca record from benthic foraminiferal calcite and its application in determining global weathering fluxes: Earth and Planetary Science Letters, v. 208, no. 1-2, p. 69–84, doi: 10.1016/S0012-821X(02)01156-1.

Locarnini, R., Mishonov, A., Antonov, J., Boyer, T., Garcia, H., Baranova, O., Zweng, M., and Johnson, D., 2010, World Ocean Atlas 2009, *in* Levitus, S. ed., NOAA Atlas NESDIS 68, U.S. Government Printing Office, Washington, D.C., p. 184.

Louderback, L.A., Grayson, D.K., and Llobera, M., 2010, Middle-Holocene climates and human population densities in the Great Basin, western USA: The Holocene, v. 21, no. 2, p. 366–373, doi: 10.1177/0959683610374888.

Malamud-Roam, F.P., Lynn Ingram, B., Hughes, M., and Florsheim, J.L., 2006, Holocene paleoclimate records from a large California estuarine system and its watershed region: linking watershed climate and bay conditions: Quaternary Science Reviews, v. 25, no. 13-14, p. 1570–1598, doi: 10.1016/j.quascirev.2005.11.012.

McGann, M., 2008, High-resolution foraminiferal, isotopic, and trace element records from Holocene estuarine deposits of San Francisco Bay, California: Journal of Coastal Research, v. 245, p. 1092–1109, doi: 10.2112/08A-0003.1.

Mensing, S., Benson, L., Kashgarian, M., and Lund, S., 2004, A Holocene pollen record of persistent droughts from Pyramid Lake, Nevada, USA: Quaternary Research, v. 62, no. 1, p. 29–38.

Milliken, R., Fitzgerald, R., Hylkema, M., Groza, R., Origer, R., Bieling, D., Levanthal, A., Wilberg, R., Gottsfield, A., Gillette, D., Bellefemine, V., Strother, E., Cartier, R., and Fredrickson, D., 2007, Punctuated Culture Change in the San Francisco Bay Area, *in* Jones, T. and Klar, K. eds., California Prehistory: Colonization, Culture, and Complexity, Altamira Press, Lanham, MD.

Milne, G., Long, A., and Bassett, S., 2005, Modelling Holocene relative sea-level observations from the Caribbean and South America: Quaternary Science Reviews, v. 24, no. 10-11, p. 1183–1202, doi: 10.1016/j.quascirev.2004.10.005.

Mix, A.C., Lund, D.C., Pisias, N.G., Boden, P., Bornmalm, L., Lyle, M., and Pike, J., 1999, Rapid climate oscillations in the northeast Pacific during the last deglaciation reflect Northern and Southern Hemisphere sources: Geophysical Monograph - AGU, v. 112, p. 127–148.

Newsome, S., Phillips, D., Culleton, B., Guilderson, T., and Koch, P., 2004, Dietary reconstruction of an early to middle Holocene human population from the central California coast: insights from advanced stable isotope mixing models: Journal of archaeological science, v. 31, no. 8, p. 1101–1115.

Ostertag-Henning, C., and Stax, R., 2000, Carbonate records from sites 1012, 1013, 1017, and 1019 and alkenone-based sea-surface temperatures from site 1017: Proceedings of the Ocean Drilling Program, Scientific Results, v. 167, p. 297–302.

Pennington, J., and Chavez, F., 2000, Seasonal fluctuations of temperature, salinity, nitrate, chlorophyll and primary production at station H3/M1 over 1989-1996 in Monterey Bay, California: Deep Sea Research Part II: Topical Studies in Oceanography, v. 47, no. 5-6, p. 947–973.

Pisias, N., Mix, A., and Heusser, L., 2001, Millennial scale climate variability of the northeast Pacific Ocean and northwest North America based on radiolaria and pollen: Quaternary Science Reviews, v. 20, no. 14, p. 1561–1576.

Putten, E.V., Dehairs, F., Keppens, E., and Baeyens, W., 2000, High resolution distribution of trace elements in the calcite shell layer of modern Mytilus edulis: Environmental and biological controls: Geochimica et Cosmochimica Acta, v. 64, no. 6, p. 997–1011.

Reimer, P.J., Baillie, M.G.L., Bard, E., Bayliss, A., Beck, J.W., Blackwell, P.G., Ramsey, C.B., Buck, C.E., Burr, G.S., Edwards, R.L., Friedrich, M., Grootes, P., Guilderson,

T., Hajdas, I., et al., 2009, IntCal09 and Marine09 radiocarbon age calibration curves, 0–50,000 years cal BP:.

Reinemann, S.A., Porinchu, D.F., Bloom, A.M., Mark, B.G., and Box, J.E., 2009, A multi-proxy paleolimnological reconstruction of Holocene climate conditions in the Great Basin, United States: Quaternary Research, v. 72, no. 3, p. 347–358, doi: 10.1016/j.yqres.2009.06.003.

Robinson, S., and Thompson, G., 1981, Radiocarbon corrections for marine shell dates with application to southern Pacific Northwest Coast prehistory: Syesis, v. 14, p. 45–57.

Rosenfeld, L., Schwing, F., Garfield, N., and Tracy, D., 1994, Bifurcated flow from an upwelling center: a cold water source for Monterey Bay: Continental Shelf Research, v. 14, no. 9, p. 931–964.

Sabin, A., and Pisias, N., 1996, Sea surface temperature changes in the northeastern Pacific Ocean during the past 20,000 years and their relationship to climate change in northwestern North America: Quaternary Research, v. 46, no. 1, p. 48–61.

Schlagheck, J., 2011, Obsidian Trade at Sand Hill Bluff: Society for California Archaeology, v. 25.

Schweikhardt, P., Sloan, D., and Ingram, B.L., 2010, Early Holocene Evolution of San Francisco Estuary, Northern California: Journal of Coastal Research, v. 264, p. 704–713, doi: 10.2112/08-1039.1.

Shackleton, N., 1973, Oxygen isotope analysis as a means of determining season of occupation of prehistoric midden sites: Archaeometry, v. 15, no. 1, p. 133–141.

Starratt, S.W., 2009, Holocene climate on the Modoc Plateau, northern California, USA: the view from Medicine Lake: Hydrobiologia, v. 631, no. 1, p. 197–211, doi: 10.1007/s10750-009-9811-z.

Stine, S., 1990, Late holocene fluctuations of Mono Lake, eastern California: Palaeogeography Palaeoclimatology Palaeoecology, v. 78, no. 3-4, p. 333–381.

Stuiver, M., and Polach, H., 1977, Discussion: Reporting of 14C data: Radiocarbon, v. 19, no. 3, p. 355–363.

Stuiver, M., and Reimer, P., 2009, CALIB 6.0:.

Stuiver, M., Pearson, G.W., and Braziunas, T.F., 1986, Radiocarbon age calibration of

marine samples back to 9000 cal yr BP: Radiocarbon, v. 28, no. 2B, p. 980–1021.

Surge, D., Lohmann, K., and Goodfriend, G., 2003, Reconstructing estuarine conditions: oyster shells as recorders of environmental change, Southwest Florida: Estuarine, Coastal and Shelf Science, v. 57, no. 5-6, p. 737–756.

Takesue, R., and Van Geen, A., 2004, Mg/Ca, Sr/Ca, and stable isotopes in modern and Holocene Protothaca staminea shells from a northern California coastal upwelling region: Geochimica et Cosmochimica Acta, v. 68, no. 19, p. 3845–3861.

Van Geen, A., Luoma, S., Fuller, C., Anima, R., Clifton, H., and Trumbore, S., 1992, Evidence from Cd/Ca ratios in foraminifera for greater upwelling off California 4, 000 years ago: Nature, v. 358, no. 6381, p. 54–56.

Vogel, J.S., Nelson, D., and Southon, J.R., 1987, C-14 background levels in an accelerator mass-spectrometry system: Radiocarbon, v. 29, no. 3, p. 323–333.

Wheeler, A., 1992, Mechanisms of molluscan shell formation, *in* Bonucci, E. ed., Calcification in Biological Systems, CRC Press, Boca Raton, FL, p. 179–215.

Figures

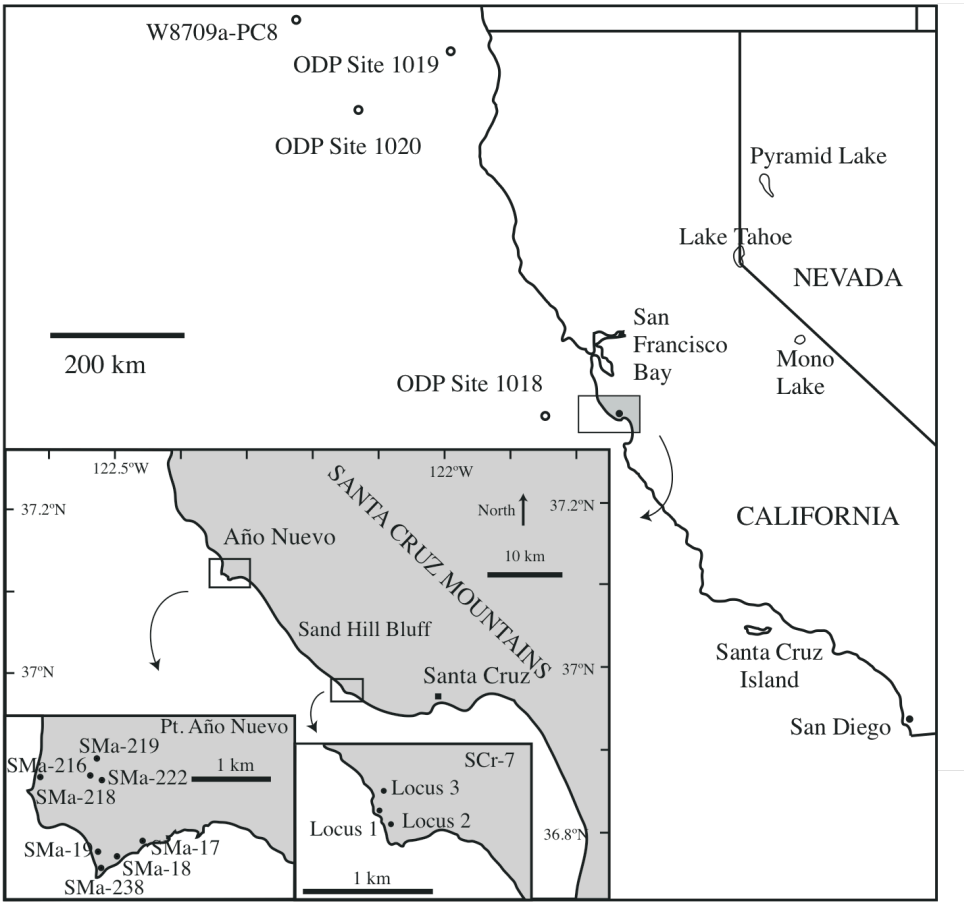

Figure 2.1. Locations of selected sites of Holocene temperature and/or salinity records (ODP Site 1019: Barron *et al*, 2003; Pyramid Lake: Mensing *et al*, 2004; Lake Tahoe: Barron *et al*, 2003; Mensing *et al*., 2004; Mono Lake: Stine, 1990). Año Nuevo State Park, is ~90 km south of San Francisco, CA and 35 km north of Santa Cruz, CA. Midden locations at Año Nuevo and SCr-7 at Sand Hill Bluff are shown in second inset.

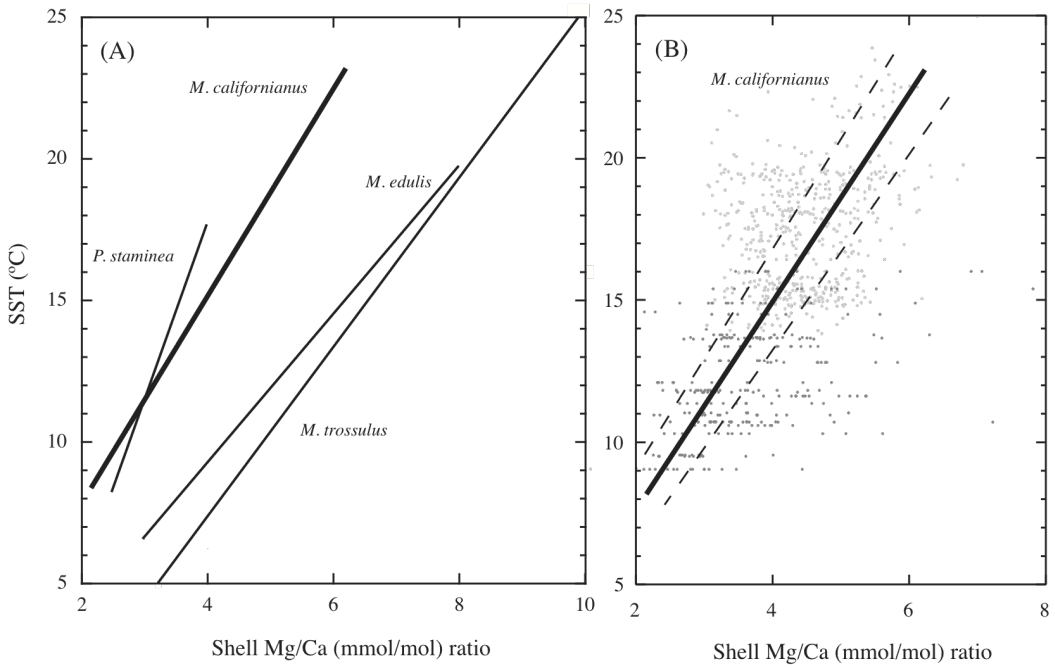

Figure 2.2. (A) Selected bivalve Mg/Ca-temperature regression lines, as determined using RMA regression analysis where data is available, and reported regression where data otherwise. (B) *M. californianus* Mg/Ca-temperature regression (solid line) with data. Data from southern California is light grey and data from central California is dark grey. Dashed lines represent 95% CI. Regression equations of modern populations as follows:

M. trossulus:	T (°C) = 2.90 (± 0.21) * Mg/Ca (mmol/mol) - 4.7 (± 1.4),	r^2 = 0.75 (Klein et al., 1996a),
M. edulis (1):	T (°C) = 2.62 (± 0.23) * Mg/Ca (mmol/mol) - 1.3 (± 1.3),	r^2 = 0.54 (Freitas et al., 2008),
P. staminea:	T (°C) = 6.25 * Mg/Ca (mmol/mol) - 7.4	(Takasue and van Geen, 2004),
M. californianus:	T (°C) = 3.65 (± 0.11) * Mg/Ca (mmol/mol) + 0.33 (± 0.47),	r^2 = 0.27 (Equation 1),

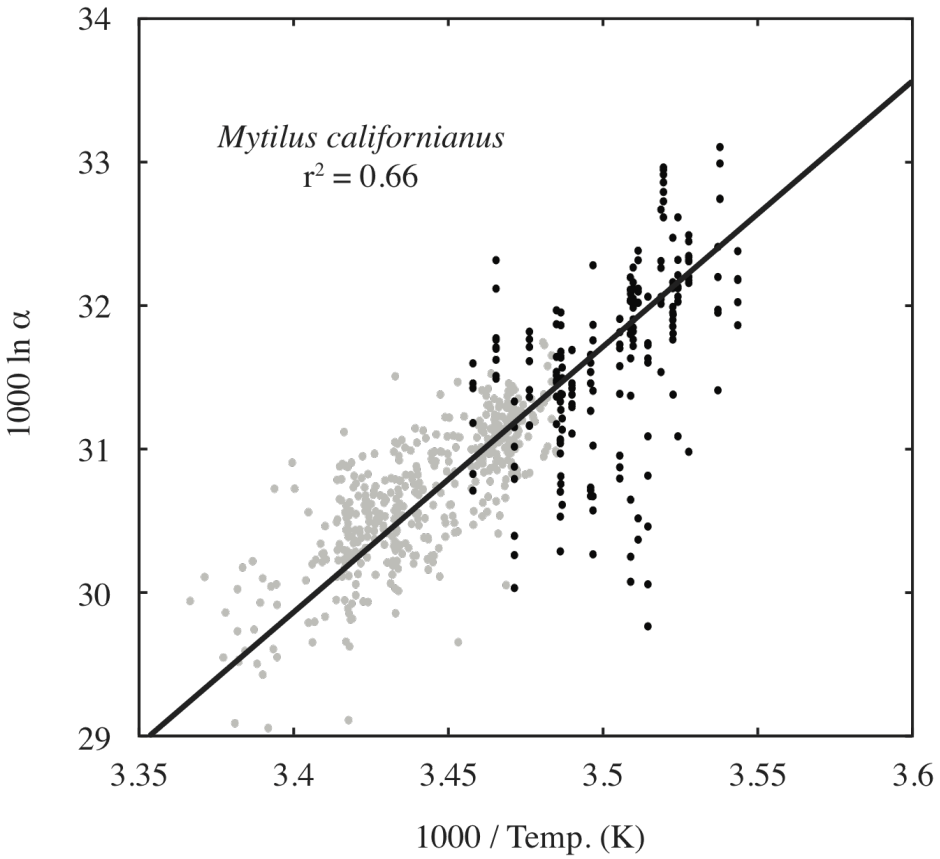

Figure 2.3. Reduced major axis regression of temperature and α values for all $\delta^{18}O$ values of *Mytilus californianus* from southern CA (grey) (Ford et al., 2010) and northern CA (black) (Forcino, 2009). Equation 2 (see text) is the regression equation for this data.

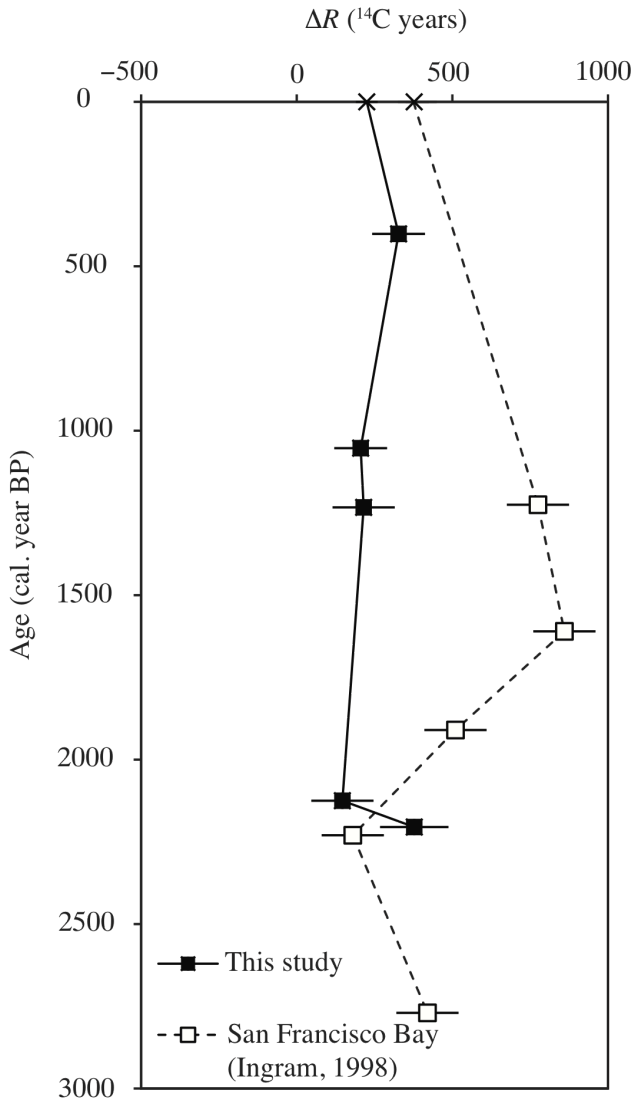

Figure 2.4. Late Holocene Δ*R* determined from coastal middens (black squares), is compared with middens within the San Francisco Bay estuary (open squares; Ingram, 1998) and pre-bomb modern values from Monterey Bay and San Francisco Bay (crosses at modern age). The age of modern (pre-bomb) San Francisco Bay water is older than coastal sites to begin with (Ingram and Southon, 1996) but was even older than coastal waters in the period ~2000-1000 years ago. Coastal reservoir ages do not show the influence of older freshwater that San Francisco Bay may have experienced in the late Holocene.

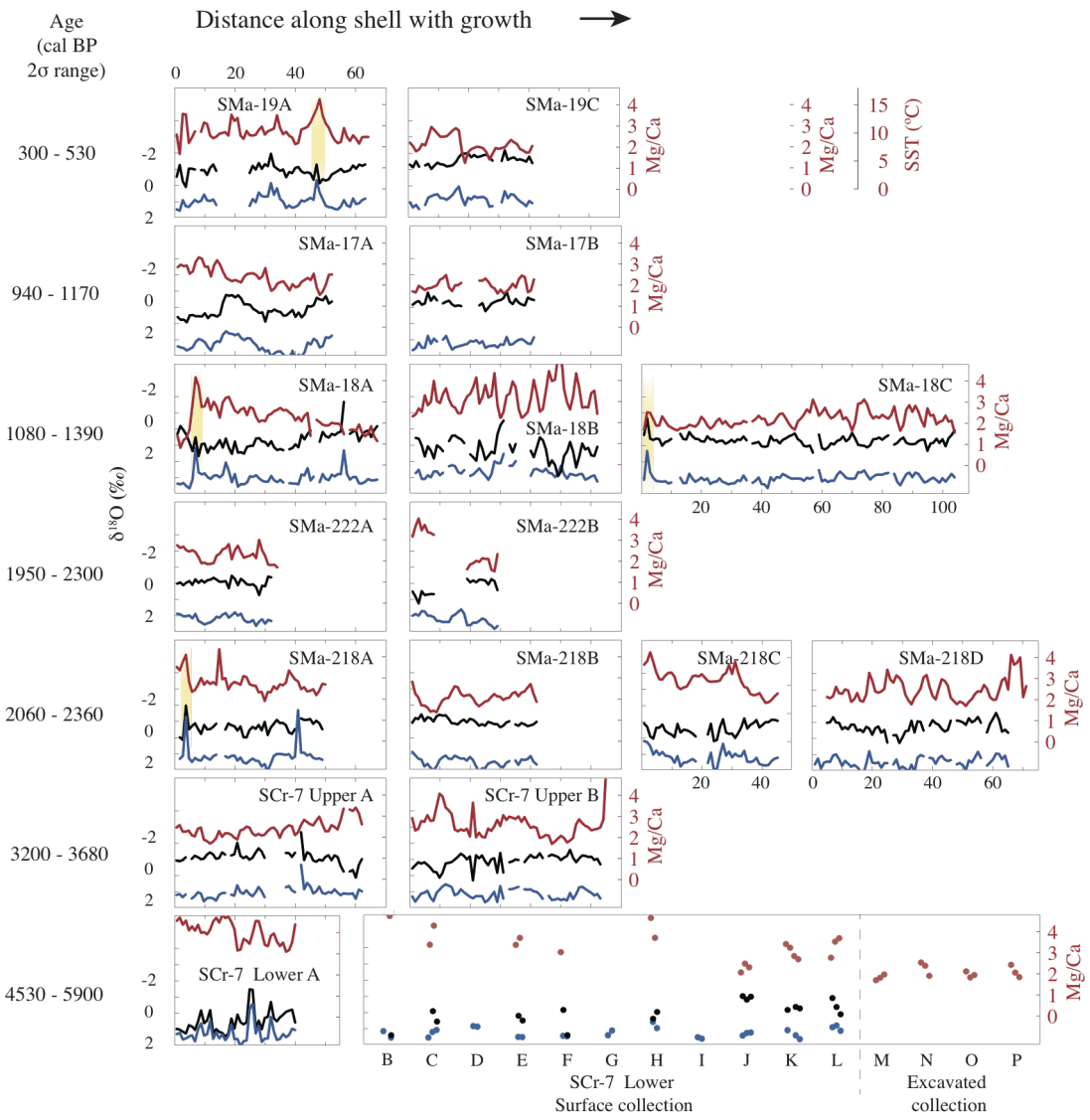

Figure 2.5. High-resolution records of temperature, $\delta^{18}O_c$, SST, and $\delta^{18}O_{sw}$ recorded by individual mollusk shells. Shells with continuous records were micromilled along growth bands, though annual cycles are difficult to discern. Shell fragments from the lower stratum of SCr-7 were milled perpendicular to growth bands to maximize time averaging since very little sample was available.

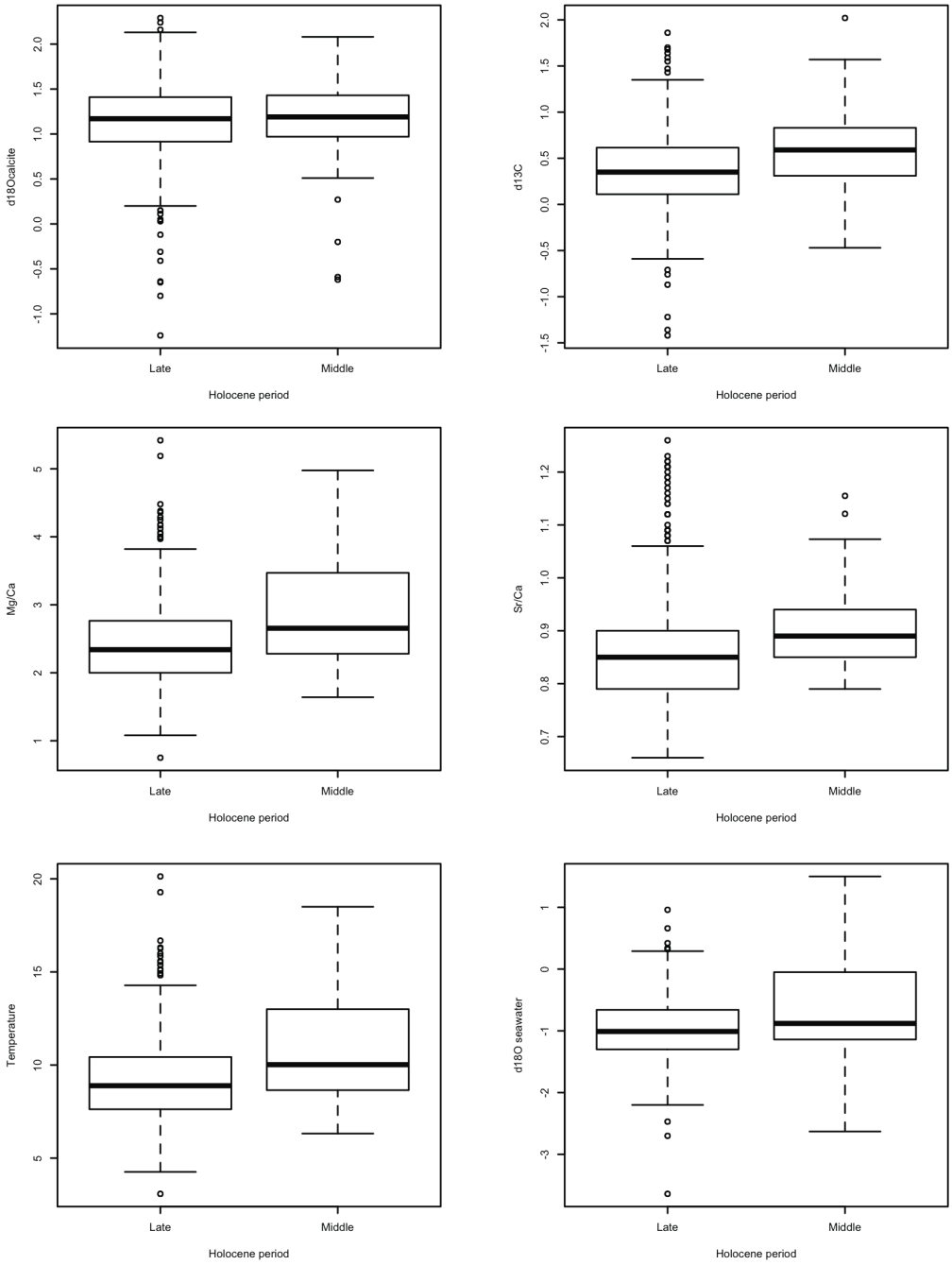

Figure 2.6. Comparisons of late and middle Holocene populations. Statistical tests suggest that the average is significantly different (at α=0.05 level) between these populations for all parameters except δ^{18}Oc.

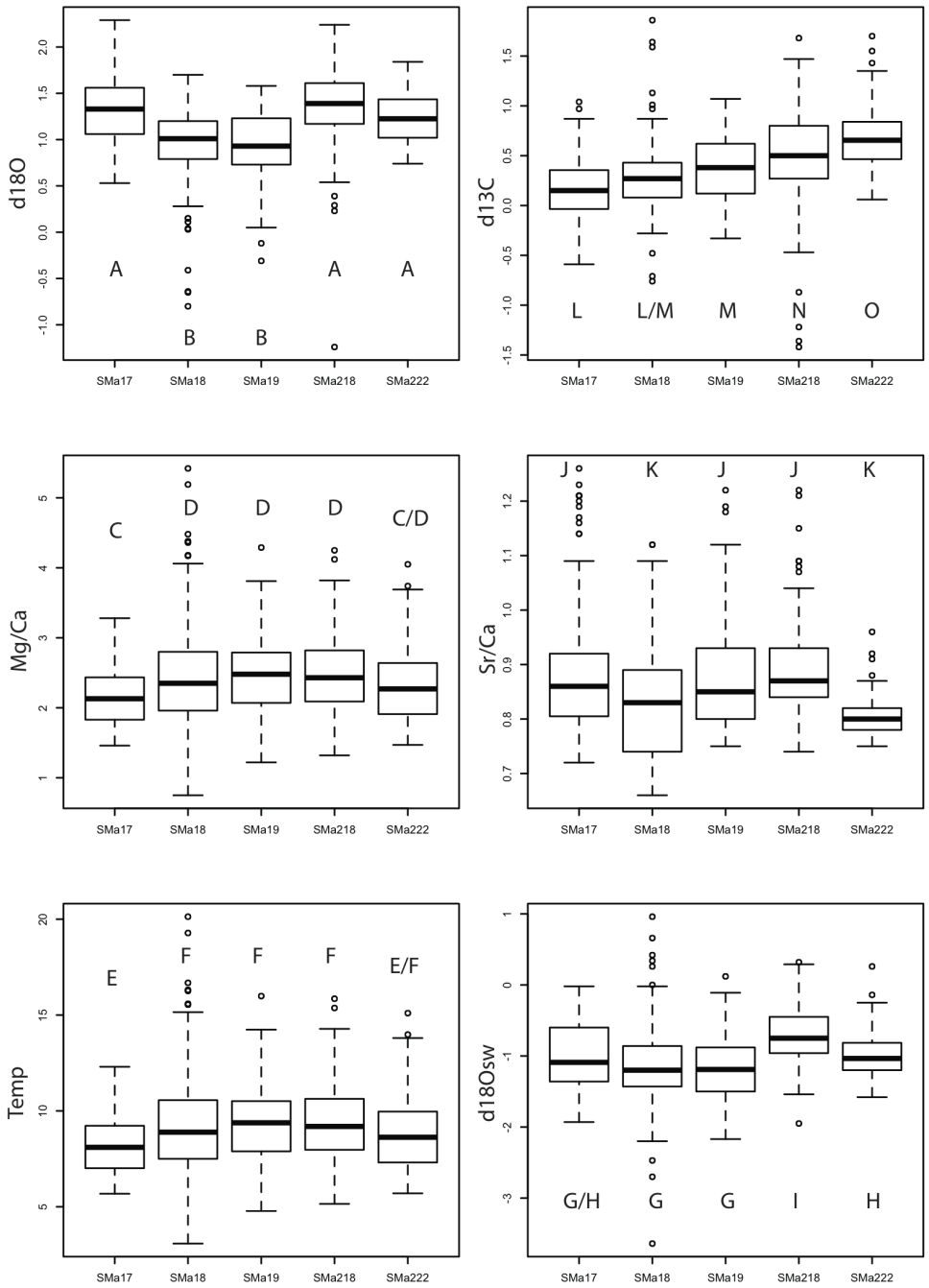

Figure 2.7. Comparisons within late Holocene middens. While Kruskal-Wallis tests suggest that no parameter is constant (at α=0.05 level) between middens, post-hoc pairwise testing may not reveal meaningful patterns among middens. Labels (A through O) correspond to geochemical parameters where the null hypothesis cannot be rejected at α=0.05 level between midden samples.

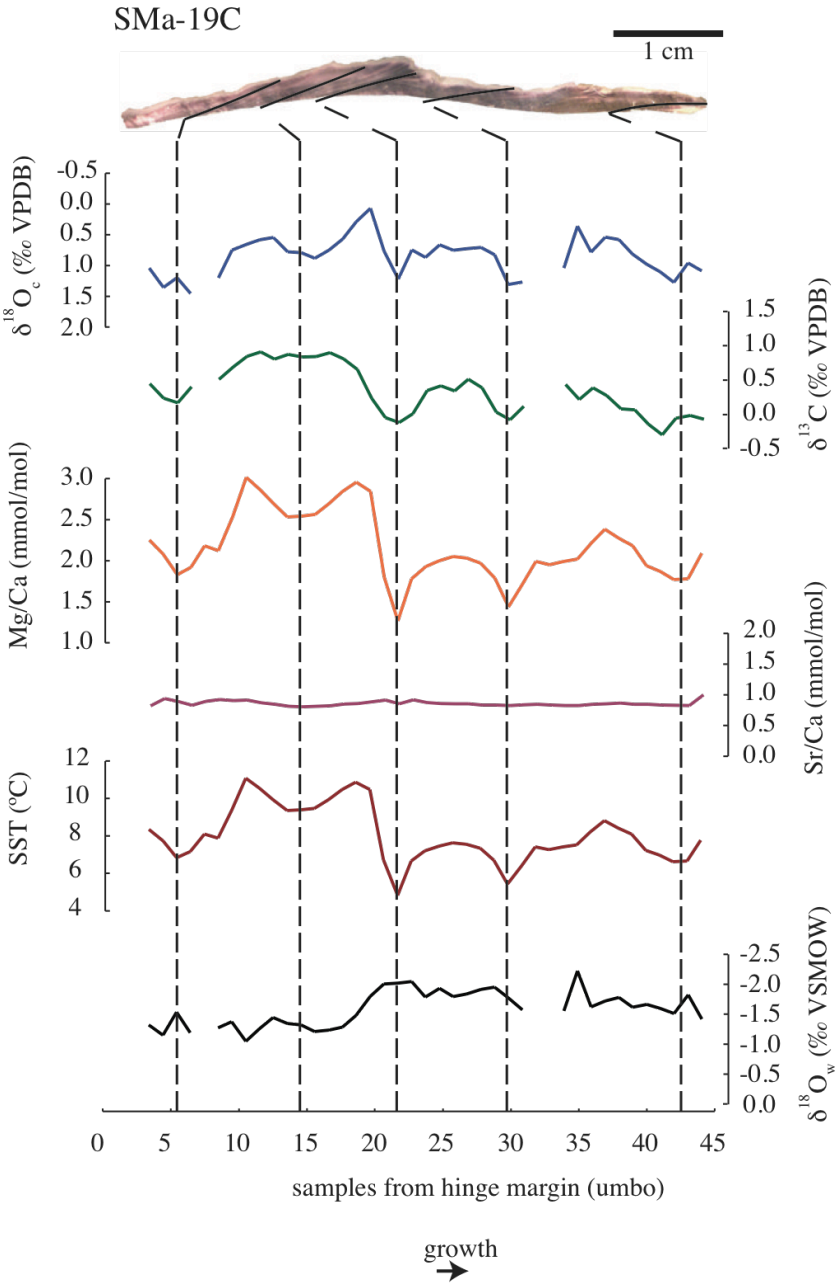

Figure 2.8. Sample mussel data from shell SMa-19C. Sample is milled along growth bands (~200 mm wide) and vertical bars represent possible winters; years are estimated from the seasonal temperature cycles.

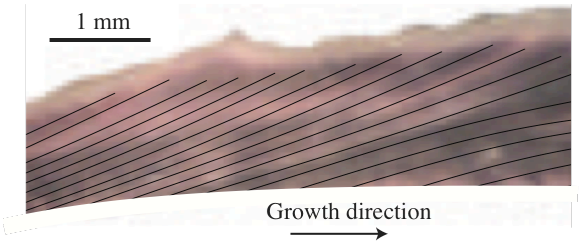

Figure 2.9. Detail of shell section (~300 μm thick) from SMa-19C with sample paths. Each path is ~150 μm wide and ~100 μm deep and milled parallel to color bands.

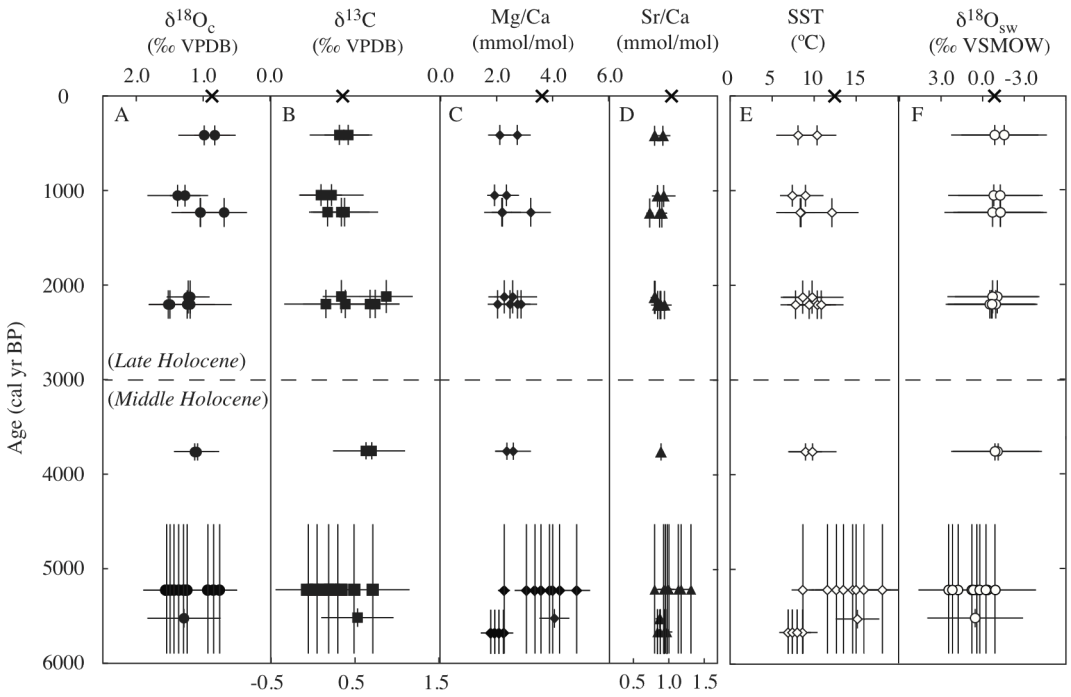

Figure 2.10. (A) Average shell $\delta^{18}O$ value, (B) average shell $\delta^{13}C$ value, (C) average shell Mg/Ca value, (D) average shell Sr/Ca value, (E) average calculated SST from Mg/Ca value, and (F) average calculated $\delta^{18}O$ of seawater. Age uncertainty is (2σ) range of charcoal dates for late Holocene and shell calcite dates for middle Holocene. Uncertainties for geochemical values are standard deviations of samples throughout the shell. Errors are propagated for uncertainty in SST and $\delta^{18}O$ seawater. Each point represents an average of 3-50+ samples. From youngest to oldest, midden layers shown are: SMa-19, SMa-17, SMa-18, SMa-222, SMa-218A, SCr-7 (upper strata), SCr-7 (Lower strata), SCr-7 (peripheral excavations, minor elements only). Modern values are marked as reported in samples from Santa Cruz, CA (Forcino, 2009).

Site	Charcoal Sample	Charcoal ^{14}C Age	CALIB 6.0 Corrected Charcoal Age (cal BP)				Components	Mean Shell ^{14}C Age (n)	Reservoir ^{14}C Age (Shell – Charcoal	ΔR
			68% (1σ) CALIB age range	Relative area under dist.	95% (2σ) CALIB age range	Relative area under dist.				
SMa-238	1	160 ± 35	0-31*	0.23	0-39*	0.19	1	810 ± 80 (5)		
			85-86	0.005	63-118	0.16				
			94-95	0.01	123-232	0.48				
			138-153	0.12	242-286	0.18				
			168-223	0.45						
			256-283	0.19						
	2	445 ± 35	489-523	1.0	335-348	0.03				
					440-440	0.001				
					454-539	0.97				
SMa-216	1	345 ± 40	318-393	0.64	310-490	1.0	1	1060 ± 70 (5)	710 ± 85	310 ± 85
			425-466	0.36						
	2	350 ± 35	320-379	0.54	315-414	0.57				
			387-391	0.03	416-493	0.43				
			427-472	0.42						
SMa-19	1	430 ± 35	475-518	1.0	332-355	0.07	>1	980 ± 90 (6)		
					434-532	0.93				
	2	315 ± 40	307-333	0.23	300-480	1.0				
			352-435	0.77						
SMa-17	1	1120 ± 35	978-1040	0.80	938-945	0.01	1	1700 ± 70 (5)	570 ± 85	170 ± 85
			1042-1058	0.20	954-1092	0.94				
					1106-1137	0.04				
					1162-1167	0.01				
	2	1135 ± 35	978-1068	1.0	963-1143	0.98				
					1160-1169	0.02				
SMa-18	1	1250 ± 35	1148-1157	0.07	1080-1274	1.0	>1	1920 ± 90 (6)	575 ± 100	175 ± 100
			1171-1263	0.93						
	2	1435 ± 35	1302-1349	1.0	1292-1386	1.0				
SMa-219	1	1540 ± 45	1379-1423	0.4	1343-1530	1.0	>1	1990 ± 70 (4)		
			1431-1443	0.09						
			1458-1516	0.51						
	2	1260 ± 35	1174-1263	1.0	1084-1113	0.06				
					1121-1282	0.94				
SMa-222	1	2120 ± 40	2009-2018	0.05	1991-2160	0.88	1	2590 ± 80 (5)	490 ± 100	90 ± 100
			2040-2148	0.95	2169-2178	0.01				
					2244-2301	0.11				
	2	2095 ± 40	2004-2027	0.21	1950-1962	0.02				
			2036-2118	0.79	1968-2153	0.97				
					2274-2291	0.02				
SMa-218	1	2290 ± 40	2185-2192	0.07	2157-2262	0.45	1	2950 ± 90 (6)	720 ± 110	320 ± 110
			2206-2230	0.23	2298-2355	0.55				
			2307-2350	0.71						
	2	2170 ± 40	2118-2182	0.46	2055-2318	1.0				
			2237-2304	0.54						

Table 2.1. Late Holocene radiocarbon data. Calibration data for charcoal is IntCal09 (Reimer *et al.*, 2009; Stuiver *et al.*, 2005), while for shells is Marine09 (Reimer *et al.*, 2009) with an average ΔR for Monterey Bay, CA of 246 ± 21 years. Samples marked with (*) are at the modern end of the calibration dataset.

SCr-7	Sample	Sample Type	^{14}C Age	CALIB 6.0 Corrected Age (cal BP) 68% (1σ) CALIB age range	Rel. area under dist.	95% (2σ) CALIB age range	Rel. area under dist.	Reference:
Locus 1 Upper Strata		Shell calcite	3780 ± 95	3325-3552	1.0	3200-3676	1.0	*Morejohn, 1976*
Locus 1 Lower Strata	A	Shell calcite	5405 ± 40	5477-5571	1.0	5426-5621	1.0	This study
	1	Shell calcite	5655 ± 35	5731-5850	1.0	5671-5889	1.0	This study
	2	Shell calcite	5015 ± 40	4932-5124	1.0	4867-5214	1.0	This study
	3	Shell calcite	4715 ± 35	4580-4722	0.90	4525-4793	1.0	This study
				4750-4768	0.10			
		Shell calcite	5390 ± 35	5475-5564	1.0	5425-5599	1.0	*Schlagheck, 2011*
		Shell calcite	5605 ± 40	5651-5793	1.0	5616-5862	1.0	*Schlagheck, 2011*
		Shell calcite	5605 ± 40	5651-5793	1.0	5616-5862	1.0	*Schlagheck, 2011*
		Shell calcite	5670 ± 35	5750-5863	1.0	5697-5902	1.0	*Schlagheck, 2011*
		Shell calcite	5390 ± 100	5363-5366	0.01	5283-5720	1.0	*Morejohn, 1976*
				5389-5614	0.99			

Table 2.2. Radiocarbon ages from shells of SCr-7; no charcoal data is available. Calibration data for this study is Marine09 (Reimer *et al.*, 2009) with an average ΔR for Monterey Bay, CA of 246 ± 21 years (Ingram and Southon, 1996). ^{14}C ages from other studies are recalibrated here using CALIB 6.0.

CAMS #	Sample ID	Site	Sample	$\delta^{13}C$	Fraction modern	±	$D^{14}C$	±	Raw ^{14}C	±
	Charcoal									
85678	SMA-238 CA	SMa-238	1	-25	0.9803	0.0037	-19.7	3.7	160	35
90087	SMA-238 CB	SMa-238	2	-25	0.9458	0.0038	-54.2	3.8	445	35
90090	SMA-216 CA	SMa-216	1	-25	0.9577	0.0046	-42.3	4.6	345	40
90091	SMA-216 CB	SMa-216	2	-25	0.9571	0.0039	-42.9	3.9	350	35
85677	SMA-19 CA	SMa-19	1	-25	0.9478	0.0036	-52.2	3.6	430	35
90086	SMA-19 CB	SMa-19	2	-25	0.9618	0.0044	-38.2	4.4	315	40
90088	SMA-17 CA	SMa-17	1	-25	0.8697	0.0035	-130.3	3.5	1120	35
90089	SMA-17 CB	SMa-17	2	-25	0.8682	0.0035	-131.8	3.5	1135	35
85676	SMA-18 CA	SMa-18	1	-25	0.8561	0.0032	-143.9	3.2	1250	35
90085	SMA-18 CB	SMa-18	2	-25	0.8362	0.0034	-163.8	3.4	1435	35
90829	SMA-219 CA	SMa-219	1	-25	0.8255	0.0046	-174.5	4.6	1540	45
90830	SMA-219 CB	SMa-219	2	-25	0.8549	0.0034	-145.1	3.4	1260	35
90825	SMA-218 CA	SMa-218	1	-25	0.7522	0.0033	-247.8	3.3	2290	40
90826	SMA-218 CB	SMa-218	2	-25	0.7977	0.0035	-202.3	3.5	2170	40
90827	SMA-222 CA	SMa-222	1	-25	0.7679	0.0034	-232.1	3.4	2120	40
90828	SMA-222 CB	SMa-222	2	-25	0.7706	0.0034	-229.4	3.4	2095	40
	Mytilus californianus									
75937	238-MC-001	SMa-238	1	0	0.9046	0.0038	-95.4	3.8	810	40
90040	238-MC-001L	SMa-238	2	1	0.8977	0.0046	-102.3	4.6	865	45
75938	238-MC-002	SMa-238	3	0	0.9028	0.0042	-97.2	4.2	820	40
90041	238-MC-002L	SMa-238	4	1	0.8996	0.0036	-100.4	3.6	850	35
80944	238-MC-003	SMa-238	5	1.4	0.8998	0.0032	-100.2	3.2	850	30
80945	238-MC-004	SMa-238	6	0.9	0.9067	0.0032	-93.3	3.2	785	30
80946	238-MC-005	SMa-238	7	1	0.9069	0.0032	-93.1	3.2	785	30
80942	216-MC-001	SMa-216	1	1	0.8842	0.0033	-115.8	3.3	990	30
80943	216-MC-002	SMa-216	2	1	0.8727	0.0032	-127.3	3.2	1095	30
80940	216-MC-003	SMa-216	3	1	0.8764	0.0032	-123.6	3.2	1060	30
80941	216-MC-004	SMa-216	4	1	0.8786	0.0027	-121.4	2.7	1040	25
90042	216-MC-005	SMa-216	5	1	0.8727	0.0035	-127.3	3.5	1095	35
75939	19-MC-001	SMa-19	1	0	0.8931	0.0038	-106.9	3.8	910	40
75940	19-MC-002	SMa-19	2	0	0.8788	0.0042	-121.2	4.2	1040	40
80953	19-MC-003	SMa-19	3	0.6	0.862	0.0029	-138	2.9	1195	30
80954	19-MC-004	SMa-19	4	1	0.8911	0.0032	-108.9	3.2	925	30
80955	19-MC-005	SMa-19	5	1	0.8867	0.0031	-113.3	3.1	965	30
80956	19-MC-006	SMa-19	6	1	0.899	0.004	-101	4	855	40
80937	17-MC-001	SMa-17	1	1	0.8136	0.003	-186.4	3	1655	30
80938	17-MC-002	SMa-17	2	1	0.8103	0.003	-189.7	3	1690	30

CAMS #	Sample ID	Site	Sample	$\delta^{13}C$	Fraction modern	±	$D^{14}C$	±	Raw ^{14}C	±
80939	17-MC-003	SMa-17	3	1	0.8143	0.0029	-185.7	2.9	1650	30
90032	17-MC-004	SMa-17	4	1	0.8011	0.0029	-198.9	2.9	1780	30
90033	17-MC-005	SMa-17	5	1	0.8087	0.0032	-191.3	3.2	1705	35
75941	18-MC-001	SMa-18	1	0	0.7802	0.0037	-219.8	3.7	1990	40
75942	18-MC-002	SMa-18	2	0	0.7826	0.0033	-217.4	3.3	1970	40
75943	18-MC-003	SMa-18	3	0	0.798	0.0038	-202	3.8	1810	40
80950	18-MC-004	SMa-18	4	0.2	0.7939	0.0027	-206.1	2.7	1855	30
80951	18-MC-005	SMa-18	5	0.7	0.7815	0.0027	-218.5	2.7	1980	30
80952	18-MC-006	SMa-18	6	1	0.7899	0.0031	-210.1	3.1	1895	35
90034	219-MC-001	SMa-219	1	1	0.7892	0.0026	-210.8	2.6	1900	30
90035	219-MC-002	SMa-219	2	1	0.7720	0.0031	-228.0	3.1	2080	35
90036	219-MC-003	SMa-219	3	1	0.7735	0.0032	-226.5	3.2	2065	35
90831	219-MC-004	SMa-219	4	0	0.7866	0.0034	-213.4	3.4	1930	40
75934	218-MC-001	SMa-218	1	0	0.7008	0.0033	-299.2	3.3	2860	40
75935	218-MC-002	SMa-218	2	0	0.6896	0.0033	-310.4	3.3	2990	40
75936	218-MC-003	SMa-218	3	0	0.6932	0.0027	-306.8	2.7	2940	40
80947	218-MC-004	SMa-218	4	0.3	0.6929	0.0029	-307.1	2.9	2945	35
80948	218-MC-005	SMa-218	5	1	0.6872	0.0025	-312.8	2.5	3015	30
80949	218-MC-006	SMa-218	6	1	0.6921	0.003	-307.9	3	2955	40
90037	222-MC-001	SMa-222	1	1	0.7284	0.0029	-271.6	2.9	2545	35
90038	222-MC-002	SMa-222	2	1	0.7213	0.0029	-278.7	2.9	2625	35
90039	222-MC-003	SMa-222	3	1	0.7219	0.0029	-278.1	2.9	2615	35
90833	222-MC-004	SMa-222	4	0	0.7274	0.0032	-272.6	3.2	2555	40
90834	222-MC-005	SMa-222	5	0	0.7207	0.0035	-279.3	3.5	2630	40
98186	007-MC-001	SCr-7	1	0	0.4945	0.0020	-505.5	2.0	5655	35
98187	007-MC-002	SCr-7	2	0	0.5355	0.0026	-464.5	2.6	5015	40
98188	007-MC-003	SCr-7	3	0	0.5559	0.0022	-444.1	2.2	4715	35
149279	SCR-7 Lower A	SCr-7	4	0.5	0.5101	0.0024	-489.9	2.4	5405	40

Table 2.3. Original data for ^{14}C meausurements. Carbon $\delta^{13}C$ values are the assumed values (Stuiver and Polach, 1977) when given without decimal places. Values measured for the material itself are given with a single decimal place. The quoted age is in radiocarbon years using the Libby half-life of 5568 years and following the conventions of Stuiver and Polach (1977). Radiocarbon concentration is given as fraction modern, $D^{14}C$, and conventional radiocarbon age. Sample preparation backgrounds have been subtracted, based on measurements of samples of ^{14}C-free calcite. Backgrounds were scaled relative to sample size.

Site	Shell	Age range (cal BP, 2σ range)	N	Average $\delta^{18}O_{calcite}$ (‰ VPDB)	Average $\delta^{13}C$ (‰)	Average* Mg/Ca (mmol/mol)	Average Sr/Ca (mmol/mol)	Average Temp. (°C)	Average $\delta^{18}O_{seawater}$ (‰ VSMOW)
SMa-19	A	300-532	63	0.99 ± 0.38	0.41 ± 0.28	2.7 ± 0.5	0.92 ± 0.10	10.3 ± 1.7	-0.9 ± 3.1
	C		44	0.38 ± 0.31	0.31 ± 0.35	2.1 ± 0.4	0.80 ± 0.04	8.0 ± 2.0	-1.6 ± 3.1
SMa-17	A	938-1169	53	1.38 ± 0.45	0.22 ± 0.38	2.4 ± 0.4	0.93 ± 0.17	8.9 ± 1.6	-0.8 ± 3.3
	B		41	1.27 ± 0.23	0.09 ± 0.25	1.9 ± 0.3	0.84 ± 0.04	7.4 ± 1.0	-1.3 ± 3.0
SMa-18	A	1080-1386	42	1.05 ± 0.43	0.37 ± 0.40	2.2 ± 0.7	0.91 ± 0.08	8.4 ± 2.4	-1.3 ± 3.4
	B		62	0.69 ± 0.34	0.33 ± 0.33	3.2 ± 0.7	0.87 ± 0.04	12.1 ± 2.6	-0.7 ± 3.5
	C		104	1.05 ± 0.28	0.17 ± 0.22	2.2 ± 0.4	0.73 ± 0.05	8.3 ± 1.3	-1.3 ± 3.1
SMa-222	A	1950-2301	34	1.20 ± 0.23	0.86 ± 0.31	2.3 ± 0.4	0.81 ± 0.04	8.6 ± 1.3	-1.1 ± 3.0
	B		30	1.23 ± 0.32	0.33 ± 0.22	2.6 ± 0.9	0.80 ± 0.05	9.7 ± 3.1	0.7 ± 3.3
SMa-218	A	2055-2355	50	1.20 ± 0.62	0.38 ± 0.50	2.7 ± 0.5	0.94 ± 0.10	10.3 ± 1.7	-0.6 ± 3.2
	B		42	1.52 ± 0.28	0.67 ± 0.35	2.0 ± 0.4	0.89 ± 0.04	7.8 ± 1.3	-1.0 ± 3.0
	C		46	1.24 ± 0.41	0.15 ± 0.49	2.9 ± 0.6	0.85 ± 0.10	10.8 ± 2.1	-0.5 ± 3.2
	D		74	1.50 ± 0.32	0.73 ± 0.29	2.5 ± 0.6	0.88 ± 0.05	9.4 ± 2.0	-0.7 ± 3.2
SCr-7 Up	A	3200-3676	56	1.10 ± 0.34	0.62 ± 0.39	2.4 ± 0.4	0.89 ± 0.04	8.9 ± 1.4	-1.1 ± 3.2
	B		62	1.14 ± 0.30	0.69 ± 0.40	2.6 ± 0.6	N/A	9.8 ± 2.3	-0.9 ± 3.2
SCr-7 Lo	A	5426-5621	40	1.29 ± 0.55	0.52 ± 0.43	4.1 ± 0.5	0.87 ± 0.06	15.1 ± 2.0	0.5 ± 3.4
	B – L	4525-5889	19	0.24 ± 0.36	1.24 ± 0.30	3.5 ± 0.9	1.0 ± 0.10	13.0 ± 3.1	-0.0 ± 3.7
	M - P	5425-5902	12	NA	NA	2.0 ± 0.3	0.91 ± 0.08	7.7 ± 1.0	NA

Table 2.4. Summary of midden shell geochemistry. Error value (±) represents standard deviation (1σ) within a specimen for measured $\delta^{13}C$, $\delta^{18}O$, Mg/Ca, and Sr/Ca. Error includes the propagation of error for the calculations of temperature and the $\delta^{18}O$ value of seawater, contributing to larger uncertainties. The age range of SCr-7 Lower is a shell-based age estimate since no charcoal was present.

3. EVALUATING DRIVERS OF PLEISTOCENE EASTERN TROPICAL PACIFIC SEA-SURFACE TEMPERATURE

Abstract

A variety of forcing mechanisms (such as insolation changes, ice sheet thickness, extent, or albedo, or greenhouse gas radiation) have been proposed as controls for the long-term eastern tropical Pacific sea-surface temperature (SST). However, the precise role each mechanism plays in controlling tropical SST is not fully known for glacial-interglacial cycles. Each hypothesis is evaluated by the direct comparison of variations in past tropical SST with variations in each forcing over long timescales. In the last decade, several long SST records have been generated which span much of the Pleistocene, here we compile new and existing data from a long record of SST on the margin of the modern cold tongue to reveal the spatial development of the cold-tongue SST pattern over the Pleistocene. We also use this high-resolution alkenone-based SST record from Ocean Drilling Program (ODP) Site 1239 between the northeastern edge of the eastern equatorial Pacific cold tongue and the Panama Basin warm pool, along with statistical coherence testing, temperature gradient analysis, and phase-lag relationships, to test previously proposed mechanisms that control long-term tropical SST change. We suggest that neither direct local insolation forcing nor ice-sheet effects are a primary control of SST in the eastern Pacific cold tongue

region in the past 1.5 Myr since both lag primary SST changes. Rather, within statistical uncertainties, high-latitude solar forcing leads or is in phase with eastern equatorial Pacific SST during the period 1500-0 kya, while radiative atmospheric greenhouse gas concentrations (where available) are closely associated with cold tongue SST. Our results verify that small changes in high-latitude insolation may have initiated the first SST changes, which were then further amplified by changing atmospheric greenhouse gas concentrations.

1. Introduction

Eastern equatorial Pacific (EEP) sea-surface temperature (SST) influences equatorial Pacific oceanic and atmospheric circulation through the zonal pressure gradient (e.g. Cane and Clement, 1999; Lawrence et al., 2006; Sarmiento et al., 2004). However, multiple mechanisms have been proposed to influence long-term eastern Pacific SST at various timescales: high and low latitude insolation changes (e.g. Clement et al., 1999; Martínez-Garcia et al., 2010; Koutavas et al., 2006; Timmermann et al., 2007; Hays et al., 1976; Philander and Fedorov, 2003), dynamics related to ice sheets (e.g. Imbrie et al., 1992), and pCO_2 changes (e.g. Lea et al., 2000). Some mechanisms even contain common elements (e.g. the role of ice sheets or signal transfer through the ventilated thermocline), though it is possible in most cases to identify the source of the forcing using the coherence and phase relationships that are revealed by time-series analysis. To perform such spectral analysis, a temporal resolution sufficient to

resolve orbital cycles is needed. Researchers are currently limited in that only a few such high-resolution geochemical SST records exist in this region that extend from the present to beyond the last few glacial cycles to test such hypotheses (e.g. Lawrence et al., 2006; Medina-Elizalde and Lea, 2005). In this study, a new alkenone-based SST record from the Ecuador margin ODP Site 1239 (0°40.32′S, 82°4.86′W; Fig. 3.1) was generated from 0 to 0.73 Ma, and was combined with previously published data from 0 to 0.5 Ma (Rincón-Martínez et al., 2010) and from 0.5 to 1.5 Ma (Etourneau et al., 2010) to create a record with higher temporal resolution than any individual record. This new record of SST change over the past 1.5 Ma is compared to other published records from other localities in the tropical SST to test proposed mechanisms for the control of Pleistocene SST patterns in the tropical Pacific.

Throughout the Pleistocene, high-latitude glacial temperatures decline, glacial cycles become more intense, resulting in thicker ice sheets at the mid-Pleistocene transition (MPT), ~1 – 0.8 Myr (McClymont et al., 2008; Clark and Pollard, 1998), possibly as a result of crossing Northern Hemisphere ice-related thresholds (Clark et al., 2006; Gildor and Tziperman, 2000; Gildor and Tziperman, 2001). By displacing atmospheric patterns equatorward, larger ice sheets also shifted latitudinal temperature fronts (Chiang and Bitz, 2005) and narrowed the band of tropical temperatures. In addition to ice volume modifications, tropical temperatures may also have been influenced by changes in the carbon cycle and deep ocean ventilation

(e.g. Kemp et al., 2010; Toggweiler, 1999), by direct insolation forcing, or by a complex interplay of insolation cycles (Huybers, 2009; Imbrie et al., 2011). Below we first outline in more detail the proposed mechanisms for eastern tropical Pacific SST change, then present the results of a new compiled paleo-temperature record from ODP Site 1239, and finally compare coherence and phasing of the temperature records with the forcing signals. Pleistocene SST patterns suggest that the eastern tropical cold tongue developed and became more geographically focused during the MPT and that the orbital variability in tropical SST is fundamentally forced by insolation changes at precession periodicity and ice-sheet changes at obliquity periodicity, along with a significant feedback response to radiative greenhouse gas forcing.

1.1 Direct local solar forcing for the eastern equatorial Pacific cold tongue

Changes in cold tongue SST patterns could have been the result of direct equatorial insolation forcing of the cold tongue (Clement et al., 1999; Clement et al., 2000; Koutavas et al., 2002) which varies primarily at precession (23-ky) frequency and modifies seasonal insolation changes. In winter and spring the Intertropical Convergence Zone (ITCZ) is roughly along the equator in both the eastern and western Pacific (Fig. 3.1); hence, equatorial insolation changes do not modify the east-west temperature gradient (Clement et al., 1999). However, in the late summer and early fall, the modern ITCZ shifts to a position north of the equator in the eastern

Pacific but remains roughly along the equator in the western Pacific warm pool. The northerly October position of the EEP ITCZ and associated divergent winds over the cold tongue are thought to allow periods of increased insolation to strengthen the east-west SST gradient by differential warming of the western Pacific where deep atmospheric convection already occurs (Mitchell and Wallace, 1992). Stronger Walker circulation in turn leads to intensified upwelling in the eastern Pacific along with even greater zonal SST asymmetry in equatorial Pacific as warm atmospheric convergence shifts farther north in the eastern Pacific. Thus, when equatorial summer-fall insolation was greater, temperatures in the cold tongue are expected to have been cooler (Koutavas et al., 2002; Clement et al., 1999).

Closely related to equatorial insolation, insolation just north of the equator (5-15°N) may also modulate eastern Pacific warm pool temperature and indirectly alter SST at Site 1239 through the seasonal southward Panama Current (Fiedler and Talley, 2006). A stronger warm Panama current could impinge on the sharp equatorial temperature front (EF) at the northern margin of the cold tongue and warm SST at Site 1239. For these reasons, the intensity of warm-season off-equatorial tropical warm pool insolation (June at 5-15°N) could potentially be positively related to EEP temperature. Using only the paleoceanographic records available, we may not be able to distinguish between these two factors (stronger Panama current vs. southward-translated ITCZ) though each is likely to reinforce the other.

1.2 High-Latitude Solar Forcing

High-latitude insolation variability is perhaps the most widely acknowledged mechanism for initiating global climate changes; as such, variations in eastern tropical SST may be related to the strong influence of 41-kyr obliquity and 23-19 kyr precession cycles at subpolar latitudes (e.g. Philander and Fedorov, 2003; Martínez-Garcia et al., 2010). The sequence of events that leads to this outcome is thought to be as follows: as the north Pacific surface ocean loses heat to the cold air masses derived from the Asian continent, surface-water cools, subducts, and flows equatorward within the subtropical thermocline. This mode water is translated equatorward and reaches the surface again in the eastern Pacific where it is heated by the sun in the tropics. The heat loss at mid-latitudes is thus balanced by heat gain at low latitudes on timescales of tens to hundreds of years (Philander and Fedorov, 2003).

Long-term changes in the ventilated thermocline circulation system may be sensitive to high-latitude insolation forcing. Earth's obliquity and precession alter high-latitude insolation; however, only changes in the angle of Earth's tilt (obliquity) modify the annual average latitudinal distribution of insolation, whereas precession affects the seasonal cycle. As the degree of Earth's tilt axis increases (from ~22^{o} to ~24^{o}), the latitudinal surface heating and density gradients in subpolar regions changed (Philander and Fedorov, 2003; Rubincam, 1994). If there is a connection

between obliquity forced insolation cycles, thermocline conditions, and low latitude SST, then the high-latitude (65°N) insolation curve and tropical SST records are expected to be coherent and in phase (within the resolution of tropical records) in the obliquity band. High-latitude insolation should also be coherent with the gradient between the eastern and western tropical Pacific since propagated changes in thermocline conditions would be expected to mainly influence SSTs in the eastern Pacific where the thermocline is shallow.

1.3 Remote Ice-Sheet Forcing

Ice-sheet size drives internal feedbacks that also may influence tropical Pacific SST (Ruddiman, 2006; Chiang and Bitz, 2005; Chiang, 2003) by influencing dust fluxes, albedo, sea level, atmospheric convection, and/or NADW formation. Early Pleistocene ice sheets were notably smaller and glacial-interglacial cycles varied at approximately 41-ky periodicity in contrast to the larger-amplitude late Pleistocene ice ages that varied at the 100-ky frequency; this shift in periodicity at 1.0 – 0.8 Ma marks the MPT (e.g. Clark and Pollard, 1998). However, ice sheets are not independent from other mechanisms of long-term climate change since high-latitude solar forcing and radiative greenhouse gases both have the potential to drive changes in ice sheet thickness and extent. Coherency, amplitude, and phase lag relationships allow us to test whether ice sheets affect tropical temperatures. Furthermore, the larger northern-hemisphere late Pleistocene ice sheets may have displaced the mean

latitude of atmospheric bands—including the ITCZ and equatorial front—south of the present position (Koutavas and Lynch-Stieglitz, 2004; Rincón-Martínez et al., 2010; Timmermann et al., 2007; Chiang and Bitz, 2005). If ice sheets do play a role in determining tropical SST, then SST and benthic $\delta^{18}O$ records, as an approximation of ice volume, should be coherent and in phase within the bands in which benthic $\delta^{18}O$ varies.

1.4 Greenhouse Gas Forcing

Tropical SST changes over the past 1500 kyr may also be related to radiative forcing due to atmospheric greenhouse gas concentrations, primarily the atmospheric carbon dioxide and methane concentrations (Lea, 2004; Medina-Elizalde and Lea, 2005; Lea et al., 2006) which account for some portion (one-third to two-thirds) of the glacial-interglacial signal (e.g. Weaver et al., 1998; Schneider von Deimling et al., 2006). Lines of evidence for this idea include the comparisons of tropical SST records that tend to co-vary (Herbert et al., 2010) with the Antarctic record of atmospheric CO_2 and CH_4 concentrations at 100-kyr and 41-kyr periodicities. One way to validate this hypothesis is to evaluate records from parts of the tropics with different regional dynamics for simultaneous surface temperatures changes (Medina-Elizalde and Lea, 2005). Another method (which is not mutually exclusive) to test whether there is a possible causal relationship between tropical SST and atmospheric CO_2 changes is to

apply cross-spectral analyses to examine whether records of those changes are coherent and in-phase.

The objective of this work is to evaluate the various hypotheses that explain tropical Pacific SST variations in the Pleistocene using cross-spectral and frequency analysis techniques of environmental (SST, GHG's, and insolation) records at orbital-scale (< ~3kya) resolution. Long continuous records of tropical SST are essential for this approach; one of which currently exists in the heart of the EEP cold tongue at ODP Site 846 (Liu and Herbert, 2004; Lawrence et al., 2006) and another in the western Pacific warm pool at ODP Site 806 (Medina-Elizalde and Lea, 2005). However, to better constrain the development and variations in the EEP cold tongue, another site is needed. In this study, we generate new SST at EEP ODP Site 1239, which combined with published data from this site (Etourneau et al., 2010; Rincón-Martínez et al., 2010), provides a record of changes in the northern margin of the cold tongue, which may be sensitive to eastern Pacific warm pool changes. Thus, we are able to evaluate controls for eastern Pacific SST and examine EF and ITCZ latitudinal changes over the past 1.5 million years.

2. Methods

2.1 Alkenone paleothermometry

At ODP Site 1239 we use samples that integrate 3 cm of sediment and are taken every 8 cm along the core splice (Shipboard Scientific Party, 2003) from 0.07 to 27.00 mcd. Using ~0.5 grams of freeze-dried sediment, lipid ketones were extracted under pressurized dichloromethane in an accelerated solvent extractor, and alkenones were quantified using an HP gas chromatograph at UCSC with an initial oven temperature of 90°C, heating by 25°C/min until 250°C, by 1°C/min until 303°C, and by 20°C/min to 330°C which was held for 30 minutes (Dekens et al., 2007). Temperatures are determined from the alkenone unsaturation index ($C_{37:2}/(C_{37:2}+C_{37:3})$) using the calibration equation of Müller et al. (1998) since cold-tongue surface waters are unlikely to encounter light or nutrient limitation. Sample precision (1-σ) is based on replicates of a liquid consistency standard in each run and sediment standard extracted alongside each run. Long-term precision of the unsaturation index is ±0.014 (±0.43°C) and ±0.009 (±0.26°C) for the liquid consistency and sediment standards, respectively.

We integrate our new data with published alkenone-based SST from ODP Site 1239 (Etourneau et al., 2010; Rincón-Martínez et al., 2010) using the common depth scale to create a continuous high-resolution SST record for the period of 0-1500 kya with a higher average sampling resolution and broader temporal window than any previous record from this site (Fig. 3.2). Replicate (identical interval) alkenone samples

analyzed at UCSC and in Kiel, Germany, show no inter-laboratory offset in the unsaturation index.

2.2 Site 1239 Timescale

The Site 1239 oxygen isotope age model is based on the benthic foraminifers *Cibicidoides wuellerstorfi* and *Uvigerina peregrina*. For this study the benthic $\delta^{18}O$ and $\delta^{13}C$ records have an average sampling interval of ~2 ky and were completed at the College of Oceanic and Atmospheric Stable Isotope Laboratory of Oregon State University. Foraminifers were picked from the >150-μm size fraction and then run using a Finnigan/MAT 251 gas-source mass spectrometer with an automated carbonate device. Precision within a species for $\delta^{18}O$ is 0.05‰ and for $\delta^{13}C$ is 0.03‰. Using the published depth scale, additional benthic isotopic measurements were incorporated into this benthic stratigraphy for the period 0-500 kya (Rincón-Martínez et al., 2010). The age model for the remainder of the core is anchored to a visual alignment of benthic foraminiferal $\delta^{18}O$ record with the robust global benthic LR04 $\delta^{18}O$ stack (Lisiecki and Raymo, 2005). Both glacial and interglacial peaks and troughs in the two curves were matched, correcting any individual segment of the original calcareous nannoplankton occurrence age model (Shipboard Scientific Party, 2003) by less than 5%. This common age model was then applied to the temperature record from 0-500 kya (Rincón-Martínez et al., 2010), from 0-730 kya (this study), and from 500-1500 kya (Etourneau et al., 2010) to build the compiled record. All changes in

ages assigned to the published temperatures from Site 1239 are small (< 3 ky). The compiled temperature record (0-1500 kya) has an average resolution of 1.1 ky for the late Pleistocene (0-800 kya) and 3.5 ky for the early Pleistocene.

2.3 Other records

We compare the Site 1239 SST record to previously published records of tropical SST from other locations, calculated changes in solar radiation, and variations in greenhouse gas concentrations. We use the published timescale for SST records at each site, which are primarily based on benthic $\delta^{18}O$ records from each core with the notable exception of Site 806 in the western Pacific. The Site 806 age model is only based on alignment of the benthic $\delta^{18}O$ record to 650 kya (Bickert et al., 1993); prior to 650 kya the age model is based on alignment of *G. ruber* $\delta^{18}O$ with Site 677 benthic $\delta^{18}O$ (Medina-Elizalde and Lea, 2005). Numerical solutions for insolation quantities on Earth are calculated from orbital parameters (Laskar et al., 2004) based on equations of motion of the solar system with uncertainty of about 0.1% over this timescale.

Carbon dioxide has previously been determined for the past 800 kya from air bubbles trapped within ice layers in Antarctic ice sheets, as compiled in Lüthi et al. (2008)and Loulergue et al. (2008), respectively. The Dome C greenhouse gas records use the EDC3 timescale. Errors in the ice core timescales become larger as samples get older

and ice layers smear out near the base of the glacier. Errors range from ±1 kyr for the past 100 kyr to as large as ±6 kyr at 800 kya (Parrenin et al., 2007).

2.4 Timeseries Analysis

To test for correlation of SST records, insolation, or greenhouse gas concentrations, we use cross-spectral analysis, coherency, and phase lag tests. Rather than to infer causality, the main purpose of this exercise is to eliminate hypotheses that are not supported by the available data. Coherency limits are set at a conservative lower bound of 80%; *i.e.*, two records are said to be coherent at a given frequency if the cross-spectral analysis reveals significant coherency greater than 80%. Crosspec and Spectral (Arand) and Analyseries software was used to determine first-order coherency and phasing relationships among paleoclimate timeseries (Palliard et al., 1996; Howell et al., 2006). In order to perform cross-spectral analyses, all records were first resampled at even spacing using piecewise linear integration interpolation (Palliard et al., 1996) at slightly higher resolution than the original records. We found that the difference between methods for sampling the timeseries' (*i.e.* cubic spline, staircase, simple interpolation, or lower resampling resolution) made very little difference in the final result, since most data is roughly evenly-spaced at high resolution before application of the new sampling protocol.

In most cases, phase analysis incorporates uncertainties associated with the 80% confidence interval of the Blackman-Tukey method but neglects the uncertainty associated with the LR04 chronology itself since the SST and benthic $\delta^{18}O$ records have been tied to the LR04 record explicitly. One exception is the phase comparison with pCO_2 reconstructions from ice cores that use the EDC3 chronology, which varies from the LR04 chronology by up to 6 kyr; comparisons with CO_2 forcing must have correspondingly large age uncertainties for much of the Pleistocene. The other exception is the phase comparison with insolation records, though the LR04 chronology is derived from tuning the $\delta^{18}O$ stack to an ice model that is based on insolation changes (Lisiecki and Raymo, 2005).

3. Results

The Site 1239 SST record shows clearly defined glacial-interglacial cycles (Fig. 3.2), shorter glacial cycles before the MPT and longer, more intense glacial cycles in the late Pleistocene. Periodicity in the Site 1239 SST record is consistent with the alkenone-based temperature record from Site 846 in the center of the cold tongue (Liu and Herbert, 2004). Both records show secular cooling of ~2 C° between 1500 – 800 kya with a constant offset between records of ~1.8 C°. At ~850 kya, the cooling trend at Sites 846 and 1239 halts and SST at Site 846 maintains a glacial-interglacial average of ~22.2°C. Conversely, at ~850 kya SST at Site 1239 begin to climb to ~26°C at ~700 ka and then slowly cool by ~1.3 C° to the present. The SST offset between

Sites 1239 and 849 correspondingly decreased since ~700 kya from almost 4 C° to a modern offset between the records of ~2 C°. Though the gradient between the two sites has changed over the Pleistocene, the amplitude of variability (1-sigma standard deviation) for both records is nearly identical at ~1.2 C° for the period of 1500 – 0 kya.

The Site 1239 benthic $\delta^{18}O$ record (Fig. 3.2), once aligned to a benthic $\delta^{18}O$ stack (Lisiecki and Raymo, 2005) to establish the chronology, lags or is in phase with the benthic Site 1239 SST record at all orbital frequencies. This is the only analysis of phase that does not depend upon which age model is used since alkenone and benthic $\delta^{18}O$ analyses used splits of the same samples.

Variance in tropical SST records shifts from obliquity to eccentricity periodicity near the MPT (Table I). Cross-spectral analysis between the Site 1239 temperature record and benthic $\delta^{18}O$ and CO_2 concentrations shows that eastern Pacific surface temperature change is coherent at all spectral frequencies with these two other signals throughout the time period where data is available (Table I). However, at minimum, both coherency and appropriate phasing are necessary to infer causality between forcing mechanisms and tropical Pacific SST, and to evaluate the prevalent theories of orbital-scale tropical SST change in the Pleistocene.

4. Discussion

In this section we first discuss the long-term shift in tropical Pacific SST patterns associated with the MPT. We suggest the long-term gradient between Sites 1239 and 846 became greater at the MPT, signaling a further development of the modern cold tongue. In sections 4.2 – 4.5, each potential mechanism for control of orbital variability in eastern tropical SST is evaluated for plausible causality both prior to and following the MPT. In each section, we consider the potential forcing mechanisms separately in the pre-MPT (1500-800 kya, '41-ky world') and the late Pleistocene (800-0 kya, '100-kyr world'), since ice age cycles are dominated by different frequencies (and thus possibly different mechanisms) in the two intervals. The division at ~800 kya also splits the records into semi-equal portions, each long enough to perform cross-spectral analysis. We suggest that in both time periods, tropical SST variability cannot be explained using proposed mechanisms in which equatorial insolation or the remote response to ice sheet size play dominant roles. Rather, orbital-scale SST variability responds to high-latitude summer insolation changes and greenhouse gas forcing.

4.1 Mid-Pleistocene transition

The shift in marine $\delta^{18}O$ records from primarily 41-kyr cycles to 100-kyr cycles that marks the MPT is enigmatic since the power of orbital insolation cycles does not change at this time (e.g. Pisias and Moore, 1981; Elkibbi and Rial, 2001). The lack of an obvious insolation-related mechanism for this shift forces us to reexamine changes

in ice sheets (Imbrie et al., 1993; Clark and Pollard, 1998) and/or oceanic carbon sequestration and periodic release (Toggweiler et al., 2006; Kemp et al., 2010) as possible explanations. Tropical Pacific temperature records can help to put the roles of ice-sheets and greenhouse gas forcing at the MPT into a global context.

Prior to ~800 kya, equatorial cold tongue temperatures progressively cooled in both glacial and interglacial intervals (at both Sites 846 and 1239); a cooling which amplified the zonal tropical Pacific temperature gradient and intensified Walker circulation (de Garidel-Thoron et al., 2005). EEP SST cooling may have been due to extratropical cooling, from 1500-800 kya (McClymont et al., 2008; Etourneau et al., 2010; Martínez-Garcia et al., 2010), that was transferred to the tropics through the thermocline (Philander and Fedorov, 2003; Liu and Herbert, 2004; Lawrence et al., 2006). A gradually cooling climate may also have changed the basal conditions below continental ice sheets that may act as a long-term modifier of ice sheet height and/or extent that alter the climate system response to insolation forcing at the MPT (e.g. Clark and Pollard, 1998). By sufficiently eroding the subglacial low-friction sediment bed (Clark et al., 2006; Roy et al., 2004), or by increasing the precipitation available to build larger ice sheets (McClymont et al., 2008; Tziperman and Gildor, 2003) glacial ice volume dramatically increased at the MPT. Larger ice sheets could have in turn shifted the position of the ITCZ to the south (Chiang and Bitz, 2005).

The SST record from ODP Site 1239 offers unique insight into the nature of the equatorial front and the average position of the ITCZ in response to these changes at the MPT. The SST at both Site 1239, at the northern margin of the cold tongue, and Site 846, in the cold tongue, cools prior to the MPT (Fig. 3.2). During the MPT between ~850 and ~650 kya, SST during both glacials and interglacials increases at Site 1239 even as high-latitude glacial temperatures cool (Etourneau et al., 2009; McClymont et al., 2008), cold-tongue temperatures cool, glacial pCO_2 concentrations are decrease (Hönisch et al., 2009), and ice volume increases. This transition to warmer, rather than colder, glacial and interglacial temperatures and a larger EF gradient at the mid-Pleistocene could reflect a southern shift of the ITCZ (Chiang and Bitz, 2005) and a more clearly defined equatorial cold tongue. An average southward shift of the ITCZ has been estimated to carry net water vapor transport out of the northern hemisphere (Vellinga and Wu, 2004; Chiang and Bitz, 2005) and may decrease the amount of water vapor transported across the Isthmus of Panama (Pahnke et al., 2007; Schmidt and Spero, 2011; Xie et al., 2008) which could, in turn, potentially alter Atlantic overturning circulation.

The Southern Ocean offers a complimentary mechanism by which deep-ocean carbon exchange may have amplified glacial-interglacial changes after the MPT via an increase in the extent of Southern Ocean stratification and an equatorward shift in the Antarctic Circumpolar Front during colder intervals (Kemp et al., 2010; Toggweiler et

al., 2006; Watson and Naveira Garabato, 2006; Schmieder et al., 2000). Today, southern hemisphere westerlies along the Antarctic Polar Front (APF) account for much of the mixing of the Southern Ocean and equilibrate deep ocean carbon with the atmospheric reservoir. During glacial maxima, the southern westerlies shifted equatorward (Kemp et al., 2010) stratifying the Southern Ocean and leading to carbon sequestration in the deep ocean and declining atmospheric pCO_2 (Toggweiler et al., 2006; Toggweiler, 2008). During the MPT the APF may have shifted northward on longer timescales from ~940 ka to ~420 ka, and increased ocean carbon storage (Kemp et al., 2010) which led to corrosive deep and intermediate waters (e.g. Lisiecki, 2010), lower atmospheric pCO_2 (Hönisch et al., 2009), and colder high-latitude temperatures. Atmospheric pCO_2 may also contribute to the change in cyclicity at the MPT; in the early Pleistocene, CO_2 concentrations seem to suggest a lower amplitude of greenhouse gas variability (Hönisch et al., 2009), a record that is consistent with, though not yet evidence for, less-intense 41-kyr cycles in greenhouse gas records in the early Pleistocene.

We next present the specific mechanisms, including tropical insolation, high-latitude, and greenhouse gas forcing, that are proposed to have modified eastern Pacific SST on orbital timescales.

4.2 Direct local solar forcing for the cold tongue

Precession of the equinoxes around Earth's eccentric orbit causes autumn solar radiation to vary by as much as 60 W/m^2 with a periodicity of 23-ky. Numerical models suggest that increased October equatorial insolation modifies zonal equatorial temperatures asymmetrically (e.g. Clement et al., 1999). In the warm west Pacific the trade winds converge at the equator, whereas in the east Pacific, the ITCZ is north of the equator (Fig. 3.1) due to interhemispheric differences in landmass geometry and distribution (Philander et al., 1996). The northern position of the ITCZ creates divergent equatorial winds, which accommodate and drive cool-water upwelling. Periods of increased equatorial insolation near the autumnal equinox are supposed to then strengthen the zonal equatorial SST asymmetry, reinforce Walker circulation and lead to cooler cold-tongue SST over long timescales (Clement et al., 1999; Koutavas et al., 2002).

However, data from the cold tongue seems to instead suggest warmer, not colder, cold-tongue SST when September-October insolation is at a maximum. Though the early Pleistocene SST record at Site 1239 is not coherent with October equatorial insolation at precession frequencies (Fig. 3.3A), at Site 846, in the cold tongue, October equatorial insolation is coherent and in phase with the SST record at the 23-ky periodicity (Fig. 3.3B), rather than inversely correlated as predicted (Clement et al., 1999; Koutavas et al., 2002). In the late Pleistocene, the results of spectral analysis are similar; the SST records at both Sites 1239 and 846 are coherent and in phase (or

nearly so) with October insolation at 23- and 19-kyr periodicity (Fig. 3.3C-D). These results suggest that periods of increased local cold-season (autumn) insolation could simply warm cold-tongue SST through direct radiative heating.

The SST record at Site 806 (western Pacific warm pool) is in phase with late summer insolation changes at precession frequency and leads the long-term record of October insolation by ~3±5 kyr at precession (not shown). Further, October equatorial insolation is not in phase with the zonal SST gradient as represented by either $\Delta SST_{806-846}$, or $\Delta SST_{806-1239}$. These results additionally confirm that equatorial insolation is not anomalously heating the western equatorial warm pool more than the cooler upwelling regions.

Tropical solar heating has also been proposed to modify the EF temperature gradient {Koutavas:2002wy}. During periods of maximum autumn insolation cold tongue SSTs may have been lower, and the eastern warm pool may have been warmer, making the EF more intense {Koutavas:2002wy}{Koutavas:2003hp}. The SST gradient between the alkenone-based SST records from Site 1239 and Site 846 ($\Delta SST_{1239-846}$) is one way to monitor changes in this front. When the SST gradient is large, the front may be sharp, and when the gradient is small, the EF may be more diffuse. When October equatorial insolation and $\Delta SST_{1239-846}$ are compared using cross-spectral analysis, $\Delta SST_{1239-846}$ is out of phase with insolation at 23-ky periodicity; confirming the

previous result that increased cold-season direct insolation warms the cold tongue, but does not seem to affect the $\Delta SST_{1239\text{-}846}$ gradient.

In the late Pleistocene, the $\Delta SST_{1239\text{-}846}$ gradient is coherent with October equatorial insolation at 23-ky periodicity, yet leads insolation by 6±1 kyr, suggesting that the ITCZ and equatorial front intensity weakens in cold-season months (September-October) at the 23-ky insolation frequency. As a further check, the SST gradient between TR163-19 (eastern Pacific warm pool, Fig. 3.1) and Site 846 also weakens alongside increased October equatorial insolation at precession. These results imply that solar heating of the warm pool is not responsible for increased upwelling and cooling in the cold tongue.

To explore whether insolation heating of the eastern Pacific warm pool, just north of the equator at 5, 10, or 15°N, controls SST at 1239 or the strength of the equatorial front, we repeated each of the above tests using warm-season insolation for the eastern Pacific warm pool, but find no additional relationship to report for either before or after the MPT. Since precession cyclicity in insolation is virtually identical in power and phase between the equator and 15°N for a given season (Fig. 3.4), each test produced similar results as equatorial insolation curves, though the phase shifted ~90° (~5 kyr insolation lead ahead of Site 846 SST) due to the choice of insolation curves from boreal summer (June 21) rather than autumn (October 1).

In sum, the late Pleistocene eastern Pacific SST records are coherent with insolation at precession frequency, but SST changes are not caused by asymmetric heating during periods of increased October equatorial insolation as suggested by modeling studies (Clement et al., 1999). Rather, the cold tongue temperature may be directly responding to precessional changes in summer-fall insolation. At Sites 806, 846, and 1239 (where coherent), tropical SST is in phase with summer-fall insolation within uncertainties. Although seasonal changes in cold-tongue SST must be affected in part by cold-water advection from the Humbolt Current and South American margin, on precession timescales changes in summer-fall solar heating seem to directly influence cold tongue SST.

4.3 High-latitude Orbital Insolation Forcing

Tropical SST records, especially those in or near upwelling regions, may also respond to extra-tropical insolation changes (Philander and Fedorov, 2003; Liu and Herbert, 2004) as mode water subducts at subtropical latitudes affecting thermocline conditions which, in turn, influence SST in the EEP where thermocline waters upwell (e.g. Philander and Fedorov, 2003). One test of such a connection between equatorial SST and extratropical insolation would be a coherent and in phase relationships between these records at the prevailing orbital bands (e.g. Hays et al., 1976; Liu and Herbert, 2004; Lee and Poulsen, 2005); summer insolation and annual insolation vary

in the precession and obliquity bands, respectively. Prior to the MPT, extratropical summer insolation forcing is coherent and in phase on obliquity timescales only with Site 846 SST (Fig. 3.5A) as previously suggested (Liu and Herbert, 2004; Lawrence et al., 2006), but leads variations in the Site 1239 SST record (even considering age-model uncertainty) (Fig. 3.5A; phase: 4±3 kyr). This result suggests that extratropical insolation may not have played a direct role in modifying Site 1239 SST since it is difficult to account for such a lag in the climate system. After the MPT, the same relationships between records exist in the obliquity band; summer insolation is in phase with Site 846 SST (phase: 2.5±3 ky) and again leads Site 1239 SST (phase: 6.5±2 kyr) (Fig. 3.5B). Extratropical insolation precession cycles could also drive tropical SST prior to the MPT; at 19-kyr periodicity, high-latitude summer insolation is in phase with cold tongue and western warm pool SST. These results validate the idea that prior to the MPT, in the '41-kyr world', extra-tropical insolation changes could have influenced equatorial SST at periodicities less than 100-ky, via oceanographic or atmospheric circulation.

4.4 Remote ice-sheet forcing

The Pleistocene ice sheets could have had a remote influence on tropical temperatures by shifting the average position of the ITCZ and by deflecting atmospheric patterns (e.g. Deser and Wallace, 2000; Chiang and Bitz, 2005; Ruddiman, 2006) on orbital timescales. If the post-MPT increased glacial ice volume displaced atmospheric bands

away from the Laurentide ice sheet and caused linear tropical temperature variations, then ice sheet and benthic $\delta^{18}O$ changes should be coherent with SST in the bands within which $\delta^{18}O$ varies. Post-MPT phase lag relationships indeed support a plausible linear relationship with tropical SST (both Site 1239 and 846) at the 100-kyr frequency (Fig. 3.6), lending credence to the theory that on long Pleistocene timescales ice sheets began to deflect atmospheric currents to the south (Broecker and Denton, 2002) and could change tropical SST at the 100-ky periodicity in the late Pleistocene.

Throughout the Pleistocene, at obliquity frequency, Site 1239 SST is in phase with minimum $\delta^{18}O$ in the global benthic stack, though Site 846 SST is not. This fact raises the possibility that at obliquity periodicity, Site 1239 SST is mainly controlled by the position of atmospheric bands and/or ice sheets whereas Site 846 SST may be primarily controlled by changes extratropical insolation through changes in the temperature or strength of oceanic upwelling and advection at obliquity. Though the uncertainties are large, the obliquity band of Site 846 SST consistently leads Site 1239 SST by ~3±4 kyr in both before and after the MPT, which may indicate different drivers for these two records at the 41-ky period.

4.5 Radiative greenhouse gas forcing

Atmospheric greenhouse gas concentrations covary with SST (Herbert et al., 2010) and through radiative heating and associated tropical feedbacks, may drive Pleistocene tropical Pacific SST changes (e.g. Medina-Elizalde and Lea, 2005). Carbon cycle changes are further proposed to have acted as an internal feedback of the climate system (Ashkenazy and Tziperman, 2004) that may have also played a role in shifting western tropical Pacific SST periodicity at the MPT (Medina-Elizalde and Lea, 2005). Here we test whether the radiative greenhouse gas forcing could have also influenced eastern Pacific SST.

Greenhouse gas records do not yet exist at sufficient temporal resolution for cross-spectral analysis prior to 800 kya. Nevertheless, preliminary atmospheric pCO_2 derived from the $\delta^{11}B$ proxy suggests a lower amplitude of variability in the period 1500-800 kya than in the late Pleistocene (Hönisch et al., 2009), consistent with global benthic $\delta^{18}O$ records (Lisiecki and Raymo, 2005). Higher glacial CO_2 concentrations prior to the MPT are consistent with warmer glacial intervals in the early Pleistocene. New orbital-scale pCO_2 records must be generated from before the MPT in order to confirm the presence of 41-kyr cycles in the atmospheric pCO_2 record to confirm this relationship.

Tropical SST records are in phase (or nearly in phase) with CO_2 concentrations (Fig. 3.6) at the eccentricity frequency supporting the idea that radiative greenhouse gas

forcing played a primary role in controlling tropical SST after the MPT (e.g. Medina-Elizalde and Lea, 2005; Herbert et al., 2010). These results are consistent with the idea that glacial terminations are influenced by an initial release of carbon from the deep ocean (Ruddiman, 2006; Shakun et al., 2012) and that oceanic controls for carbon fluxes into and out of the high-latitude ocean play an important role in determining the amplitude of glacial-interglacial temperature variability (Kemp et al., 2010) in the late Pleistocene 100-ky ice age cycles.

Atmospheric carbon dioxide records in the late Pleistocene also contain components of obliquity and precession cycles (Fig. 3.6). At the obliquity periodicity, CO_2 concentrations lag high-latitude insolation and cold-tongue temperatures; other records that lag include minimum benthic $\delta^{18}O$ and Site 1239 SST. In the precession bandwidth, SST at Site 806 and TR163-19 is in phase with or leads CO_2 (phase: 2±2 ky) (Fig. 3.6). The fact that CO_2 lags SST variations indicates that it may not have been a direct driver of temperature change at the 41-kyr or 23-kyr periodicities; rather, tropical climate or oceanographic changes may have played a role in carbon cycle feedbacks, perhaps through productivity and carbon uptake, or changes in continental vegetation on these timescales.

5. Summary

As with other parts of the globe we observe a transformation of surface conditions and temperature variability near the MPT in the east Pacific. Prior to the MPT, east Pacific surface waters cooled during both glacials and interglacials just as high-latitude glacial intervals became increasingly intense (Fig. 3.2). At ~850 kya, near the MPT, the equatorial front at the northern margin of the cold tongue steepened as the Site 1239 SST warmed over about the next 150 ky. Once developed, the larger SST gradient between Site 1239 and Site 846 remained to the present day.

Spectral analysis of insolation and SST suggest that SST change in the tropics is not inversely related to October insolation, as predicted by early models. Rather, at precession periodicities (19-23 kyr cycles) eastern Pacific SST is directly correlated to equatorial or extratropical radiation changes in the tropical cold season (summer-fall) rather than inversely correlated as previously suggested. Though the cold tongue is largely influenced by the strength and temperature of upwelling or advecting cool water on obliquity or eccentricity timescales, small precession-scale modulations of eastern tropical SST can be directly related to past insolation quantities both before and after the mid-Pleistocene transition.

At the 41-kyr periodicity, east Pacific SST changes may reflect ice-sheet volume and high-latitude forcing. Specifically, in the obliquity band of variability, phase analysis suggests that northern-hemisphere summer insolation changed first and was then

closely followed by corresponding changes in SST in the heart of the cold tongue. Over an ice age cycle, ice sheets then continue to grow and impose consequent changes in benthic $\delta^{18}O$, atmospheric CO_2, and latitudinal bands of atmospheric circulation, which are reflected in Site 1239 SST; each of these components of the climate system lag northern hemisphere insolation.

At the 100-ky periodicity radiative greenhouse gas changes seem to be the only forcing mechanism with sufficient power to amplify eastern tropical SST change. Carbon cycle interactions with the marine and terrestrial realms and the interplay of ocean overturning at high-latitudes must aid in the control of atmospheric CO_2 concentrations. However, high-resolution records are only available for the last 800 kyr; this limitation curbs our current ability to make statements about greenhouse gas forcing in the period before the mid-Pleistocene transition but acts as inspiration for reconstructions of high-resolution pCO_2 in future research.

References

Ashkenazy, Y., and Tziperman, E., 2004, Are the 41kyr glacial oscillations a linear response to Milankovitch forcing?: Quaternary Science Reviews, v. 23, no. 18-19, p. 1879–1890, doi: 10.1016/j.quascirev.2004.04.008.

Bickert, T., Berger, W., Burke, S., and Schmidt, H., 1993, Late Quaternary stable isotope record of Cibicidoides wuellerstorfi from the Ontong Java Plateau, *in* Berger, W., Kroenke, L., and Mayer, L. eds., Proc. ODP, Scientific Results, Ocean Drilling Program.

Broecker, W.S., and Denton, G.H., 2002, The role of ocean-atmosphere reorganizations in glacial cycles: Geochimica et Cosmochimica Acta, v. 53, no. 10, p. 2465–2501.

Cane, M., and Clement, A., 1999, A role for the tropical Pacific coupled ocean-atmosphere system on Milankovitch and millennial timescales. Part II: Global impacts: Mechanisms of global climate change at millennial time scales, v. 112, p. 373–383.

Chiang, J.C.H., 2003, Sensitivity of the Atlantic Intertropical Convergence Zone to Last Glacial Maximum boundary conditions: Paleoceanography, v. 18, no. 4, doi: 10.1029/2003PA000916.

Chiang, J.C.H., and Bitz, C.M., 2005, Influence of high latitude ice cover on the marine Intertropical Convergence Zone: Climate Dynamics, v. 25, no. 5, p. 477–496, doi: 10.1007/s00382-005-0040-5.

Clark, P., and Pollard, D., 1998, Origin of the middle Pleistocene transition by ice sheet erosion of regolith: Paleoceanography, v. 13, no. 1, p. 1–9.

Clark, P.U., Archer, D., Pollard, D., Blum, J.D., Rial, J.A., Brovkin, V., Mix, A.C., Pisias, N.G., and Roy, M., 2006, The middle Pleistocene transition: characteristics, mechanisms, and implications for long-term changes in atmospheric pCO2: Quaternary Science Reviews, v. 25, no. 23-24, p. 3150–3184, doi: 10.1016/j.quascirev.2006.07.008.

Clement, A., Seager, R., and Cane, M., 1999, Orbital controls on the El Nino/Southern Oscillation and the tropical climate: Paleoceanography, v. 14, no. 4, p. 441–456.

Clement, A., Seager, R., and Cane, M., 2000, Suppression of El Nino during the mid-Holocene by changes in the Earth's orbit: Paleoceanography, v. 15, no. 6, p. 731–737.

de Garidel-Thoron, T., Rosenthal, Y., Bassinot, F., and Beaufort, L., 2005, Stable sea surface temperatures in the western Pacific warm pool over the past 1.75 million years: Nature, v. 433, no. 7023, p. 294–298.

Dekens, P.S., Ravelo, A.C., and Mccarthy, M.D., 2007, Warm upwelling regions in the Pliocene warm period: Paleoceanography, v. 22, no. 3, p. PA3211, doi: 10.1029/2006PA001394.

Deser, C., and Wallace, J., 2000, Large-scale atmospheric circulation features of warm and cold episodes in the tropical Pacific: Journal of Climate, v. 3, no. 11, p. 1254–1281.

Elkibbi, M., and Rial, J.A., 2001, An outsider's review of the astronomical theory of the climate: is the eccentricity-driven insolation the main driver of the ice ages?: Earth-Science Reviews, v. 56, no. 1-4, p. 161–177.

Etourneau, J., Martinez, P., Blanz, T., and Schneider, R., 2009, Pliocene-Pleistocene variability of upwelling activity, productivity, and nutrient cycling in the Benguela region: Geology, v. 37, no. 10, p. 871–874, doi: 10.1130/G25733A.1.

Etourneau, J., Schneider, R., Blanz, T., and Martinez, P., 2010, Intensification of the Walker and Hadley atmospheric circulations during the Pliocene–Pleistocene climate transition: Earth and Planetary Science Letters,, p. 1–8, doi: 10.1016/j.epsl.2010.06.010.

Fiedler, P.C., and Talley, L.D., 2006, Hydrography of the eastern tropical Pacific: A review: Progress in Oceanography, v. 69, no. 2-4, p. 143–180, doi: 10.1016/j.pocean.2006.03.008.

Gildor, H., and Tziperman, E., 2001, A sea ice climate switch mechanism for the 100-kyr glacial cycles: Journal of Geophysical Research, v. 106, no. C5, p. 9117–9133.

Gildor, H., and Tziperman, E., 2000, Sea ice as the glacial cycles' climate switch: Role of seasonal and orbital forcing: Paleoceanography, v. 15, no. 6, p. 605–615.

Hays, J., Imbrie, J., and Shackleton, N., 1976, Variations in the earth's orbit: pacemaker of the ice ages: Science, v. 194, no. 4270, p. 1121–1132.

Herbert, T.D., Peterson, L.C., Lawrence, K.T., and Liu, Z., 2010, Tropical Ocean Temperatures Over the Past 3.5 Million Years: Science, v. 328, no. 5985, p. 1530–1534, doi: 10.1126/science.1185435.

Howell, P., Ballance, J., Baughman, J., and Ochs, L., 2006, ARAND Time Series Analysis Software: Providence, RI.

Hönisch, B., Hemming, N., Archer, D., Siddall, M., and McManus, J., 2009, Atmospheric carbon dioxide concentration across the mid-Pleistocene transition: Science, v. 324, no. 5934, p. 1551.

Huybers, P., 2009, Antarctica's orbital beat: Science, v. 325, no. 5944, p. 1085.

Imbrie, J., Berger, A., Boyle, E., Clemens, S., Duffy, A., Howard, W., Kukla, G., Kutzbach, J., Martinson, D., McIntyre, A., Mix, A., Molfino, B., Morley, J., Peterson, L., et al., 1993, On the Structure and Origin of Major Glaciation cycles. 2. The 100,000-year cycle: Paleoceanography, v. 8, no. 6, p. 699–735.

Imbrie, J., Boyle, E., Clemens, S., Duffy, A., Howard, W., Kukla, G., Kutzbach, J., Martinson, D., McIntyre, A., Mix, A.C., Molfino, B., Morley, J., Peterson, L.C., Pisias, N., et al., 1992, On the structure and origin of major glaciation cycles 1. Linear resonses to Milankovitch forcing: Paleoceanography, v. 7, no. 6, p. 701–738.

Imbrie, J.Z., Imbrie-Moore, A., and Lisiecki, L.E., 2011, A phase-space model for Pleistocene ice volume: Earth and Planetary Science Letters, v. 307, no. 1-2, p. 94–102, doi: 10.1016/j.epsl.2011.04.018.

Kemp, A.E.S., Grigorov, I., Pearce, R.B., and Garabato, A.C.N., 2010, Migration of the Antarctic Polar Front through the mid-Pleistocene transition: evidence and climatic implications: Quaternary Science Reviews, v. 29, no. 17-18, p. 1993–2009, doi: 10.1016/j.quascirev.2010.04.027.

Koutavas, A., and Lynch-Stieglitz, J., 2003, Glacial-interglacial dynamics of the eastern equatorial Pacific cold tongue-Intertropical Convergence Zone system reconstructed from oxygen isotope records: Paleoceanography, v. 18, no. 4, p. 1089, doi: 10.1029/2003PA000894.

Koutavas, A., and Lynch-Stieglitz, J., 2004, Variability of the marine ITCZ over the eastern Pacific during the past 30,000 years: Regional perspective and global context: The Hadley Circulation: Present, Past, and Future,, p. 347–369.

Koutavas, A., Demenocal, P.B., Olive, G.C., and Lynch-Stieglitz, J., 2006, Mid-Holocene El Niño–Southern Oscillation (ENSO) attenuation revealed by individual foraminifera in eastern tropical Pacific sediments: Geology, v. 34, no. 12, p. 993, doi: 10.1130/G22810A.1.

Koutavas, A., Lynch-Stieglitz, J., Marchitto, T., and Sachs, J., 2002, El Nino-like pattern in ice age tropical Pacific sea surface temperature: Science, v. 297, no. 5579, p. 226.

Laskar, J., Robutel, P., Joutel, F., Gastineau, M., Correia, A.C.M., and Levrard, B.,

2004, A long-term numerical solution for the insolation quantities of the Earth: Astronomy and Astrophysics, v. 428, no. 1, p. 261–285, doi: 10.1051/0004-6361:20041335.

Lawrence, K., Liu, Z., and Herbert, T., 2006, Evolution of the eastern tropical Pacific through Plio-Pleistocene glaciation: Science, v. 312, no. 5770, p. 79.

Lea, D., 2004, The 100 000-yr cycle in tropical SST, greenhouse forcing, and climate sensitivity: Journal of Climate, v. 17, no. 11, p. 2170–2179.

Lea, D., Pak, D., and Spero, H., 2000, Climate impact of late Quaternary equatorial Pacific sea surface temperature variations: Science, v. 289, no. 5485, p. 1719.

Lea, D., Pak, D., Belanger, C., Spero, H., Hall, M., and Shackleton, N., 2006, Paleoclimate history of Galapagos surface waters over the last 135,000 yr: Quaternary Science Reviews, v. 25, no. 11-12, p. 1152–1167, doi: 10.1016/j.quascirev.2005.11.010.

Lee, S.-Y., and Poulsen, C.J., 2005, Tropical Pacific climate response to obliquity forcing in the Pleistocene: Paleoceanography, v. 20, no. 4, p. PA4010, doi: 10.1029/2005PA001161.

Lisiecki, L.E., 2010, A benthic $\delta^{13}C$-based proxy for atmospheric pCO_2 over the last 1.5 Myr: Geophysical Research Letters, v. 37, no. 21, p. L21708, doi: 10.1029/2010GL045109.

Lisiecki, L.E., and Raymo, M.E., 2005, A Pliocene-Pleistocene stack of 57 globally distributed benthic $\delta^{18}O$ records: Paleoceanography, v. 20, no. 1, p. PA1003, doi: 10.1029/2004PA001071.

Liu, Z., and Herbert, T.D., 2004, High-latitude influence on the eastern equatorial Pacific climate in the early Pleistocene epoch: Nature, v. 427, no. 6976, p. 720–723.

Loulergue, L., Schilt, A., Spahni, R., Masson-Delmotte, V., Blunier, T., Lemieux, B., Barnola, J.-M., Raynaud, D., Stocker, T.F., and Chappellaz, J., 2008, Orbital and millennial-scale features of atmospheric CH4 over the past 800,000 years: Nature, v. 453, no. 7193, p. 383–386, doi: 10.1038/nature06950.

Lüthi, D., Le Floch, M., Bereiter, B., Blunier, T., Barnola, J.-M., Siegenthaler, U., Raynaud, D., Jouzel, J., Fischer, H., Kawamura, K., and Stocker, T.F., 2008, High-resolution carbon dioxide concentration record 650,000–800,000 years before present: Nature, v. 453, no. 7193, p. 379–382, doi: 10.1038/nature06949.

Martínez-Garcia, A., Rosell-Melé, A., McClymont, E., Gersonde, R., and Haug, G.,

2010, Subpolar link to the emergence of the modern Equatorial Pacific cold tongue: Science, v. 328, no. 5985, p. 1550.

McClymont, E.L., Rosell-Melé, A., Haug, G.H., and Lloyd, J.M., 2008, Expansion of subarctic water masses in the North Atlantic and Pacific oceans and implications for mid-Pleistocene ice sheet growth: Paleoceanography, v. 23, no. 4, doi: 10.1029/2008PA001622.

Medina-Elizalde, M., and Lea, D., 2005, The mid-Pleistocene transition in the Tropical Pacific: Science, v. 310, no. 5750, p. 1009.

Mitchell, T.P., and Wallace, J.M., 1992, The annual cycle in equatorial convection and sea surface temperature: Journal of Climate, v. 5, no. 10, p. 1140–1156.

Müller, P., Kirst, G., Ruhland, G., Storch, Von, I., and Rosell-Melé, A., 1998, Calibration of the alkenone paleotemperature index U^{37}_{K}' based on core-tops from the eastern South Atlantic and the global ocean (60 N-60 S): Geochimica et Cosmochimica Acta, v. 62, no. 10, p. 1757–1772.

Pahnke, K., Sachs, J.P., Keigwin, L., Timmermann, A., and Xie, S.-P., 2007, Eastern tropical Pacific hydrologic changes during the past 27,000 years from D/H ratios in alkenones: Paleoceanography, v. 22, no. 4, p. PA4214, doi: 10.1029/2007PA001468.

Palliard, D., Labeyrie, L., and Yiou, P., 1996, Macintosh program performs time-series analysis: Eos Trans. AGU 77, 379 p.

Parrenin, F., Barnola, J., Beer, J., Blunier, T., Castellano, E., Chappellaz, J., Dreyfus, G., Fischer, H., Fujita, S., and Jouzel, J., 2007, The EDC3 chronology for the EPICA Dome C ice core: Climate of the Past, v. 3, p. 485–497.

Philander, S., Gu, D., Halpern, D., Lambert, G., Lau, N., Li, T., and Pacanowski, R., 1996, Why the ITCZ is mostly north of the equator: Journal of Climate, v. 9, no. 12, p. 2958–2972.

Philander, S.G., and Fedorov, A.V., 2003, Role of tropics in changing the response to Milankovich forcing some three million years ago: Paleoceanography, v. 18, no. 2, p. 1045, doi: 10.1029/2002PA000837.

Pisias, N.G., and Moore, T., Jr, 1981, The evolution of Pleistocene climate: a time series approach: Earth and Planetary Science Letters, v. 52, no. 2, p. 450–458.

Rincón-Martínez, D., Lamy, F., Contreras, S., Leduc, G., Bard, E., Saukel, C., Blanz, T., Mackensen, A., and Tiedemann, R., 2010, More humid interglacials in Ecuador during the past 500 kyr linked to latitudinal shifts of the equatorial front

and the Intertropical Convergence Zone in the eastern tropical Pacific: Paleoceanography, v. 25, no. 2, p. PA2210, doi: 10.1029/2009PA001868.

Roy, M., Clark, P.U., Raisbeck, G.M., and Yiou, F., 2004, Geochemical constraints on the regolith hypothesis for the middle Pleistocene transition: Earth and Planetary Science Letters, v. 227, no. 3-4, p. 281–296, doi: 10.1016/j.epsl.2004.09.001.

Rubincam, D., 1994, Insolation in terms of Earth's orbital parameters: Theoretical and applied climatology, v. 48, no. 4, p. 195–202.

Ruddiman, W., 2006, Orbital changes and climate: Quaternary Science Reviews, v. 25, no. 23-24, p. 3092–3112.

Sarmiento, J., Gruber, N., Brzezinski, M., and Dunne, J., 2004, High-latitude controls of thermocline nutrients and low latitude biological productivity: Nature, v. 427, no. 6969, p. 56–60.

Schmidt, M.W., and Spero, H.J., 2011, Meridional shifts in the marine ITCZ and the tropical hydrologic cycle over the last three glacial cycles: Paleoceanography, v. 26, no. 1, doi: 10.1029/2010PA001976.

Schmieder, F., Dobeneck, von, T., and Bleil, U., 2000, The Mid-Pleistocene climate transition as documented in the deep South Atlantic Ocean: initiation, interim state and terminal event: Earth and Planetary Science Letters, v. 179, no. 3-4, p. 539–549.

Schneider von Deimling, T., Held, H., Ganopolski, A., and Rahmstorf, S., 2006, Climate sensitivity estimated from ensemble simulations of glacial climate: Climate Dynamics, v. 27, no. 2-3, p. 149–163, doi: 10.1007/s00382-006-0126-8.

Shakun, J.D., Clark, P.U., He, F., Marcott, S.A., Mix, A.C., Liu, Z., Otto-Bliesner, B., Schmittner, A., and Bard, E., 2012, Global warming preceded by increasing carbon dioxide concentrations during the last deglaciation: Nature, v. 484, no. 7392, p. 49–54, doi: 10.1038/nature10915.

Shipboard Scientific Party, 2003, Site 1239, *in* Mix, A.C., Tiedemann, R., and Blum, P. eds., Proc. ODP, Init. Repts, Ocean Drilling Program, College Station, TX, p. 1–93.

Timmermann, A., Lorenz, S.J., An, S.-I., Clement, A., and Xie, S.-P., 2007, The Effect of Orbital Forcing on the Mean Climate and Variability of the Tropical Pacific: Journal of Climate, v. 20, no. 16, p. 4147–4159, doi: 10.1175/JCLI4240.1.

Toggweiler, J.R., 2008, Origin of the 100,000-year timescale in Antarctic temperatures and atmospheric CO 2: Paleoceanography, v. 23, no. 2, p. PA2211, doi: 10.1029/2006PA001405.

Toggweiler, J.R., 1999, Variation of atmospheric CO_2 by ventilation of the ocean's deepest water: Paleoceanography, v. 14, no. 5, p. 571–588.

Toggweiler, J.R., Russell, J.L., and Carson, S.R., 2006, Midlatitude westerlies, atmospheric CO 2, and climate change during the ice ages: Paleoceanography, v. 21, no. 2, doi: 10.1029/2005PA001154.

Tziperman, E., and Gildor, H., 2003, On the mid-Pleistocene transition to 100-kyr glacial cycles and the asymmetry between glaciation and deglaciation times: Paleoceanography, v. 18, no. 1, doi: 10.1029/2001PA000627.

Vellinga, M., and Wu, P., 2004, Low-latitude freshwater influence on centennial variability of the Atlantic thermohaline circulation: Journal of Climate, v. 17, no. 23, p. 4498–4511.

Watson, A.J., and Naveira Garabato, A.C., 2006, The role of Southern Ocean mixing and upwelling in glacial-interglacial atmospheric CO2 change: Tellus B, v. 58, no. 1, p. 73–87, doi: 10.1111/j.1600-0889.2005.00167.x.

Weaver, A.J., Eby, M., Fanning, A.F., and Wiebe, E.C., 1998, Simulated influence of carbon dioxide, orbital forcing and ice sheets on the climate of the Last Glacial Maximum: Nature, v. 394, no. 6696, p. 847–853.

Xie, S.-P., Okumura, Y., Miyama, T., and Timmermann, A., 2008, Influences of Atlantic Climate Change on the Tropical Pacific via the Central American Isthmus: Journal of Climate, v. 21, no. 15, p. 3914–3928, doi: 10.1175/2008JCLI2231.1.

Figures

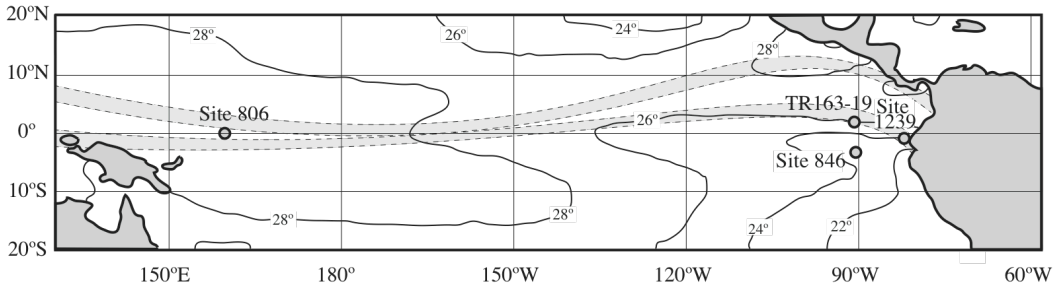

Figure 3.1. Location map showing core locations for SST records. Modern mean annual SST is contoured using the World Ocean Atlas (Locarnini et al., 2010) dataset. Light gray shading represents approximate average modern position of ITCZ in July (north) and January (south).

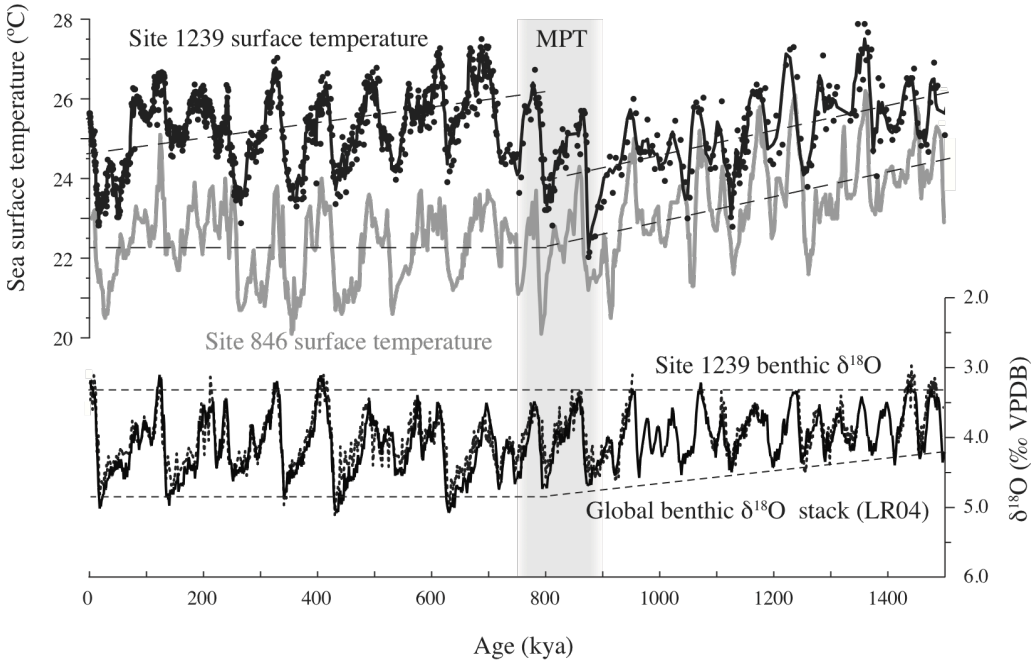

Figure 3.2. Site 1239 compiled temperature record (black, original data and resampled curve) compared with Site 846 SST (grey) (Liu and Herbert, 2004) in the heart of the cold tongue. The Site 1239 benthic $\delta^{18}O$ record (with *cibicidoides wuellerstofi* record offset by 0.66‰) is aligned with a global benthic $\delta^{18}O$ stack. Temperatures are warmer on the northeastern margin of the cold tongue; the two sites show secular cooling in the early Pleistocene, an abrupt increase in the SST gradient at the MPT, then secular cooling at Site 1239 after ~800 kya. Plotted below is the benthic $\delta^{18}O$ age model (dotted) from Site 1239 aligned with global benthic stack LR04 (solid).

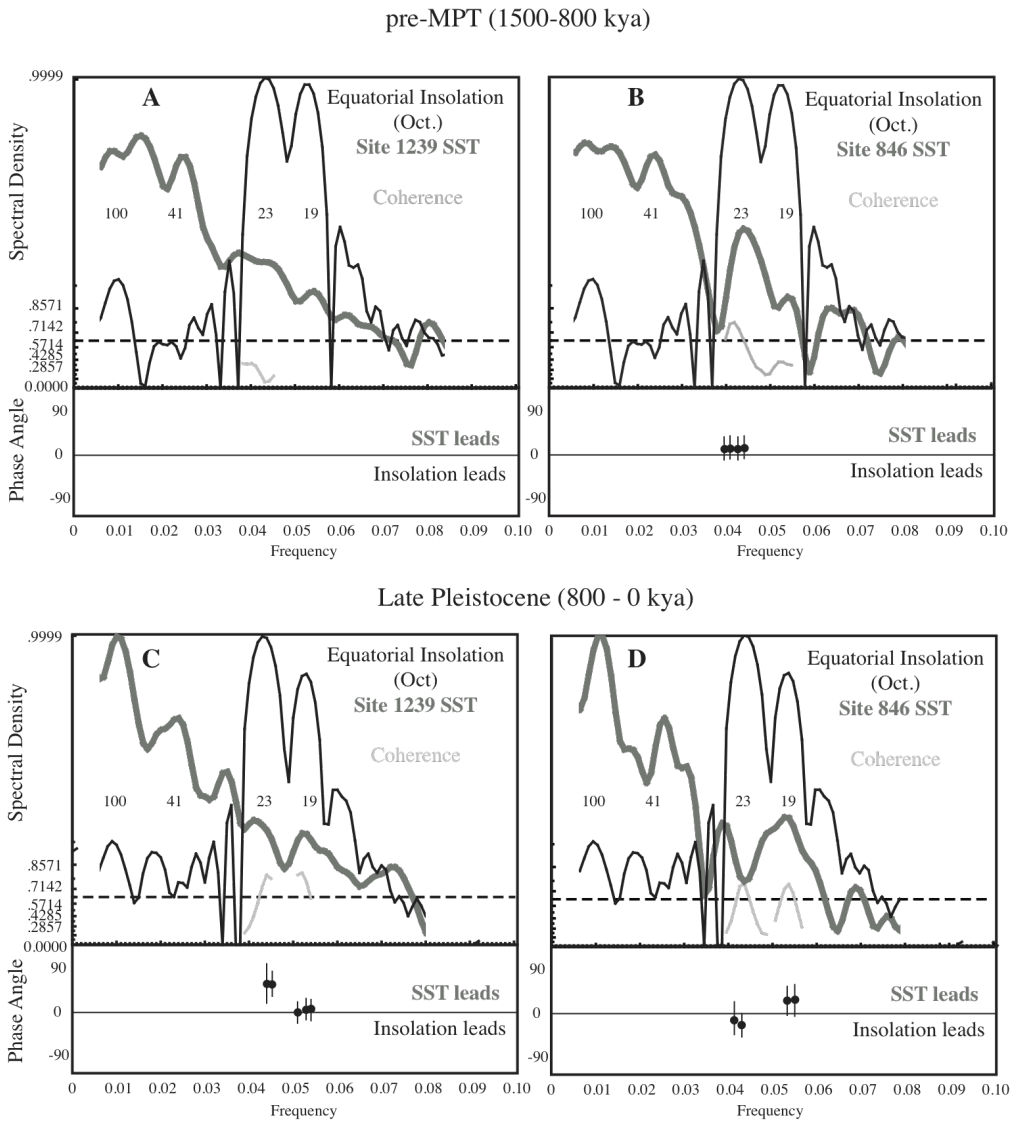

Figure 3.3. Cross-spectral analysis (spectral density, coherence, and phase angle) of pre- and post-MPT equatorial insolation and SST at Site 846 and 1239. Horizontal dashed line represents limit of non-zero coherence at 80% confidence interval, phase only plotted when coherence is above 80% level. (A) Pre-MPT Site 1239 SST spectrum (thick grey line) is not coherent with direct insolation (thin black line) at any frequency. (B) Site 846 SST (thick grey line) is in phase with insolation (thin black line) at 23-ky periodicity rather than being 180° out of phase as expected. (C) Late Pleistocene Site 1239 SST is coherent with equatorial insolation at precession frequencies, though SST leads October insolation at 23-ky periods and in phase at 19-ky periods. (D) Same result as pre-MPT, though both 23- and 19-kyr periodicity is in phase.

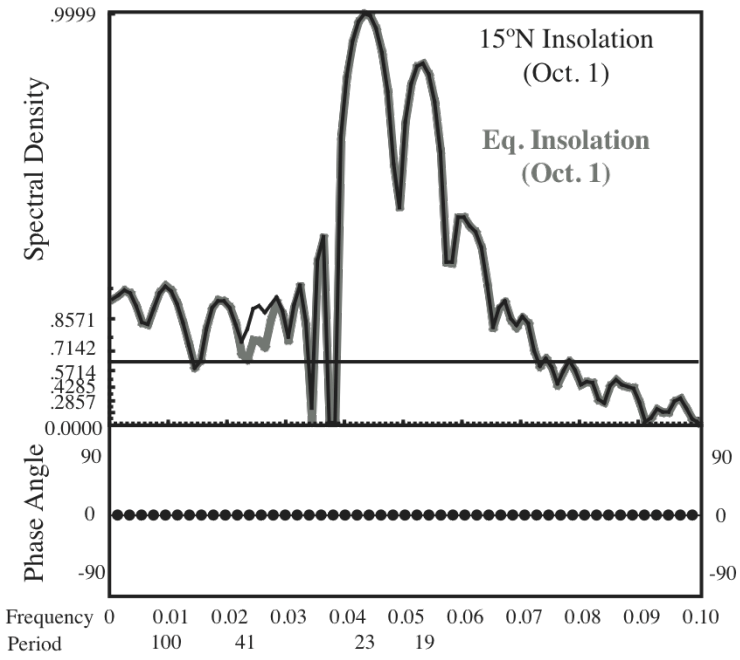

Figure 3.4: Cross-spectral analysis of autumn insolation at the equator and 15°N. Records are coherent and in phase for all frequencies.

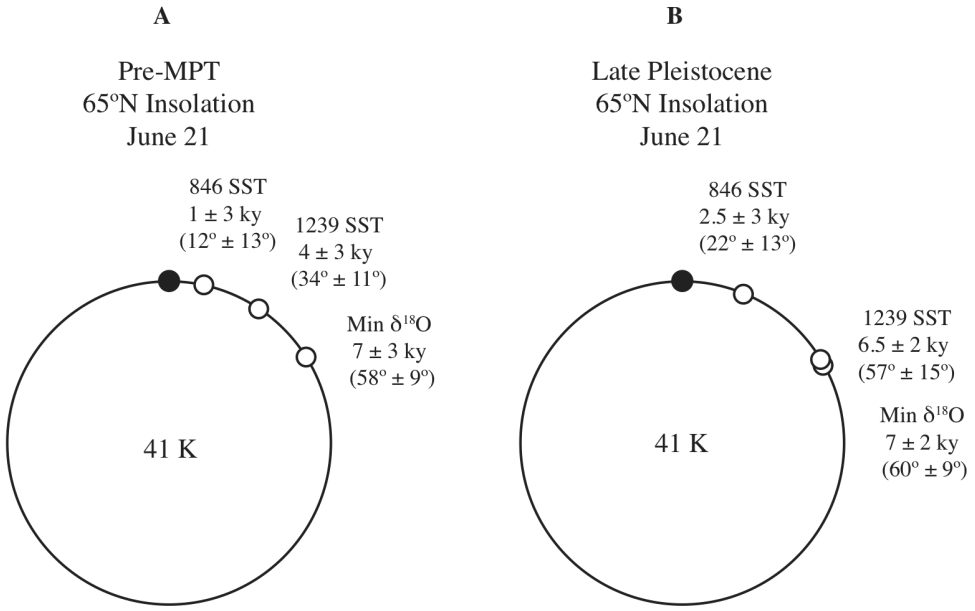

Figure 3.5: Obliquity phase wheels for SST at Sites 846 and 1239 compared with high-latitude summer insolation and ice volume (estimated using minimum benthic $\delta^{18}O$) forcing for pre- and post-MPT time periods. Extratropical insolation is at the 12 o'clock position (black circle); phase is reported in both ky and phase angle with error. Pre-MPT cold tongue SST lags high-latitude insolation but leads minimum ice volume; in the late Pleistocene Site 1239 SST may be in phase with minimum ice volume.

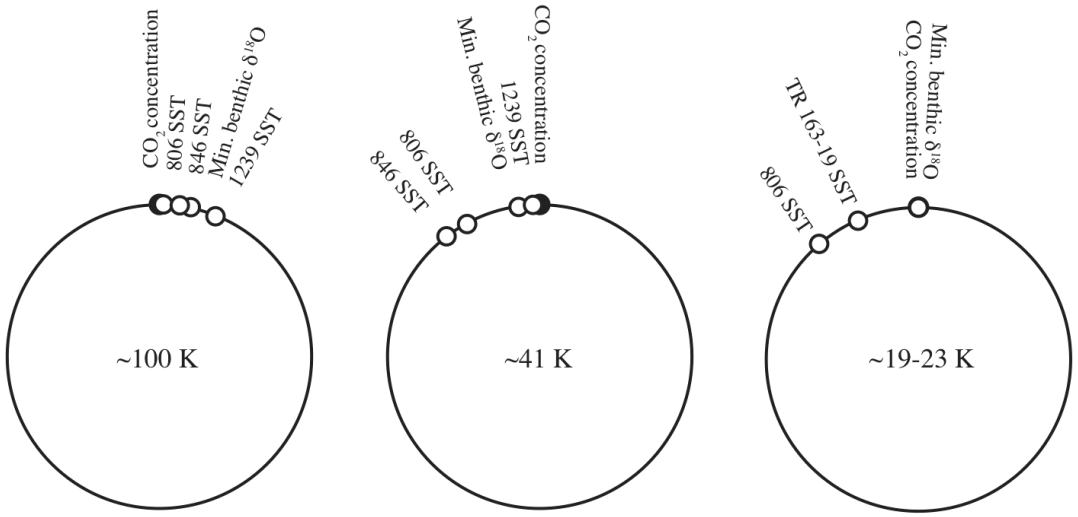

Figure 3.6: Phase wheels for records related to atmospheric greenhouse gas concentrations (CO_2 concentration is the black circle at 12 o'clock position). At 100-ky periodicity only Site 1239 SST lags CO_2, whereas at 41-ky periodicity Site 846 SST and Site 806 SST lead CO_2. Site 1239 SST and CO_2 are only coherent in the precessional bandwidth (0.041-0.054 ky^{-1}) at 23-ky periodicity; at this frequency the records are in phase. Phase relationships are presented in Table II.

Period	Record	% of variance (spectral density) in each band: Precession 18-24 kyr	Obliquity 37-45 kyr	Eccentricity 90-111 kyr	% of variance (spectral density) coherent with: Solar Insol. June 21, 65°N	Benthic $\delta^{18}O$ stack (LR04)	Global Atm. CO_2
Pre-MPT (1500-800 kya)	**Site 1239 SST**	3%	17%	12%	20%	98%	N/A
	Site 846 SST	6%	17%	12%	24%	97%	N/A
Post-MPT (800-0 kya)	**Site 1239 SST**	2%	8%	30%	13%	98%	98%
	Site 846 SST	6%	12%	25%	22%	95%	95%

Table 3.1: Percent of variance as determined by spectral density coherent among records.

	100-kyr period		41-kyr period		19-23-kyr period	
Record	**Lag (ky)**	**Lag (phase angle)**	**Lag (ky)**	**Lag (phase angle)**	**Lag (ky)**	**Lag (phase angle)**
Site 806 SST	0 ± 4 ky	-1° ± 13°	3 ± 2 ky	29° ± 14°	3 ± 2 ky	41° ± 25°
Site 846 SST	-2 ± 4 ky	-8° ± 13°	4 ± 2 ky	38° ± 18°		
Benthic $\delta^{18}O$ (min. ice)	-4 ± 1 ky	-13° ± 4°	1 ± 2 ky	7° ± 15°	0 ± 2 ky	0° ± 34°
Site 1239 SST	-6 ± 4 ky	-21° ± 16°	0 ± 2 ky	2° ± 15°		
TR 163-19 SST					1 ± 1 ky	23° ± 16°

Table 3.2: Data table for Fig. 3.6.

4. LATE PLEISTOCENE TROPICAL PACIFIC TEMPERATURE SENSITIVITY TO RADIATIVE GREENHOUSE GAS FORCING

ABSTRACT

Understanding how global temperature changes with increasing atmospheric greenhouse gas concentrations, or climate sensitivity, is of central importance to climate change research. Climate models provide sensitivity estimates that may not fully incorporate slow, long-term feedbacks such as those involving ice sheets and vegetation. Geological studies, on the other hand, can provide estimates that integrate long and short-term climate feedbacks to radiative forcing. Because high latitudes are thought to be most sensitive to greenhouse gas forcing owing to, for example, ice-albedo feedbacks, we focus on the tropical Pacific to derive a minimum value for long-term climate sensitivity. Using Mg/Ca-paleothermometry from the planktonic foraminifera *G. ruber* from the past 500 kyr at Ocean Drilling Program (ODP) Site 871 in the western Pacific warm pool, we estimate the tropical Pacific climate sensitivity parameter (λ) to be 0.94 – 1.06 ^{o}C $(W\ m^{-2})^{-1}$, which is higher than that predicted by model simulations of the Last Glacial Maximum or by models of doubled greenhouse gas concentration forcing. This result suggests that models may not yet adequately represent the long-term feedbacks related to ocean circulation,

vegetation and associated dust, the cryosphere and/or may underestimate the effects of tropical clouds or other short-term feedback processes.

INTRODUCTION

Greenhouse gas (GHG) forcing directly and indirectly affects sea-surface temperature (SST) on geologic timescales (Lea, 2004; Hansen and Sato, 2011) yet remains a key uncertainty for future climate change (Knutti and Hegerl, 2008). Models estimate that global equilibrium climate sensitivity ranges from about 2 – 4.5 °C, but do not fully account for 'slow' feedbacks (e.g., those involving deep ocean circulation, vegetation, dust, or ice sheets); thus, the potential long-term warming may lie outside this range (Knutti and Hegerl, 2008). Geological paleoclimate studies provide estimates of tropical equilibrium climate system sensitivity, the SST response to CO_2 and CH_4 radiative forcing after all fast and slow internal climate feedbacks are included (Lea, 2004). Our strategy uses atmospheric CO_2 and CH_4 concentrations as the initial forcing, rather than considering radiative balance terms separately (as in Rohling et al., 2012) since albedo, dust, and GHG concentrations are interrelated (IPCC, 2007). Thus, our approach indicates how GHG concentrations affect temperature change with all the other feedbacks integrated. As previously defined, this relationship between SST and GHG forcing (λ, in °C $(W\ m^{-2})^{-1}$) is the past equilibrium climate sensitivity parameter (Otto-Bliesner et al., 2009; Lea, 2004).

Models tend to agree on temperature change in the tropics for the Last Glacial Maximum (LGM, Otto-Bliesner et al., 2009) and future warming scenarios (DiNezio et al., 2009), making tropics data-model comparisons less model-dependent. The tropics also avoid the strong ice-albedo feedbacks, which increase climate sensitivity at the high latitudes (Lea, 2004; Holland and Bitz, 2003; Hansen and Sato, 2011). Thus, tropical climate sensitivity provides a firm 'lower bound' for global climate sensitivity without the confounding effects of high latitude feedbacks.

While model-derived past tropical climate sensitivity (0.67-0.83 ^{o}C $(W\,m^{-2})^{-1}$) generally agrees with observational estimates (Knutti and Hegerl, 2008; Otto-Bliesner et al., 2009; Schmittner et al., 2011), some models tend to rely on the MARGO SST reconstruction (Knutti and Hegerl, 2008; Waelbroeck et al., 2009). Particularly in the tropical Pacific, MARGO is largely based on SSTs derived from foraminiferal assemblage distributions, which are often biased by ecological shifts (Lea, 2004; Mix et al., 2001) and more strongly correlated with mixed layer and thermocline depth than SST (as in Rohling et al., 2012; Andreasen and Ravelo, 1997). Geochemical SST reconstructions from the tropical Pacific show a larger amplitude of glacial-interglacial change (IPCC, 2007; Medina-Elizalde and Lea, 2005) and represent a more accurate indicator of past climate sensitivity than foraminifera transfer functions in the tropics (Otto-Bliesner et al., 2009; Lea, 2004; Lea, 2004).

Excellent spatial coverage is not possible with available cores; thus, our approach is to generate a high quality geochemical SST record in an important section of the tropical oceans. The western equatorial Pacific warm pool covers a large area of the surface ocean, plays an important role in atmospheric convection, and gives an overall sense of tropical climate sensitivity. The most desirable record also avoids the dynamic effects associated with equatorial upwelling or proximity to strong SST gradients and includes multiple glacial cycles to provide many realizations of warm and cold extremes in climate and in greenhouse gas concentrations. Finally, the ideal site is in relatively shallow water to minimize the high-Mg-calcite dissolution associated with deeper waters. For these reasons, we selected ODP Site 871 in the western Pacific. Its location (5°33.1'N, 172°20.7'E, Fig. 4.1) is far from sharp modern oceanographic gradients and its depth (1255m) is well above the lysocline (LGM, Otto-Bliesner et al., 2009; Shipboard Scientific Party, 1993), ideal for Mg/Ca-based SST estimates.

The Mg/Ca paleotemperature technique is based on the temperature dependence of Mg substitution in calcite (DiNezio et al., 2009; Anand et al., 2003), though calcite with higher Mg/Ca composition preferentially dissolves from carbonate shells at depth, decreasing the original Mg/Ca value. Most attempts to correct for this effect (e.g. Dekens et al., 2002), add a linear dissolution correction after calculating SST with the exponential relationship, which overestimates the associated range of temperature variability. Correcting the Mg/Ca value for dissolution before applying the Mg/Ca-

temperature relationship (after Rosenthal and Lohmann, 2002) is a more reasonable technique to constrain the amplitude of SST change in the tropical warm pool and to formulate a lower bound for climate sensitivity. We use this method to demonstrate that late Pleistocene equatorial Pacific SST is more sensitive to GHG radiative forcing than most models predict.

METHODS AND APPROACH

A new dissolution-corrected *Globigerinoides ruber* Mg/Ca SST record, for the past 500 ky, from western tropical Pacific ODP Site 871 was compared to the published records of GHG concentrations from air bubbles trapped in ice cores (Siegenthaler et al., 2005; Loulergue et al., 2008) to calculate past climate sensitivity. For age model control, the benthic $\delta^{18}O$ stratigraphy for Site 871 was aligned with a benthic $\delta^{18}O$ stack (Lisiecki and Raymo, 2005 and Supplemental Material). The glacial-interglacial amplitude of both records is ~2.0 ‰. Sediment representing the most recent 43,000 years of the record was disturbed in the coring process and is removed from further analysis.

To correct for high-Mg calcite dissolution at depth, we assigned a depth-dependent correction to the measured Mg/Ca value (after Rosenthal and Lohmann, 2002) before applying the exponential SST-Mg/Ca calibration to calculate SST. The depth-dependent correction for *G. ruber* is derived from calculating the residual between

published core-top Mg/Ca data from the tropical warm pool regions and calculated surface Mg/Ca values at each core top location. Since no dissolution is likely in surface waters, this correction should not be extended to very shallow water without additional data. We derived a new *G. ruber* equation for tropical Pacific SST, $SST = \ln[(Mg/Ca_{measured} + 0.259 * Depth(km) + 0.537) / 0.38] / 0.09$, after the calibration equation of Anand et al., (2003). A detailed explanation of the derivation and error analysis for this new correction can be found in the Supplementary Material.

Changes in the down-core SST record (ΔT, difference between past and modern SST (Locarnini et al., 2010)) and radiative forcing from GHGs (ΔRF, difference between past radiative forcing and preindustrial values) are the foundation of the calculation of past tropical Pacific equilibrium climate sensitivity to radiative forcing. We compare these estimates of past climate sensitivity to model simulations of the LGM to assess the importance of glacial boundary conditions (e.g., ice albedo) in model simulations and discuss the relevance of our results to validating tropical climate sensitivity predicted by climate models.

RESULTS AND DISCUSSION

A number of techniques to calculate the past tropical climate sensitivity parameter (λ) are considered: (1) comparison of the resampled ΔT and ΔRF records at even time steps, (2) comparison of the average glacial and interglacial values for each record,

and (3) comparison of the relationship between the amplitude of the coherent bandwidth of each record at 100-ky periodicity. Each technique, described in detail below, yields notably similar results (λ = 0.94 – 1.06 ^{o}C (W m^{-2})$^{-1}$).

While teleconnections with ice-sheet albedo and orbital-scale oscillations in solar radiation play a small role in driving tropical SST over this time period, we first consider radiative forcing by GHGs to be the primary factor driving changes in warm pool SST (e.g. Lea, 2004) and later evaluate the role of other glacial boundary conditions for determining tropical climate change. This assumption is the starting point of our analysis for several reasons. First, direct GHG radiative forcing is an order of magnitude greater than that of annual average solar radiation. Using black body calculations, the direct effect of glacial-interglacial GHG changes (combined radiative change of ~2.6 W m^{-2}; (IPCC, 2007)) on surface temperature is ~0.4 C^{o} while, in comparison, the direct effect of a change in local annual average solar radiation due to changes in eccentricity is ~0.04 C^{o} (or < 0.2 W m^{-2}) (Hartmann, 1994). Therefore, though orbital parameters are potential 'triggers' of glacial-interglacial change, they are considered negligible as direct tropical radiation changes. Further, ice sheet albedo has a direct radiative effect on surface temperature up to ~2000 km from the southern edge of the ice sheet (Jackson and Broccoli, 2003), still far from the tropics. Ice sheets indirectly influence wind fields, which can impact ocean vertical density structure, mixing, and upwelling (Lee and Poulsen, 2005).

However, these effects are minimal for tropical SST at off-equator non-upwelling sites such as ODP Site 871. Finally, frequency analyses of changes in climate parameters suggest that even if orbital variations pace glacial-interglacial cycles, GHG variations are the major forcing of tropical warm pool SST in the Late Pleistocene time period (Lea, 2004). For these reasons, we first assume that GHGs are the primary forcing of past warm pool SST and later consider the role of other changes in glacial boundary conditions when we compare our results to climate simulations of the LGM.

Surface temperature change (ΔT; Fig. 4.2) was directly related to radiative forcing (ΔRF) using the formula $\Delta T = \lambda^{*}\Delta RF$ (IPCC, 2007; Lea, 2004). The slope of ΔT and ΔRF (method 1) at Site 871 yields a past climate sensitivity parameter (λ_1) of 1.06 (± 0.05) $^{o}C\ (W\ m^{-2})^{-1}$ (Fig. 4.3). The second method for calculating λ uses only the average glacial and interglacial temperatures and radiative forcing as determined from visual inspection of the global benthic oxygen isotope stack (Table S1) and yields λ_2 = 0.94 (± 0.12) $^{o}C\ (W\ m^{-2})^{-1}$. By eliminating transitional periods between glacial and interglacial intervals, this method depends less on the accuracy of the age model and reduces apparent λ by <0.15 $^{o}C\ (W\ m^{-2})^{-1}$. The third method compares the relative amplitude in the frequency band most coherent between the temperature and radiative forcing records, the ~100-kyr band, resulting in λ_3 = 0.97 $^{o}C\ (W\ m^{-2})^{-1}$. Thus, even when other frequency bands are excluded, λ_3 is 92% of λ_1; this result is not surprising given that most of the variance in ΔT and ΔRF is highly coherent and in

phase and occurs in the 100-kyr-frequency band. The techniques described above give a range of values for λ (0.94 - 1.06 °C $(W m^{-2})^{-1}$ and, taking into account uncertainties in the climate sensitivity regression and timescale uncertainties, a total range of 0.82 – 1.11 °C $(W m^{-2})^{-1}$. This range is equivalent to an equilibrium tropical climate sensitivity to a doubling of GHG concentration of 3.5 – 3.9 °C (full range, including uncertainty, of 3.03 – 4.12 °C).

Potential biases in the Site 871 SST record include low sedimentation rate, possible bioturbation, and uncertainties in the dissolution calibration. If the low sedimentation rate or bioturbation reduced the apparent Mg/Ca amplitude at Site 871, the actual climate sensitivity could be greater than we observe. However, the amplitude similarity between Site 871 benthic $\delta^{18}O$ and the benthic $\delta^{18}O$ stack suggests that bioturbation is not impacting the amplitude of long-timescale cycles at Site 871 any more severely than at the higher sedimentation rate open ocean sites used in the stack. Our dissolution correction assumed 0.9 mmol/mol (~18%) dissolution at 1255 m water depth. If less dissolution occurred at this depth, the resulting past climate sensitivity may be greater (up to 1.29 °C $(W m^{-2})^{-1}$; Supplemental Material). Each potential bias equates to higher λ and does not resolve the model-data mismatch for past climate sensitivity estimates.

We also calculated past climate sensitivity at other warm-pool tropical Pacific SST records for comparison. As an example, the piecewise technique (1) using the Mg/Ca record from Site 806 yields a value of $\lambda_1 = 1.13 \pm 0.05$ °C $(W\,m^{-2})^{-1}$. The higher sensitivity at Site 806 than off-equator Site 871 suggests that local ocean dynamics (equatorial upwelling strength, etc) amplified equatorial SST changes and cooled Site 806 more during glacial intervals. At site TR163-19 in the eastern Pacific (Lea et al., 2000) SST was even more sensitive ($\lambda_1 = 1.25\ (\pm 0.05)$ °C $(W\,m^{-2})^{-1}$) possibly since Site TR163-19 is near an oceanographic front or was influenced by shifts of the ITCZ or upwelling changes (Koutavas and Lynch-Stieglitz, 2003).

The climate sensitivity parameter estimated from Site 871 is 0.11 – 0.39 °C $(W\,m^{-2})^{-1}$ higher than PMIP2 models (Otto-Bliesner et al., 2009) suggest for the tropical LGM (Fig. 4.4). Comparisons of observation-based estimates of λ to LGM model estimates present an interesting case study since many of the slow feedbacks (ice sheets, etc) are prescribed as model boundary conditions (Otto-Bliesner et al., 2009). The fact that models underestimate the observed tropical cooling when ice sheets are prescribed implies that the relatively high tropical climate sensitivity we determine is unlikely to be related to neglecting high latitude albedo changes due to glaciation.

Since LGM model simulations incorporate ice volume, sea level, and GHG concentrations as given fields and make adjustments for deep ocean circulation

changes (Otto-Bliesner et al., 2009), the climate sensitivity mismatch between observational and modeled estimates of past sensitivity may be rooted in the way other boundary conditions are treated. In LGM simulations, both vegetation and dust aerosol boundary conditions are prescribed as present-day values. However, cold glacial conditions tend to favor vegetation types with higher albedo and more atmospheric dust (Yue et al., 2011), which cool the climate further during glacial periods if incorporated into the model simulations. Our results, which incorporate dust implicitly, are consistent within error with paleoclimate estimations of the global climate sensitivity parameter when dust is treated as a feedback (Rohling et al., 2012).

The past tropical climate sensitivity parameter is also 0.37 – 0.49 ^{o}C (W m^{-2})$^{-1}$ higher than predicted by the CMIP3 models (DiNezio et al., 2009) of future doubling of CO_2 (Fig. 4.4). The primary reason for the difference may simply be that our data-based estimates of past climate sensitivity intrinsically include slow feedbacks related to such components of the Earth system as deep ocean dynamics and ice-volume changes, which are not captured by models of future climate change. The complexity of simulating the effects of clouds (e.g. Delworth et al., 2006) and other short-term feedback mechanisms may also explain why models of future tropical climate might underestimate climate sensitivity (Knutti and Hegerl, 2008). Such effects are especially important near the equator where cloud-related feedbacks play a large role.

As paleoclimate data directly informs our understanding of the past, it may not be appropriate to scale observational estimates of glacial-interglacial climate sensitivity to future warming scenarios since nonlinear feedbacks add uncertainty to such an extrapolation at low latitudes (Crucifix, 2006). Numerical simulations of climate are needed to accurately estimate future tropical climate sensitivity. Yet, until simulations are able to capture the full range of tropical SST suggested by the paleoclimate data, models may underestimate future climate sensitivity. Resolution of this data-model mismatch in past glacial cycles is required to refine predictions of future climate sensitivity.

SUMMARY

This work shows that past long-term equilibrium climate sensitivity of the tropical Pacific region to forcing by GHG concentration changes is 0.94 – 1.06 ^{o}C $(W\ m^{-2})^{-1}$, larger than suggested by multi-model projections of either past glacial tropical sensitivity or future tropical sensitivity to doubled CO_2 concentrations. It also shows that a pre-exponential dissolution correction is necessary for accurate reconstructions of past temperature using Mg/Ca ratios from foraminifera. Methodology to construct tropical Pacific temperature records using Mg/Ca in foraminifera will benefit from a more comprehensive core-top calibration from the region, including a greater range of shallow (<1500m) core-top Mg/Ca data.

Past climate sensitivity calculated in this study focuses on tropical regions and does not represent global equilibrium climate sensitivity. Global and high latitude climate sensitivities are thought to be larger than that in the tropics (e.g. Holland and Bitz, 2003) due to extreme amplification of climate perturbations where ice-albedo feedbacks operate. Since tropical SSTs are expected to be less responsive to GHG forcing than high-latitude SST, our tropical equilibrium sensitivity estimates (3.5 – 3.9 ^{o}C for a doubling of CO_2) may be a lower bound for long-term global climate sensitivity.

ACKNOWLEDGEMENTS

This research was supported by the Schlanger Fellowship from the Consortium for Ocean Leadership and by National Science Foundation grant # OCE-0902047. We thank the Ocean Drilling Program for providing sample access, Jessica Macias and Victor Castro for assistance in sample processing, and two anonymous reviewers for constructive comments.

FIGURES

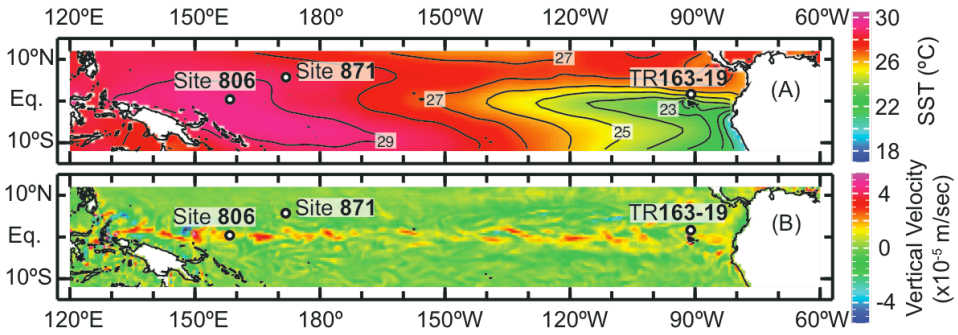

Figure 4.1: Location map for three core locations: ODP Site 806, ODP Site 871, and core TR163-19. Mapped are (A) modern average SST (Locarnini et al., 2010) and (B) vertical velocity at 25m water depth for the month of July 2000 (Carton and Giese, 2008).

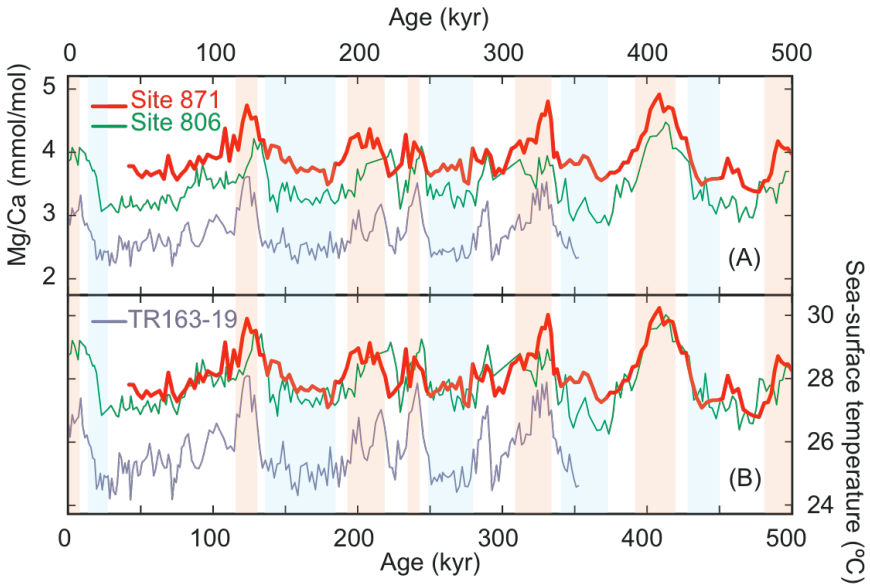

Figure 4.2: Mg/Ca and SST records from equatorial Pacific sites, ODP Site 806 (Medina-Elizalde and Lea, 2005), TR163-19 (Lea et al., 2000) and ODP Site 871 (this study). (A) Measured Mg/Ca records. (B) SST calculated with new pre-exponential dissolution correction. Blue and red bars are glacial and interglacial periods, respectively. The sedimentation rate for this core is 1.0 (± 0.1) cm/ky.

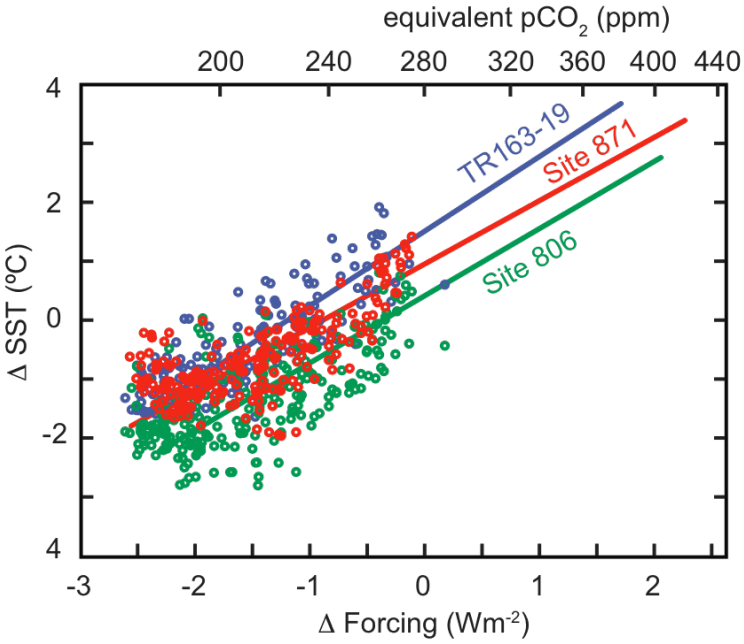

Figure 4.3: Past climate sensitivity to changes in GHG forcing. The regression for Site 871 is $\Delta T = 1.06(\pm 0.05) * \Delta RF + 0.91(\pm 0.08)$, $r^2=0.53$, for Site 806 is $\Delta T = 1.12(\pm 0.05) * \Delta RF + 0.38(\pm 0.09)$, $r^2=0.47$, and for site TR163-19 is $\Delta T = 1.25(\pm 0.05) * \Delta RF + 1.48(\pm 0.09)$, $r^2=0.70$.

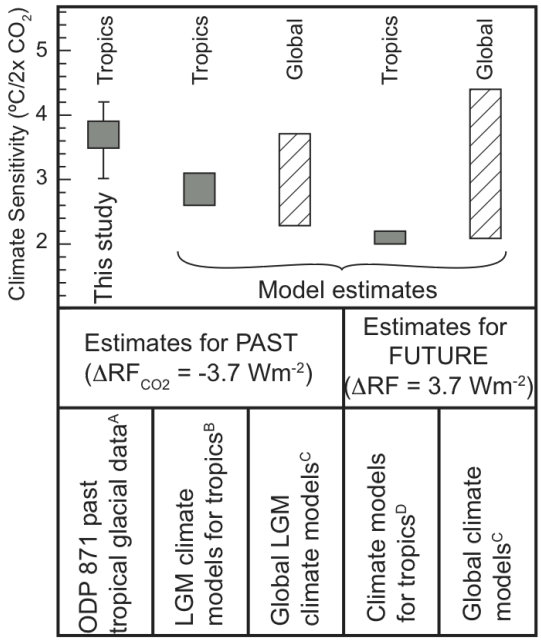

Figure 4.4: Comparison of climate sensitivity results from this study (paleoclimate data) with tropical and global modeling results for the LGM and future warming. (A) This study (with uncertainties), (B) Otto-Bliesner et al., (2009), (C) IPCC, (2007), (D) DiNezio et al., (2009).

SUPPLEMENTAL MATERIAL

Primary data for this study are from Ocean Drilling Program (ODP) Site 871 at the Limilok Guyot (5°33.13'N, 172°20.66'E, water depth 1255m, (Shipboard Scientific Party, 1993)). The site has a modern annual average SST of 28.8°C (Locarnini et al., 2010). One sample was taken every 3 cm downcore; ~40-60 *Globigerinoides ruber* (white) tests and 1-5 *Uvigerina spp.* tests were picked from the 250-355 μm size fraction of each sample.

Samples of the surface mixed-layer foraminifer *G. ruber* were cleaned following established protocols including oxidation and reduction steps (e.g. Boyle and Keigwin, 1985; Mashiotta et al., 1999) just as in other studies (Dekens et al., 2002; Lea et al., 2000; Medina-Elizalde and Lea, 2005). Mg/Ca ratios were measured using an ICP-OES at the University of California Santa Cruz; 1-σ standard deviation for repeated measurements of an internal foraminifera reference standard is 0.21 mmol/mol, or ~0.5 C°.

Dissolution Correction

Carbonate shells preferentially lose high-Mg calcite to dissolution with depth; thus a dissolution correction for Mg/Ca must be applied to reconstruct the accurate range of tropical SST (e.g. Brown and Elderfield, 1996; Rosenthal et al., 2000). Since dissolution lowers the Mg/Ca value of the shell and the resulting temperature, one

common method to correct for dissolution is to add a specified term to the temperature, depending on the degree of dissolution, commonly associated with the depth of the sediment core (Dekens et al., 2002). For example, applying a correction for dissolution to the published Mg/Ca-based temperature record from ODP Site 806 (Medina-Elizalde and Lea, 2005) using this method (Dekens et al., 2002) produces the range in temperature shown in Fig. 4.5-A. Since dissolution affects the Mg/Ca values of the shell, and not the temperature directly, it is more appropriate to correct the Mg/Ca value for dissolution first, before using the exponential relationship (between Mg/Ca and temperature) to estimate temperature, similar in theory to that suggested by Rosenthal et al. (2002).

Our new dissolution correction is applied to measured Mg/Ca values in order to estimate the original surface Mg/Ca value before dissolution occurs at depth. We established a regional depth-based dissolution correction from published modern annual average SST and core top Mg/Ca data (Broecker and Peng, 1982; Lea et al., 2000; Dekens et al., 2002) from the tropical Pacific warm pool region and create a linear (r^2=0.93) correction for dissolution with depth (Fig. 4.5-B) assuming that core-top planktonic foraminifera formed in waters directly over the core location at modern SST. Cold tongue values were excluded since dissolution within the sediments likely increases with large differences in organic matter productivity. While a linear relationship may be an oversimplification, it is a reasonable estimation over

the given range of ocean depths and data available. The 'residual' Mg/Ca is calculated from the difference between the calculated and measured Mg/Ca values of *G. ruber* from each core top. For each coretop location, the surface Mg/Ca value was calculated using the modern surface temperature (Locarnini et al., 2010) and the Anand et al. (2003) equation of Mg/Ca = 0.38 e^[0.09*SST]. This equation is indistinguishable from the Dekens et al. (2002) equation at zero water depth. The Mg/Ca (residual) represents the shift in Mg/Ca value that occurs due to dissolution. A simple linear regression against water depth (Fig. 4.5B), with errors, yields:

$$Mg/Ca(residual) = 0.26(\pm 0.03) * Depth(km) + 0.54(\pm 0.08)$$

The y-intercept of 0.54 (±0.08) implies that if we extrapolate the regression to the sea surface (zero water depth) there is significant dissolution, which contradicts the idea that dissolution is only a serious problem at depths close to the lysocline and below (Sadekov et al., 2010). However, the shallowest of the sites used in this calibration is 1.6 km; deeper than 1.6 km, the linear regression is constrained by the calibration data, but above 1.6 km, dissolution must actually decrease more quickly, perhaps non-linearly, than the regression fit implies. Thus, the application of this formula to shallow sites must be approached with caution (as explained in more detail below). We use this linear regression formula to develop a complete equation for sea-surface paleotemperature using the depth-based dissolution correction of sediment Mg/Ca to surface Mg/Ca and the exponential Mg/Ca-temperature relationship (Anand et al., 2003). The complete equation for sea-surface paleotemperature, including errors, is:

$$SST = \frac{\ln(\frac{Mg/Ca(surf.)}{0.38(\pm 0.02)})}{0.090(\pm 0.003)}, \qquad \text{where}$$

$$Mg/Ca(surf.) = Mg/Ca(measured) + 0.26(\pm 0.03) * Depth(km) + 0.54(\pm 0.08)$$

or, for an overall equation for Mg/Ca:

$$Mg/Ca_{ruber}(mmol/mol) = -0.26(\pm 0.03) * Depth(km) - 0.54(\pm 0.08) + 0.38(\pm 0.02) * e^{0.09(\pm 0.003)*T}$$

Conceptually, this dissolution correction shifts the exponential Mg/Ca-temperature calibration curve vertically (lower) through Mg/Ca-SST-space rather than adding a (horizontal) constant temperature correction as in previous work (Fig. 4.5-D). When uncertainties in the depth-dissolution regression are propagated in the temperature calibration, the dissolution correction could add up to 1.3 C° of uncertainty to the SST calculation. In this study the dissolution correction is assumed to be unchanging through time and shifts all temperature estimates by approximately the same amount. Further work is warranted to minimize this uncertainty at shallow water depths.

Since the calibration equation derived above is based on coretop data from sites that are deeper than 1.6 km, the question is: How should we then apply this calibration to data from ODP Site 871, which has a shallower water depth of 1.3 km? Our preferred method is conservative, and simply uses the original linear regression and extrapolates the core-top calibration from 1.6 km to 1.3 km water depth (Fig. 4.5B). This method results in smaller amplitudes of SST (Fig. 4.5-C) compared to the traditional method where an offset correction is applied to the SST values (e.g. Dekens et al., 2007 Fig. 4.5-A). Furthermore, compared to other methods explained below to

extrapolate the calibration to 1.3 km, this conservative method using our new calibration yields the lowest climate sensitivity values (open square in Fig. 4.5-B).

Another approach to extrapolating the calibration to the depth of our core site (1.3 km) assumes that the Mg/Ca offset at zero water depth is zero (Fig. 4.5B). At one extreme, this is represented by a second regression from the shallowest depth at which there is calibration data (1.6 km) and through the origin (though the artificial sudden change in slope at 1.6 km water depth seems unlikely). This yields corrected Mg/Ca values that are 0.14 mmol/mol higher than the first approach. This small difference is within the measured Mg/Ca error, suggesting that the original calibration is sufficient for this depth.

At the opposite extreme, we can assume that there was no dissolution shallower than 1.6 km (Fig. 4.5B). In this case there would be no dissolution correction at ODP site 871. The resulting climate sensitivity estimates would then be higher than any formulation that attempts to correct for dissolution ($\lambda = 1.29$ °C $(W\,m^{-2})^{-1}$), and the estimates of previous interglacial temperatures in the western Pacific would be consistently ~2 C° cooler than modern, rendering this scenario unlikely.

The dissolution calibration also depends on the paleotemperature equation used to calculate surface Mg/Ca (from which the residual is calculated, Figure S1B). We tried

7 different equations (Anand et al., 2003; Elderfield and Ganssen, 2000; Hastings et al., 2001; Hendry et al., 2009; McConnell and Thunell, 2005; Pak et al., 2004; Regenberg et al., 2009), though most cluster around the original Anand equation. Equations that do not correct for dissolution result in cooler absolute temperatures, higher glacial-interglacial amplitude of change, and higher climate sensitivity, compared to our new calibration that corrects for significant dissolution.

Overall, directly applying our new calibration equation, which assumes that the Mg/Ca-residual due to dissolution changes linearly with depth (Fig. 4.5B) and extrapolates that linear relationship to 1.2 km (the depth of ODP Site 871), produces the lowest climate sensitivity values compared to other methods that either ignore dissolution or correct for dissolution using a different approach. Even these lowest estimates of climate sensitivity are higher than those predicted by models; this main point is a robust result that is not undermined by uncertainties in the dissolution correction.

In general, our new calibration has the overall effect of, given a change in measured Mg/Ca values, reducing the calculated amplitude of SST compared to the commonly used correction (Dekens et al., 2002). This difference between the dissolution corrections becomes greater at deeper water depths (Fig. 4.6). Overall, our new Mg-based dissolution-corrected temperature record demonstrates the smaller amplitude

of glacial-interglacial temperature change compared to other calibrations when applied to Mg/Ca records in the tropics.

When our new Mg-based dissolution correction is applied to existing long Mg/Ca records from the tropical Pacific (Site 806B and TR163-19) the resulting cold glacial temperatures are warmer than previous studies suggested while the interglacial temperatures are relatively unchanged (Fig. 4.7) from published temperature estimates (Lea, 2004; Medina-Elizalde and Lea, 2005).

For this study we use the foraminifera species *Globigerinoides ruber* (white). No differentiation was made among morphotypes of *G. ruber*, though small differences have been shown to exist in Mg/Ca-SST calibrations (Steinke et al., 2005). This choice is reasonable given the morphotypes of *G. ruber* are gradational (Sadekov et al., 2008) and temperature differences among morphotypes are likely to be small (Bolton et al., 2011) in areas with a deep thermocline and minimal upwelling.

Tropical climate sensitivity error calculations

Tropical climate sensitivity is determined by comparing the forcing associated with greenhouse gas concentrations (CO_2 and CH_4) and the change in temperature at tropical ODP Site 871 (Fig. 4.8). The correlation coefficient (Pearson's r) for the Site 871 temperature record and the atmospheric CO_2 record is 0.74 while the correlation

for the Site 871 temperature record and the atmospheric CH_4 record is 0.67. Comparison of this climate sensitivity parameter with models is made in the text under the Results and Discussion section. Error in the climate sensitivity parameter incorporates 95% confidence intervals in the dissolution correction and the RMA regressions of ΔSST and ΔRF. The 95% confidence interval for the resulting climate sensitivity parameter is 0.82 – 1.11 $^{o}C\ (W\ m^{-2})^{-1}$) and for the climate sensitivity (Fig. 4.4) is 3.03 - 4.12 C^{o}. The non-zero intercept in each regression (Fig. 4.3) is due to past interglacial timeperiods that were slightly warmer than pre-industrial temperatures (Lea, 2004; Hansen and Sato, 2011).

The role of dynamics

While some small amount of surface temperature change at Site 871 may be due to shifts in the local temperature gradients, it is unlikely that local dynamics could have much of an impact on SST since the gradients in the western Pacific warm pool are weak, less than 1^{o}C change over 6^{o} of latitude (670 km). Furthermore, during the glacial periods, SST at Site 871 was warmer than at Site 806; a reversal in the direction of the gradient between the two sites cannot be explained by expansion or contraction of modern gradients. Rather it implies that dynamics, such as upwelling, may have cooled temperatures at equatorial Site 806 slightly during glacial periods. Cooler temperatures at Site 806 on the equator may support the notion that Site 871 is a

more ideal location for examining western Pacific warm pool heat flux adjustments to radiative forcing.

Radiative forcing calculations

For carbon dioxide, we use (Ramaswamy et al., 2001):

$\Delta F_{CO2} = 4.841 \ln ([CO_2]/[CO_2]_0) + 0.0906 (\sqrt{[CO_2]} - \sqrt{[CO_2]_0})$.

For methane, we use (Ramaswamy et al., 2001):

$\Delta F_{CH4} = 0.036 (\sqrt{[CH_4]} - \sqrt{[CH4]_0}) -$

$[0.47 \ln\{1 + 2.01x10^{-5} ([CH_4] [N_2O]_0)^{0.75} + 5.31x10^{-15} [CH_4] ([CH_4] [N_2O]_0)^{1.52}\}] -$

$[0.47 \ln\{1 + 2.01x10^{-5} ([CH_4]_0 [N_2O]_0)^{0.75} + 5.31x10^{-15} [CH_4]_0 ([CH4]_0 [N_2O]_0)^{1.52}\}]$

where $[CO_2]_0 = 280$ ppmv, $[CH_4]_0 = 700$ ppb, and $[N_2O]_0 = 280$ ppb.

The total radiative forcing is $\Delta F_{TOT} = \Delta F_{CO2} + \Delta F_{CH4}$. As in other studies (Lea, 2004), past changes in N_2O are ignored since N_2O has a relatively small radiative influence and lacks a continuous record.

Timescale

Each Mg/Ca record treated in this study is associated with a benthic $\delta^{18}O$ record at a similar resolution from the same core. Modern bottom-water temperature at Site 871

is 3.5°C, salinity 34.5 (Locarnini et al., 2010). These $\delta^{18}O$ records covary in time and space and are aligned with a global 'stack' of benthic $\delta^{18}O$ data. For this study, we generated the benthic $\delta^{18}O$ record for Site 871 using *Uvigerina spp*. from the same samples and size fraction as the Site 871 temperature record. From the 250-355 μm size fraction, 1-3 individual shells were analyzed, at a resolution of one sample every 3 cm. Samples were analyzed at the University of California Stable Isotope Laboratory using a Fisons PRISM mass spectrometer with a common acid bath carbonate preparation system. Standard error for 46 measurements of an internal CM05 $\delta^{18}O$ standard was ±0.05‰. The benthic $\delta^{18}O$ data from Site 806 and TR163-19 is from *Uvigerina spp.* and *C. wuellerstorfi* from previous studies (Bickert et al., 1993; Lea et al., 2002) at a similar temporal resolution. Site-specific benthic $\delta^{18}O$ records were visually aligned (Fig. 4.9) with a common timescale using glacial and interglacial maxima (Lisiecki and Raymo, 2005) with only small corrections in alignment with Analyseries software (Palliard et al., 1996).

On average the Site 871 temperature record seems to lead global benthic $\delta^{18}O$ (LR04 stack) by about 9(± 2) kyr at the 100-kyr frequency. At other frequencies there does not appear to be any lead between the signals. The temperature lead varies among terminations: at T-II (~130 kya) SST leads, though at other terminations SST and the benthic $\delta^{18}O$ stack covary. The early temperature increase in MIS 6 is also seen at other west Pacific sites (e.g. de Villiers, 2003). The out-of-phase behavior between SST

and benthic $\delta^{18}O$ record is inconsequential to our calculation of climate sensitivity since we are comparing SST and CO_2 records which are in-phase within error at orbital frequencies. The fact that all three approaches for calculating climate sensitivity provide the same result within error further suggests that the correlation with CO_2 is good. To check this observation, we also removed the data prior to 150 ka, retaining the parts of the Site 871 SST record that look similar to more common tropical sites, and re-calculated the sensitivity. The result is $\lambda = 1.08$ °C $(W\,m^{-2})^{-1}$, the same result as when data from Termination II is included, within error.

Regression

The relationships for regression through temperature and radiative forcing data are developed using the Reduced Major Axis (RMA) approach (1000 iterations, Sokal and Rohlf, 2011) which is reasonable when the independent variable x is measured with error (Fig. 4.10).

SUPPLEMENTARY FIGURES

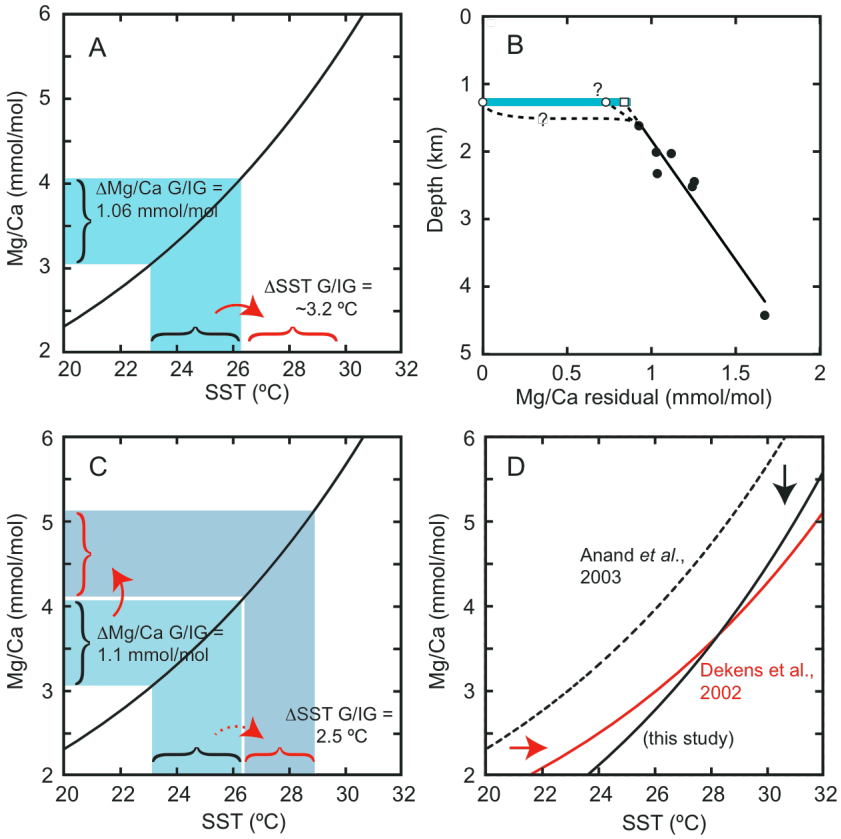

Figure 4.5: Comparison of calibration techniques using Site 806B *G. ruber* Mg/Ca record (Medina-Elizalde and Lea, 2005), which has a glacial-interglacial (G-IG) amplitude of 1.06 mmol/mol as an example. (A) Previous calibration technique correcting temperatures for dissolution by adding an offset to the derived temperature (Dekens et al., 2002) results in a G-IG amplitude of 3.2 C°. (B) The relationship between water depth and Mg/Ca residual, from core top data (filled circles) outside the Cold Tongue where dissolution may be greater. The relationship is $Mg/Ca_{residual}$ = 0.26 (±0.03)*Depth(km) + 0.54 (±0.08). R^2 = 0.93. Core top data and locations are presented in Dekens et al. (2002), Tables 1 and 4. The equation is extrapolated 12% beyond the shallowest core to the depth of Site 871 (open square). Open circles are possibilities that cannot be eliminated, though each produces even higher climate sensitivity and greater data-model mismatch. (C). The new calibration, derived in this study, to correct Mg/Ca for dissolution first before calculating paleotemperature, results in a G-IG amplitude of 2.5 C°. (D) The calibration for this study shifts the surface Mg/Ca-temperature curve vertically while other calibrations appear to shift the curve horizontally.

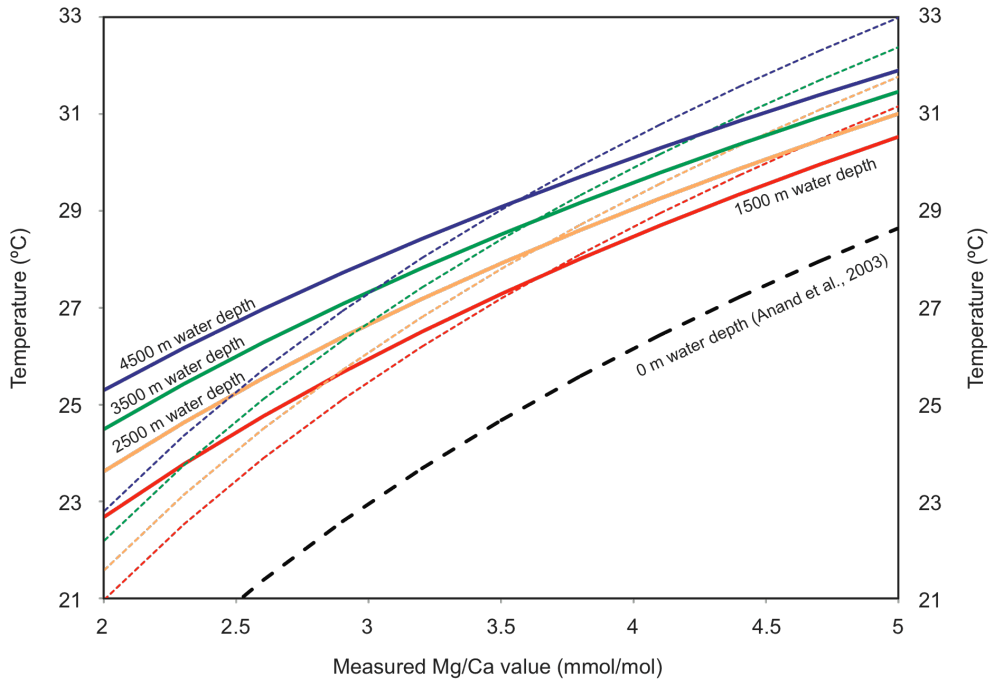

Figure 4.6: Comparison of Mg/Ca-corrected calibration (this study, solid lines) and previous calibration (Dekens et al., 2002). Using the new Mg-based dissolution correction results in a smaller range of tropical Pacific glacial-interglacial temperatures for cores at any depth.

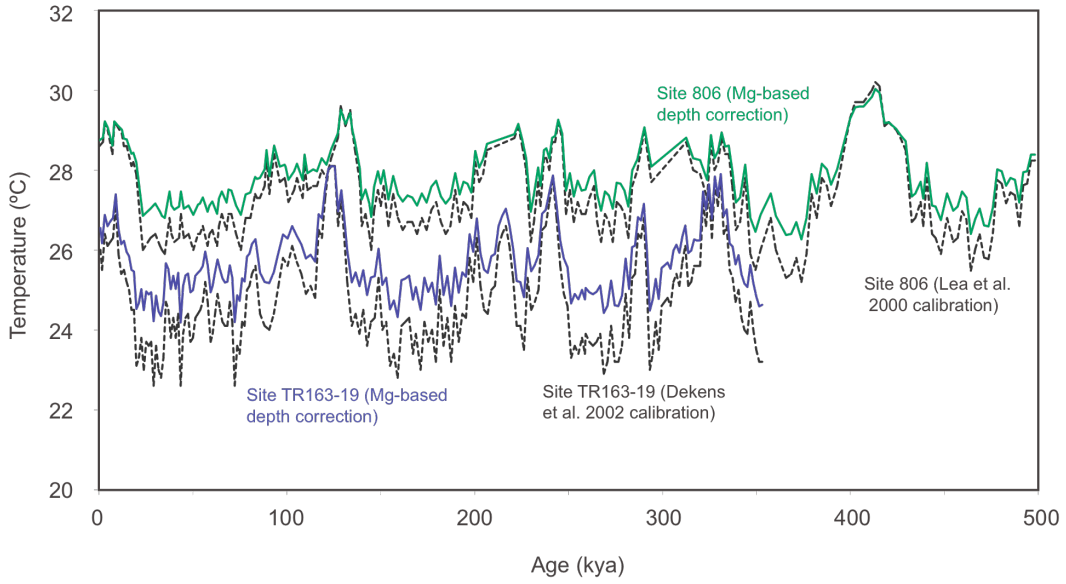

Figure 4.7: Existing Mg/Ca records (Medina-Elizalde and Lea, 2005; Lea et al., 2000; black lines) corrected using the Mg-based dissolution correction as described (solid lines). In general, our new calibration shifts glacial temperatures toward warmer values, while interglacials remain unchanged.

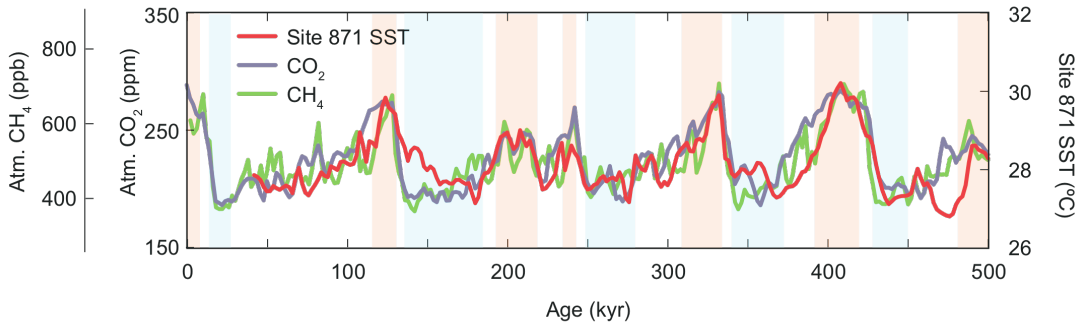

Figure 4.8: Site 871 SST compared through time with atmospheric greenhouse gas concentrations. Blue and red vertical bars are glacial and interglacial times, respectively.

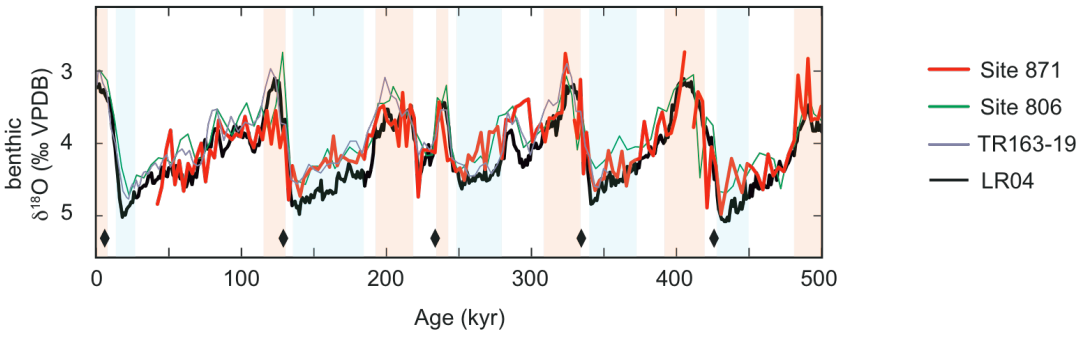

Figure 4.9: Benthic $\delta^{18}O$ records measured from Site 871, Site 806, and TR163-19 mentioned in the text compared to a global stack (Lisiecki and Raymo, 2005) for temporal alignment and age determination. Blue and red vertical bars are glacial and interglacial times, respectively. The correlation coefficient (Pearson's r) for the Site 871 benthic $\delta^{18}O$ record and the benthic LR04 stack is 0.79. Tie points are indicated by black diamonds.

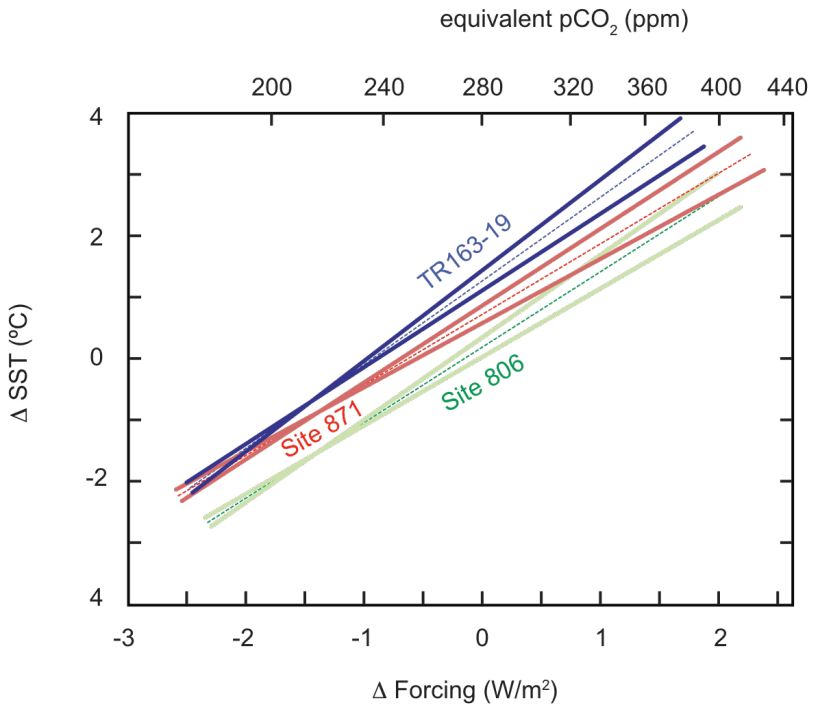

Figure 4.10: Regressions through data from TR163-19, Site 871, and Site 806 with regression errors plotted.

	Glacial or Interglacial period	
	Termination (kya)	Inception (kya)
Stage 1	0	11
Stage 2	17	28
Stage 5e	114	130
Stage 6	135	185
Stage 7(a)	192	220
Stage 7(b)	234	243
Stage 8	248	280
Stage 9	308	334
Stage 10	340	373
Stage 11	391	421
Stage 12	428	472
Stage 13	482	498

Table 4.1: Glacial and Interglacial periods visually identified from global benthic oxygen-isotope stack (Lisiecki and Raymo, 2005).

REFERENCES

Anand, P., Elderfield, H., and Conte, M.H., 2003, Calibration of Mg/Ca thermometry in planktonic foraminifera from a sediment trap time series: Paleoceanography, v. 18, no. 2, doi: 10.1029/2002PA000846.

Andreasen, D., and Ravelo, A., 1997, Tropical Pacific Ocean thermocline depth reconstructions for the last glacial maximum: Paleoceanography, v. 12, no. 3, p. 395–413.

Bickert, T., Berger, W., Burke, S., and Schmidt, H., 1993, Late Quaternary stable isotope record of Cibicidoides wuellerstorfi from the Ontong Java Plateau: en.scientificcommons.org.

Bolton, A., Baker, J.A., Dunbar, G.B., Carter, L., Smith, E.G.C., and Neil, H.L., 2011, Environmental versus biological controls on Mg/Ca variability in Globigerinoides ruber(white) from core top and plankton tow samples in the southwest Pacific Ocean: Paleoceanography, v. 26, no. 2, p. PA2219, doi: 10.1029/2010PA001924.

Boyle, E., and Keigwin, L., 1985, Comparison of Atlantic and Pacific paleochemical records for the last 215,000 years: Changes in deep ocean circulation and chemical inventories: Earth and Planetary Science Letters, v. 76, no. 1-2, p. 135–150.

Broecker, W.S., and Peng, T.H., 1982, Tracers in the Sea: Lamont-Doherty Geological Observatory, Palisades, NY.

Brown, S., and Elderfield, H., 1996, Variations in Mg/Ca and Sr/Ca ratios of planktonic foraminifera caused by postdepositional dissolution: Evidence of shallow Mg-dependent dissolution: Paleoceanography, v. 11, no. 5, p. 543–551.

Carton, J.A., and Giese, B.S., 2008, A Reanalysis of Ocean Climate Using Simple Ocean Data Assimilation (SODA): Monthly weather review, v. 136, no. 8, p. 2999–3017, doi: 10.1175/2007MWR1978.1.

Crucifix, M., 2006, Does the Last Glacial Maximum constrain climate sensitivity?: Geophysical Research Letters, v. 33, no. 18, doi: 10.1029/2006GL027137.

de Villiers, S., 2003, Dissolution effects on foraminiferal Mg/Ca records of sea surface temperature in the western equatorial Pacific: Paleoceanography, v. 18, no. 3, doi: 10.1029/2002PA000802.

Dekens, P., Lea, D., Pak, D., and Spero, H., 2002, Core top calibration of Mg/Ca in tropical foraminifera: Refining paleotemperature estimation: Geochemistry Geophysics Geosystems, v. 3, p. 1022, doi: 10.1029/2001GC000200.

Dekens, P.S., Ravelo, A.C., and Mccarthy, M.D., 2007, Warm upwelling regions in the Pliocene warm period: Paleoceanography, v. 22, no. 3, p. PA3211, doi: 10.1029/2006PA001394.

Delworth, T., Broccoli, A., Rosati, A., Stouffer, R., Balaji, V., Beesley, J., Cooke, W., Dixon, K., Dunne, J., and Dunne, K., 2006, GFDL's CM2 global coupled climate models. Part I: Formulation and simulation characteristics: Journal of Climate, v. 19, no. 5, p. 643–674.

DiNezio, P.N., Clement, A.C., Vecchi, G.A., Soden, B.J., Kirtman, B.P., and Lee, S.-K., 2009, Climate Response of the Equatorial Pacific to Global Warming: Journal of Climate, v. 22, no. 18, p. 4873–4892, doi: 10.1175/2009JCLI2982.1.

Elderfield, H., and Ganssen, G., 2000, Past temperature and δ18O of surface ocean waters inferred from foraminiferal Mg/Ca ratios: Nature, v. 405, no. 6785, p. 442–445.

Hansen, J., and Sato, M., 2011, Paleoclimate Implications for Human-Made Climate Change, *in* Berger, A., Mesinger, F., and Šijači, D. eds. Climate Change at the Eve of the Second Decade of the Century: Inferences from Paleoclimate and Regional Aspects: Proceedings of the Milutin Milankovitch 130th Anniversary Symposium, Springer, p. 1–32.

Hartmann, D.L., 1994, Global Physical Climatology: Academic Press, San Diego, CA.

Hastings, D., Kienast, M., Steinke, S., and Whitko, A., 2001, A comparison of three independent paleotemperature estimates from a high resolution record of deglacial SST records in the tropical South China Sea: Eos Trans. AGU, v. 82, no. 47.

Hendry, K.R., Rickaby, R.E.M., Meredith, M.P., and Elderfield, H., 2009, Controls on stable isotope and trace metal uptake in Neogloboquadrina pachyderma (sinistral) from an Antarctic sea-ice environment: Earth and Planetary Science Letters, v. 278, no. 1-2, p. 67–77, doi: 10.1016/j.epsl.2008.11.026.

Holland, M.M., and Bitz, C.M., 2003, Polar amplification of climate change in coupled models: Climate Dynamics, v. 21, no. 3-4, p. 221–232, doi: 10.1007/s00382-003-0332-6.

IPCC, 2007, Climate Change 2007: The Physical Science Basis. Contributions of

Working Group I to the Fourth Assessment Report of the Intergovernmental Panel on Climate Change (S. Solomon, D. Qin, M. Manning, Z. Chen, M. Marquis, K. Averyt, & M. Tignor, Eds.): Cambridge University Press, United Kingdom and New York, NY USA.

Jackson, C.S., and Broccoli, A.J., 2003, Orbital forcing of Arctic climate: mechanisms of climate response and implications for continental glaciation: Climate Dynamics, v. 21, no. 7-8, p. 539–557, doi: 10.1007/s00382-003-0351-3.

Knutti, R., and Hegerl, G.C., 2008, The equilibrium sensitivity of the Earth's temperature to radiation changes: Nature Geoscience, v. 1, no. 11, p. 735–743, doi: 10.1038/ngeo337.

Koutavas, A., and Lynch-Stieglitz, J., 2003, Glacial-interglacial dynamics of the eastern equatorial Pacific cold tongue-Intertropical Convergence Zone system reconstructed from oxygen isotope records: Paleoceanography, v. 18, no. 4, p. 1089, doi: 10.1029/2003PA000894.

Lea, D., 2004, The 100 000-yr cycle in tropical SST, greenhouse forcing, and climate sensitivity: Journal of Climate, v. 17, no. 11, p. 2170–2179.

Lea, D., Martin, P., Pak, D., and Spero, H., 2002, Reconstructing a 350 ky history of sea level using planktonic Mg/Ca and oxygen isotope records from a Cocos Ridge core: Quaternary Science Reviews, v. 21, no. 1-3, p. 283–293.

Lea, D., Pak, D., and Spero, H., 2000, Climate impact of late Quaternary equatorial Pacific sea surface temperature variations: Science, v. 289, no. 5485, p. 1719.

Lee, S.-Y., and Poulsen, C.J., 2005, Tropical Pacific climate response to obliquity forcing in the Pleistocene: Paleoceanography, v. 20, no. 4, p. PA4010, doi: 10.1029/2005PA001161.

Lisiecki, L.E., and Raymo, M.E., 2005, A Pliocene-Pleistocene stack of 57 globally distributed benthic $\delta^{18}O$ records: Paleoceanography, v. 20, no. 1, p. PA1003, doi: 10.1029/2004PA001071.

Locarnini, R., Mishonov, A., Antonov, J., Boyer, T., Garcia, H., Baranova, O., Zweng, M., and Johnson, D., 2010, World Ocean Atlas 2009, *in* Levitus, S. ed. NOAA Atlas NESDIS 68, U.S. Government Printing Office, Washington, D.C.

Loulergue, L., Schilt, A., Spahni, R., Masson-Delmotte, V., Blunier, T., Lemieux, B., Barnola, J.-M., Raynaud, D., Stocker, T.F., and Chappellaz, J., 2008, Orbital and millennial-scale features of atmospheric CH4 over the past 800,000□years: Nature, v. 453, no. 7193, p. 383–386, doi: 10.1038/nature06950.

Mashiotta, T., Lea, D., and Spero, H., 1999, Glacial-interglacial changes in Subantarctic sea surface temperature and [delta] 18O-water using foraminiferal Mg: Earth and Planetary Science Letters, v. 170, no. 4, p. 417–432.

McConnell, M.C., and Thunell, R.C., 2005, Calibration of the planktonic foraminiferal Mg/Ca paleothermometer: Sediment trap results from the Guaymas Basin, Gulf of California: Paleoceanography, v. 20, no. 2, doi: 10.1029/2004PA001077.

Medina-Elizalde, M., and Lea, D., 2005, The mid-Pleistocene transition in the Tropical Pacific: Science, v. 310, no. 5750, p. 1009.

Mix, A.C., Bard, E., and Schneider, R., 2001, Environmental processes of the ice age: land, oceans, glaciers (EPILOG): Quaternary Science Reviews, v. 20, no. 4, p. 627–657.

Otto-Bliesner, B.L., Schneider, R., Brady, E.C., Kucera, M., Abe-Ouchi, A., Bard, E., Braconnot, P., Crucifix, M., Hewitt, C.D., Kageyama, M., Marti, O., Paul, A., Rosell-Melé, A., Waelbroeck, C., et al., 2009, A comparison of PMIP2 model simulations and the MARGO proxy reconstruction for tropical sea surface temperatures at last glacial maximum: Climate Dynamics, v. 32, no. 6, p. 799–815, doi: 10.1007/s00382-008-0509-0.

Pak, D.K., Lea, D.W., and Kennett, J.P., 2004, Seasonal and interannual variation in Santa Barbara Basin water temperatures observed in sediment trap foraminiferal Mg/Ca: Geochemistry Geophysics Geosystems, v. 5, p. Q12008.

Palliard, D., Labeyrie, L., and Yiou, P., 1996, Macintosh program performs time-series analysis: Eos Trans. AGU 77, 379 p.

Ramaswamy, V., Boucher, O., Haigh, J., Hauglustaine, D., Haywood, J., Myhre, G., Nakajima, T., Shi, G., Solomon, S., and Betts, R., 2001, Radiative forcing of climate change:.

Regenberg, M., Steph, S., Nürnberg, D., Tiedemann, R., and Garbe-Schönberg, D., 2009, Calibrating Mg/Ca ratios of multiple planktonic foraminiferal species with δ18O-calcification temperatures: Paleothermometry for the upper water column: Earth and Planetary Science Letters, v. 278, no. 3-4, p. 324–336, doi: 10.1016/j.epsl.2008.12.019.

Rohling, E.J., Medina-Elizalde, M., Shepherd, J.G., Siddall, M., and Stanford, J.D., 2012, Sea Surface and High-Latitude Temperature Sensitivity to Radiative Forcing of Climate over Several Glacial Cycles: Journal of Climate, v. 25, no. 5, p. 1635–1656, doi: 10.1175/2011JCLI4078.1.

Rosenthal, Y., and Lohmann, G.P., 2002, Accurate estimation of sea surface temperatures using dissolution-corrected calibrations for Mg/Ca paleothermometry: Paleoceanography, v. 17, no. 3, p. 1044.

Rosenthal, Y., Lohmann, G., Lohmann, K., and Sherrell, R., 2000, Incorporation and preservation of Mg in Globigerinoides sacculifer: Implications for reconstructing the temperature and 18O/16O of seawater: Paleoceanography, v. 15, no. 1, p. 135–145.

Sadekov, A., Eggins, S.M., De Deckker, P., and Kroon, D., 2008, Uncertainties in seawater thermometry deriving from intratest and intertest Mg/Ca variability in Globigerinoides ruber: Paleoceanography, v. 23, no. 1, doi: 10.1029/2007PA001452.

Sadekov, A.Y., Eggins, S.M., Klinkhammer, G.P., and Rosenthal, Y., 2010, Effects of seafloor and laboratory dissolution on the Mg/Ca composition of Globigerinoides sacculifer and Orbulina universa tests — A laser ablation ICPMS microanalysis perspective: Earth and Planetary Science Letters, v. 292, no. 3-4, p. 312–324, doi: 10.1016/j.epsl.2010.01.039.

Schmittner, A., Urban, N., Shakun, J., and Mahowald, N., 2011, Climate Sensitivity Estimated from Temperature Reconstructions of the Last Glacial Maximum: Science.

Shipboard Scientific Party, 1993, Site 871, *in* Silva, P.I., Haggerty, J., and Rack, R. eds. Proceedings of the Ocean Drilling Program, Initial Reports, Vol. 144, Ocean Drilling Program, p. 105–144.

Siegenthaler, U., Stocker, T., Monnin, E., Lüthi, D., Schwander, J., Stauffer, B., Raynaud, D., Barnola, J., Fischer, H., and Masson-Delmotte, V., 2005, Stable carbon cycle–climate relationship during the late Pleistocene: Science, v. 310, no. 5752, p. 1313.

Sokal, R.R., and Rohlf, F.J., 2011, Biometry: The Principles and Practices of Statistics in Biological Research: W. H. Freeman, New York, NY.

Steinke, S., Chiu, H.-Y., Yu, P.-S., Shen, C.-C., Löwemark, L., Mii, H.-S., and Chen, M.-T., 2005, Mg/Ca ratios of two Globigerinoides ruber(white) morphotypes: Implications for reconstructing past tropical/subtropical surface water conditions: Geochemistry Geophysics Geosystems, v. 6, no. 11, p. Q11005, doi: 10.1029/2005GC000926.

Waelbroeck, C., Paul, A., Kucera, M., Rosell-Melé, A., Weinelt, M., Schneider, R., Mix, A.C., Abelmann, A., Armand, L., Bard, E., Barker, S., Barrows, T.T., Benway,

H., Cacho, I., et al., 2009, Constraints on the magnitude and patterns of ocean cooling at the Last Glacial Maximum: Nature Geoscience, v. 2, no. 2, p. 127–132, doi: 10.1038/ngeo411.

Yue, X., Wang, H., Liao, H., and Jiang, D., 2011, Simulation of the Direct Radiative Effect of Mineral Dust Aerosol on the Climate at the Last Glacial Maximum: Journal of Climate, v. 24, no. 3, p. 843–858, doi: 10.1175/2010JCLI3827.1.

5. PLEISTOCENE EVOLUTION OF THE TROPICAL PACIFIC WARM POOL

Abstract

The temperature of the western equatorial Pacific warm pool impacts meridional and zonal atmospheric circulation; therefore, accurate warm pool surface paleotemperatures are critical for estimating the magnitude of zonal and meridional heat transport and testing models of past climate change. Here we use the Mg/Ca value of *G. ruber* to reconstruct past sea surface temperature (SST) from the margin (~5°N) of the modern western Pacific warm pool (represented by ODP Site 871) from the period 0-1.5 Ma. We contrast this record with an existing sea-surface temperature (SST) record on the equator in the warm pool in order to determine mean annual sea-surface temperature (SST) gradients between the center and northeast margin of the warm pool on glacial-interglacial timescales. The reconstructed gradient is similar to the modern gradient during past interglacial intervals; however, during many past glacial intervals, this gradient is reversed: cooler temperatures are recorded at the equator than at the marginal site, consistent with cooler waters upwelling from an elevated thermocline along the equator. The evolution of peak glacial and interglacial SST of available tropical temperature records further demonstrates early Pleistocene intensification of Walker circulation and the subsequent stabilization of zonal tropical temperature gradients after the mid-Pleistocene transition.

1. Introduction

The heat content of the tropical Pacific affects global atmospheric and oceanic convection and climate patterns throughout the North Pacific region and beyond [*Cane*, 1998]. The modern warm pool is warmest in the center (along the equator) and tends to cool heterogeneously toward the margins (Fig. 5.1). Numerical models suggest that the latitudinal extent of warm surface water expands in response to increasing global temperature [*Sun*, 2003; *Liu et al.*, 2005; *Brierley et al.*, 2009]. However, others argue against the expansion of warm surface waters due to three stabilizing negative feedbacks in the tropical climate system: either warm temperatures facilitate more vigorous atmospheric convection and increased evaporative cooling [e.g. *Knutson and Manabe*, 1995], warm temperature amplify high-altitude clouds in the tropics that shield the surface from incoming shortwave radiation [e.g. *Ramanathan and Collins*, 1991], or that a greater latitudinal SST gradient drives enhanced atmospheric heat transport from the tropics to higher latitudes [e.g. *Wallace*, 1992]. Surface temperature gradients from the past have the potential to test such theories. Here we use records of Pleistocene SST to examine how tropical SST patterns change from glacial to interglacial climate states.

Equatorial upwelling in the western Pacific warm pool is suggested to occur at rates similar to the central and eastern Pacific though western upwelling sources water

from deeper within the water column [*Helber and Weisberg*, 2001]. Could glacial-interglacial changes in global temperature be accompanied by changes in the temperature or strength of western equatorial upwelling and thus the pattern of surface temperature? Testing this idea requires geochemical SST records from both the equator and off-equator sites within the western equatorial Pacific warm pool. An existing Mg/Ca-based SST record from the center of the warm pool at ODP Site 806 [*Medina-Elizalde and Lea*, 2005] offers a critical indication of glacial-interglacial SST change on the equator but does not quantify the temperature of the surrounding warm pool: comparison to an additional off-equatorial temperature record from a similar latitude would provide a measure of the meridional temperature gradient within the tropical west Pacific: here use employ Site 871 (5°33'N, 172°21'E, water depth 1255m) [*Shipboard Scientific Party*, 1993] for this purpose. Additionally, the equatorial to off-equator temperature gradient in the eastern Pacific can be examined using existing SST records from the eastern Pacific cold tongue (Site 846) compared to a site (Sites 1239 or TR163-19) [*Lea et al.*, 2000; *Liu and Herbert*, 2004; *Etourneau et al.*, 2010] located in the warm water just to the north of the modern equatorial front. Furthermore, comparing records from west and east sites, can provide estimates of the changes in the intensity of Walker circulation as global climate changes.

While studies of SST gradients in the tropical Pacific exist for the last glacial maximum [e.g. *Kienast et al.*, 2001; *Koutavas et al.*, 2002] a more robust quantification of the relationship between spatial SST patterns and global climate requires a broader study that includes many iterations of glacial-interglacial cycles. The SST record from ODP Site 871 extends through Marine Isotope Stage (MIS) 50, which allows us to examine changes over the course of ~25 glacial cycles and across the mid-Pleistocene transition (MPT), a shift from climate cycles dominated by 41-kyr periodicity to 100-kyr periodicity. Greater than modern global temperatures are consistent with an expansion of the tropical warm pool [*Brierley et al.*, 2009]. In contrast, in this study we show that during most glacial intervals in the Pleistocene, the warm pool SST was warmer at 5°N of the equator (the location of our new record) than SST on the equator, consistent with cooler or stronger upwelling along the equator. We also use this new SST record to show that the zonal tropical SST gradient and Walker circulation intensified in the early Pleistocene, culminating in the establishment of a strong large-scale zonal SST gradient at the mid-Pleistocene transition.

2. Data

A new dissolution-corrected SST record (Fig. 5.2A) for the past 1.5 Ma was generated from *Globigerinoides ruber* Mg/Ca at ODP Site 871. For each sample 40-60 *G. ruber* (white) tests and 1-5 *Uvigerina spp.* tests were picked from the 250-355 μm size

fraction. The *G. ruber* tests were cleaned following established protocols including oxidation and reduction steps [*Boyle and Keigwin*, 1985; *Mashiotta et al.*, 1999]. Mg/Ca ratios were measured using an ICP-OES at the University of California Santa Cruz; 1-σ standard deviation for repeated measurements of an internal foraminifera reference standard is 0.21 mmol/mol, or ~0.5 C°. The Uvigerina spp. tests were analyzed at the University of California Stable Isotope Laboratory using a Fisons PRISM mass spectrometer with a common acid bath carbonate preparation system. Standard error for 46 measurements of an internal CM05 $\delta^{18}O$ standard was ±0.05‰.

To correct for high-Mg calcite dissolution at depth, we assigned a depth-dependent correction to the measured Mg/Ca value before applying the exponential Mg/Ca-SST calibration [*Dyez and Ravelo*, n.d.]. The dissolution correction for *G. ruber* was derived from calculating the residual Mg/Ca between published core-tops from the tropical warm pool regions and calculated surface Mg/Ca values at each core top location. This correction should not be extended to less than ~600m water depth in the west Pacific since no dissolution is likely in surface waters with $[CO_3^{2-}]$ greater than ~25 umol/kg [*Regenberg et al.*, 2006]. Once Mg/Ca values were corrected for dissolution, we calculate SST based on the derived surface Mg/Ca value [*Anand et al.*, 2003]. The overall equation relating tropical Pacific SST to *G. ruber* Mg/Ca and depth is: $SST = \ln[(Mg/Ca_{measured} + 0.259 * Depth(km) + 0.537) / 0.38] / 0.09$ [*Dyez and Ravelo*, n.d.]. We also recalculated SST from previously published Mg/Ca data from

Sites 806 and TR163-19 [*Lea et al.*, 2000; *Medina-Elizalde and Lea*, 2005] using this technique to reconstruct regional temperature gradients. Our study uses these records to assess regional oceanic and atmospheric circulation and circulation changes from glacial to interglacial times, and through the MPT.

For age model control (Fig. 5.2B), the benthic $\delta^{18}O$ stratigraphy for Site 871 was aligned with a benthic $\delta^{18}O$ stack [*Lisiecki and Raymo*, 2005]. The glacial-interglacial amplitude of both records is ~2.0‰ in the late Pleistocene and ~1.5‰ in the early Pleistocene. The most recent 43 kyr of the record was removed since sediment was disturbed when cored. Peak glacial and interglacial intervals are defined by calculating from the benthic $\delta^{18}O$ stack both a moving average and moving 1-σ standard deviation. The period of time averaged is 100-ky in the late Pleistocene and 40-ky prior to the MPT. For the purpose of this study peak interglacial intervals are defined by benthic $\delta^{18}O$ values lower than the 1-σ standard deviation while peak glacials are defined by benthic $\delta^{18}O$ values higher than the 1-σ standard deviation. Peak glacial and interglacial SSTs were determined using the same technique; though peak SST may not necessary align perfectly with the peak $\delta^{18}O$ values due to assumptions associated with the age model. Since this simplified method of calculating peak glacial and peak interglacial temperatures does not rely on a single point from each interval (maximum or minimum) it represents a robust depiction of peak temperature within

an age model uncertainty of 6 kyr for the period before 1 Ma and 4 kyr for the period 1-0 Ma.

3. Results and Discussion

The cyclicity of the SST record from ODP Site 871 shows a strong similarity to the pattern of glacial-interglacial cycles in other western tropical Pacific temperature records [e.g. *Medina-Elizalde and Lea*, 2005] and in a benthic $\delta^{18}O$ stack [*Lisiecki and Raymo*, 2005] and the benthic $\delta^{18}O$ record from Site 871 (Fig. 5.2). In each record, spectral power in the 41-kyr cycle is greater prior to the MPT than in the late Pleistocene while the reverse is true for the 100-kyr cycle. This change in cyclicity is consistent with a similar mid-Pleistocene shift in the frequency of spectral power of records of bottom water temperature, ice volume, and, hypothetically, atmospheric GHG concentrations. Additionally, similar to other warm pool records, the average value of SST at Site 871 is nearly constant between the early and late Pleistocene which is suggestive of relatively little change in the radiative heat budget of the warm pool [*de Garidel-Thoron et al.*, 2005].

Today, surface temperatures at Site 806 are 0.5°C greater at Site 806 than at Site 871 on the margin of the warm pool. A similar SST difference between the two sites exists during most interglacial periods of the past 1.5 Ma (Fig. 5.3), within the error of the SST measurements. However, in most glacial intervals SST is cooler at Site 806 than at

Site 871, suggesting that waters just north of the equator are warmer than water on the equator. T-test results suggest the difference in the SST gradient between the two sites during glacials compared to interglacials is significant ($p<0.05$).

Such a 'bifurcated' warm pool during the glacial periods resembles the surface temperature pattern of the eastern tropical Pacific today, with cooler temperature on the equator compared to off the equator. However, the temperature gradient over 5° of latitude is smaller, ~1°C, in the west Pacific compared to ~3±1°C in the east Pacific. This temperature pattern may represent stronger upwelling or a source of cooler water upwelling at the equator than 5°N north of the equator, and must be a result of glacial oceanic or atmospheric dynamics includes stronger equatorial winds and/or a shallower thermocline depth. Increased terrigenous dust in the glacial periods is thought to represent stronger trade winds [*Winckler et al.*, 2008] during glacial intervals. Stronger trades may set up a stronger pressure gradient and cause the thermocline to deepen, but at the same time, they may drive stronger Ekman transport away from the equator allowing a thin band of relatively cool water upwelling along the equator. While no western Pacific SST record is yet available for 5°S latitude, if upwelling is confined to the equator we might expect such a record to also demonstrate warmer glacial SST compared to an equatorial site from the same latitude.

The temperature gradient reconstruction described above uses our relatively new method for overcoming the effects of dissolution on the Mg/Ca of foraminifera so that accurate changes in SST can be quantified. By using the same dissolution correction at each site, we eliminate differences due to the choice of Mg/Ca-temperature calibration or due to the choice of method to correct for dissolution effects on Mg/Ca of calcite. If we had instead applied the calibration used previously for generating a Site 806 SST record [*Medina-Elizalde and Lea*, 2005], to both sites, the calculated SST would be warmer at Site 871 than at Site 806, though for both glacial and interglacial intervals. Relatively cool SST on the equator in the middle of the warm pool at interglacial intervals seems implausible, given that the present interglacial has the opposite (warmer temperatures at the equator). While dissolution occurs at both sites today, another possibility is that during glacial intervals the lysocline and [CO_3^{2-}] isopleths were deeper [*Farrell and Prell*, 1989] which would yield a smaller correction for high-Mg calcite dissolution in the past. Less corrosive glacial waters, though, would be expected to influence both sites similarly and also cannot account for the warmer glacial surface temperatures at Site 871 than at Site 806. Overall, the primary observation, that cooling was more intense on the equator than off the equator during glacials, is robust and cannot be an artifact of dissolution nor of a poor choice of calibration.

When we compare SST records across the Pacific (Fig. 5.4) a number of important patterns emerge. In the early Pleistocene the tropical Pacific zonal gradient slowly increased; this secular cooling occurred during glacial and interglacial periods in the eastern tropical Pacific while western Pacific SST maintained an average of ~29°C. The increasing zonal gradient in the early Pleistocene may be due to a gradually strengthening Walker circulation that drove increased upwelling in the eastern Pacific [*McClymont and Rosell-Melé*, 2005; *Etourneau et al.*, 2010]. At the MPT (~0.9 Ma), a strong SST gradient developed between the center of the eastern Pacific cold tongue (represented by Site 846 SST) and margin of the eastern Pacific warm pool (represented here by Site 1239) just as larger, longer-lasting ice sheets began to appear in the northern hemisphere. This steepened gradient could be related to a southerly shift in the average position of Intertropical Convergence Zone (ITCZ), a band of atmospheric vertical convection. By the late Pleistocene average zonal tropical Pacific SST gradients were roughly stable, suggesting that changes in major tectonic or other long—term boundary conditions (other than orbital-scale variability) have not occurred since the mid-Pleistocene.

The progression of tropical SST during peak glacial and peak interglacial periods (Fig. 5.5) shows that glacials and interglacials have diverging evolution histories. Linear regressions show declining glacial SST from 1.5 Ma to present with cold tongue SST (represented by Site 846) declining at a faster rate than other tropical records. The

long-term glacial cooling in the tropics may indicate a reflection of increased glacial pCO_2 drawdown from the early Pleistocene to present. In contract, linear regressions of interglacial intervals outside of the cold eastern cold tongue, are relatively unchanged and may represent a recovery to nearly identical pCO_2 values for each interglacial. Moving averages (Fig. 5.5) of peak warm pool glacial SST graphically show the ~0.8°C difference between 5°N and the equator of the (represented by Site 871 and 806, respectively) and the strengthening equatorial front at the MPT between the center and margin of the cold tongue (represented by Sites 846 and 1239, respectively) in both glacial and interglacial intervals.

4. Summary

A new high-resolution SST record is generated from the margin of the modern western tropical Pacific warm pool in order to reconstruct tropical SST variability from 1.5 Ma to present. After applying identical dissolution corrections and Mg/Ca-SST calibrations to a previously published Mg/Ca record from Site 806 [*Medina-Elizalde and Lea*, 2005] on the equator, we show warmer SST at 5°N than at the equator during past glacial intervals. This consistent pattern of cooler temperatures along the equator implies stronger (or cooler) glacial equatorial upwelling along the equator in the western tropical Pacific region. We argue that warmer SST at 5°N is not a consequence of biased application of calibrations or to neglecting potentially less glacial dissolution. Such a pattern of SST may be instead be attributed to stronger

glacial trade winds that enhanced surface water advection away from the equator to accommodate cooler glacial upwelling along the equator in the western Pacific.

Our comparison with other Pleistocene tropical SST records also confirms that the average zonal SST gradient increased in the early Pleistocene due to eastern tropical Pacific cooling and then stabilized after the mid-Pleistocene transition. This result suggests that the bulk of long-term Pleistocene cooling was complete by the MPT and that once the 100-ky cycle of large ice sheets was established the trend of intensified glacial climate essentially halted, possibly due to climate thresholds that maintain minimum pCO_2 levels during glacial intervals.

Acknowledgements. This research was supported by the Schlanger Fellowship from the Consortium for Ocean Leadership and by National Science Foundation grant # OCE-0902047. The authors would also like to thank the Ocean Drilling Program for providing samples, and Jessica Macias and Victor Castro for assistance in sample processing.

References

Anand, P., H. Elderfield, and M. H. Conte (2003), Calibration of Mg/Ca thermometry in planktonic foraminifera from a sediment trap time series, *Paleoceanography*, *18*(2), doi:10.1029/2002PA000846.

Boyle, E., and L. Keigwin (1985), Comparison of Atlantic and Pacific paleochemical records for the last 215,000 years: Changes in deep ocean circulation and chemical inventories, *Earth and Planetary Science Letters*, *76*(1-2), 135–150.

Brierley, C., A. Fedorov, Z. Liu, T. Herbert, K. Lawrence, and J. LaRiviere (2009), Greatly expanded tropical warm pool and weakened Hadley circulation in the early Pliocene, *Science*, *323*(5922), 1714.

Cane, M. A. (1998), CLIMATE CHANGE:A Role for the Tropical Pacific, *Science*, *282*(5386), 59–61, doi:10.1126/science.282.5386.59.

de Garidel-Thoron, T., Y. Rosenthal, F. Bassinot, and L. Beaufort (2005), Stable sea surface temperatures in the western Pacific warm pool over the past 1.75 million years, *Nature*, *433*(7023), 294–298.

Dyez, K. A., and A. C. Ravelo (n.d.), Late Pleistocene tropical Pacific temperature sensitivity to radiative greenhouse gas forcing, *Geology*, *XX*.

Etourneau, J., R. Schneider, T. Blanz, and P. Martinez (2010), Intensification of the Walker and Hadley atmospheric circulations during the Pliocene–Pleistocene climate transition, *Earth and Planetary Science Letters*, 1–8, doi:10.1016/j.epsl.2010.06.010.

Farrell, J. W., and W. L. Prell (1989), Climatic change and CaCO3 preservation: an 800,000 year bathymetric reconstruction from the central equatorial Pacific Ocean, *Paleoceanography*, *4*(4), 447–466.

Helber, R. W., and R. H. Weisberg (2001), Equatorial upwelling in the western Pacific warm pool, *Journal of Geophysical Research-Oceans*, *106*(C5), 8989.

Kienast, M., S. Steinke, K. Stattegger, and S. Calvert (2001), Synchronous tropical South China Sea SST change and Greenland warming during deglaciation, *Science*, *291*(5511), 2132.

Knutson, T., and S. Manabe (1995), Time-mean response over the tropical Pacific to increased CO2 in a coupled ocean-atmosphere model, *Journal of Climate*, *8*(9), 2181–2199.

Koutavas, A., J. Lynch-Stieglitz, T. Marchitto, and J. Sachs (2002), El Nino-like pattern in ice age tropical Pacific sea surface temperature, *Science*, *297*(5579), 226.

Lea, D., D. Pak, and H. Spero (2000), Climate impact of late Quaternary equatorial Pacific sea surface temperature variations, *Science*, *289*(5485), 1719.

Lisiecki, L. E., and M. E. Raymo (2005), A Pliocene-Pleistocene stack of 57 globally distributed benthic $\delta^{18}O$ records, *Paleoceanography*, *20*(1), PA1003, doi:10.1029/2004PA001071.

Liu, Z., and T. D. Herbert (2004), High-latitude influence on the eastern equatorial Pacific climate in the early Pleistocene epoch, *Nature*, *427*(6976), 720–723.

Liu, Z., S. Vavrus, F. He, N. Wen, and Y. Zhong (2005), Rethinking Tropical Ocean Response to Global Warming: The Enhanced Equatorial Warming, *Journal of Climate*, *18*(22), 4684–4700.

Locarnini, R., A. Mishonov, J. Antonov, T. Boyer, H. Garcia, O. Baranova, M. Zweng, and D. Johnson (2010), World Ocean Atlas 2009, in *NOAA Atlas NESDIS 68*, vol. Volume 1: Temperature, edited by S. Levitus, p. 184, U.S. Government Printing Office, Washington, D.C.

Mashiotta, T., D. Lea, and H. Spero (1999), Glacial-interglacial changes in Subantarctic sea surface temperature and [delta] 18O-water using foraminiferal Mg, *Earth and Planetary Science Letters*, *170*(4), 417–432.

McClymont, E. L., and A. Rosell-Melé (2005), Links between the onset of modern Walker circulation and the mid-Pleistocene climate transition, *Geology*, *33*(5), 389, doi:10.1130/G21292.1.

Medina-Elizalde, M., and D. Lea (2005), The mid-Pleistocene transition in the Tropical Pacific, *Science*, *310*(5750), 1009.

Ramanathan, V., and W. Collins (1991), Thermodynamic regulation of ocean warming by cirrus clouds deduced from observations of the 1987 El Niño, *Nature*, *351*(6321), 27–32.

Regenberg, M., D. Nürnberg, S. Steph, J. Groeneveld, D. Garbe-Schönberg, R. Tiedemann, and W.-C. Dullo (2006), Assessing the effect of dissolution on planktonic foraminiferal Mg/Ca ratios: Evidence from Caribbean core tops, *Geochemistry Geophysics Geosystems*, *7*(7), doi:10.1029/2005GC001019.

Shipboard Scientific Party (1993), Site 871, in *Proceedings of the Ocean Drilling Program, Initial Reports, Vol. 144*, vol. 144, edited by P. I. Silva, J. Haggerty, and

R. Rack, pp. 105–144, Ocean Drilling Program.

Sun, D. Z. (2003), A possible effect of an increase in the warm-pool SST on the magnitude of El Niño warming, *Journal of Climate*, *16*(2), 185–205.

Wallace, J. (1992), Effect of deep convection on the regulation of tropical SST, *Nature*, *377*, 230–231.

Winckler, G., R. F. Anderson, M. Q. Fleisher, D. McGee, and N. Mahowald (2008), Covariant glacial-interglacial dust fluxes in the equatorial Pacific and Antarctica, *Science*, *320*(5872), 93–96.

Figures

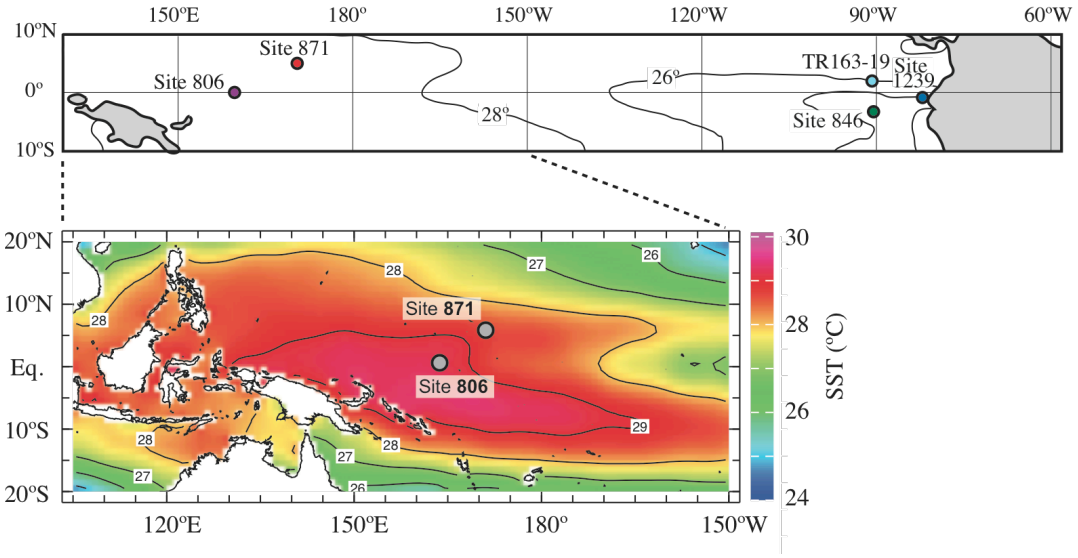

Figure 5.1. Location and average annual surface temperature [*Locarnini et al.*, 2010] map of the tropical Pacific and expanded map of the western tropical Pacific warm pool with selected Mg/Ca-based records.

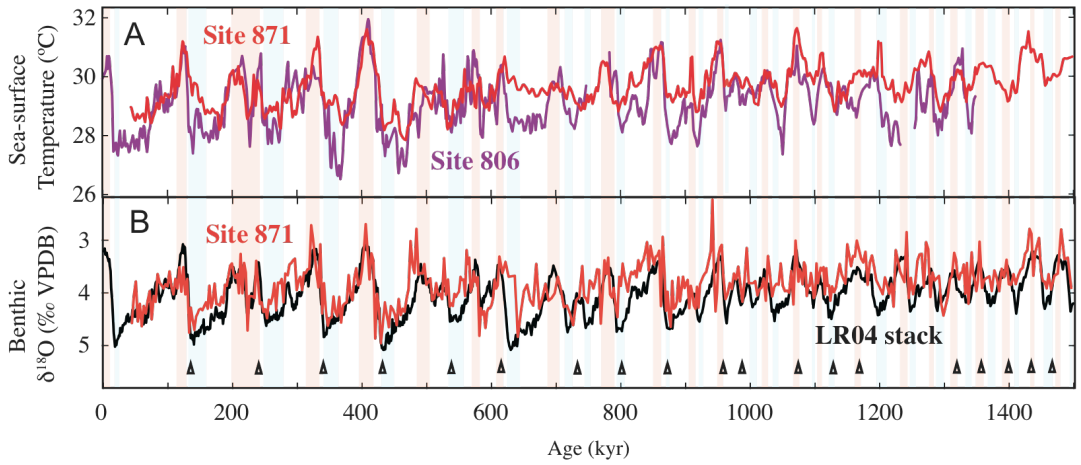

Figure 5.2. (A) SST records from the western Pacific warm pool sites, ODP Site 806 [*Medina-Elizalde and Lea*, 2005] and ODP Site 871 (500-1500 kya, this study). (B) Age model for Site 871 is based on measured benthic $\delta^{18}O$ values compared to a global benthic $\delta^{18}O$ stack [*Lisiecki and Raymo*, 2005].

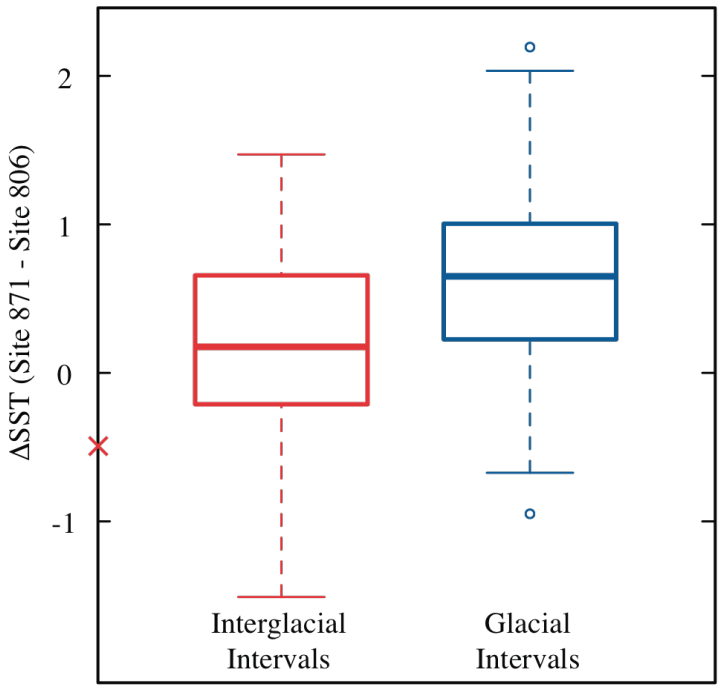

Figure 5.3. Comparison of SST gradient between Sites 871 and 806 based on glacial vs. interglacial interval. Box-plots of the SST gradient (ΔSST (Site 871-806)) as resampled every 2 ky for comparison. Modern SST gradient is marked on scale bar. Interglacial intervals display a homogeneous SST pattern; glacial intervals tend to have cooler temperatures at the equator (Site 806) and the difference is significant ($p<0.05$).

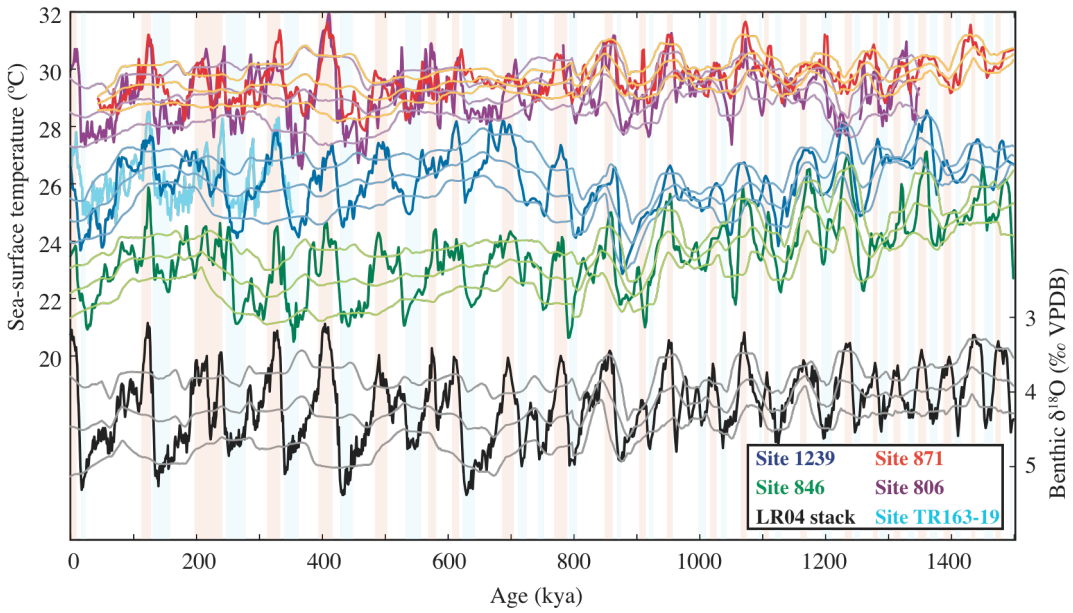

Figure 5.4. Long cross-equatorial surface temperature timeseries (846: [*Liu and Herbert*, 2004], 1239: [*Etourneau et al.*, 2010], TR163-19: [*Lea et al.*, 2000], 806: [*Medina-Elizalde and Lea*, 2005], 871: this study) compared with benthic $\delta^{18}O$ stack [*Lisiecki and Raymo*, 2005]. Running mean and 1-σ standard deviation for each timeseries show interglacial (glacial) maxima (minima). Vertical bars represent glacial and interglacial intervals defined by benthic $\delta^{18}O$ variations outside 1-σ standard deviation.

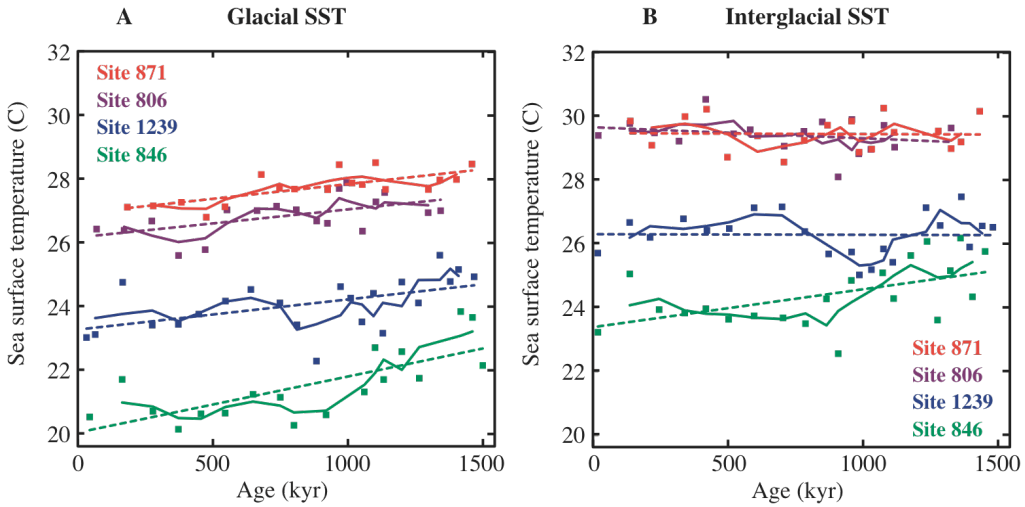

Figure 5.5. Progression of tropical SST for (A) glacial and (B) interglacial intervals is defined by the average SST from excursions beyond 1-σ standard deviation over the past 1.5 Ma. Linear fit (dashed line) and 3-point moving average (solid line) are superimposed.

Marine Isotope Stage	Age (kyr) Start	Age (kyr) End
1	11	0
2	25	17
5	127	116
6	157	135
7	242	199
8	277	250
9	334	315
10	363	340
11	417	397
12	448	429
13	503	484
14	556	536
15	616	572
16	640	626
17	704	690
18	750	716
19	788	774
20	840	794
21	860	850
22	876	872
23	914	908
24	926	918
25	956	948
26	966	962
27	980	978
28	1008	986
29	1024	1022
30	1044	1034
31	1074	1068
32	1099	1097
33	1112	1106
34	1128	1122
35	1168	1160
36	1208	1198
37	1240	1230
38	1254	1248
39	1282	1276
40	1298	1288
41	1318	1310
42	1340	1334
43	1358	1350
44	1378	1368
45	1400	1392
46	1414	1410
47	1440	1436
48	1464	1454
49	1480	1474
50	1500	1496

Table 5.1. Peak glacial and interglacial intervals.

6. CONCLUDING REMARKS AND FUTURE DIRECTIONS

The four projects presented in this dissertation aim to increase our understanding of the relationship between the Pacific Ocean sea-surface temperature and incoming solar radiation, ice volume, and greenhouse gas concentrations. Taken together, these projects offer new observations that lend insight to the mechanisms and theories of past climate change. Through these projects I provide a case study of the most recent interglacial period (the Holocene), compare tropical SST records with potential forcing mechanisms, add to our understanding of tropical climate history, and develop new approaches to proxy analysis.

Chapter 2 examines new records of temperature, ^{14}C activity, and the $\delta^{18}O$ value of seawater from anthropological middens on a previously unstudied portion of the California coast from the mid-Holocene and late Holocene within the established climate context. Though existing sediment-core records from the California Current show a slight cooling in the mid-Holocene, the high Mg/Ca ratios in selected mid-Holocene coastal mollusks suggest warmer intervals of warmer SST in the mid-Holocene. Calculations of $\delta^{18}O_{sw}$ from these same warm intervals also suggest smaller inputs of low-$\delta^{18}O$ freshwater, and less precipitation. These drier conditions are consistent with mid-Holocene evidence of extreme drought in eastern California.

Over the past 4 ky, records of SST and $\delta^{18}O_{sw}$ are consistent with the range of values in the modern system. This result suggests that very little environmental change has occurred over the past 4 kya on the central California coast. However, the accuracy of such estimates is partially obscured by the uncertainty associated with the SST and $\delta^{18}O_{sw}$ calibrations for this species of mollusk. Additional lake records from lakes in coastal California may be able to confirm that warmer and drier intervals extended from inland areas to the coast.

In Chapter 3, I show that a new compiled record of SST from Site 1239 reveals a fundamental shift in the development of the eastern Pacific cold tongue at the mid-Pleistocene transition. The Site 1239 SST record is the only record in which both glacial and interglacial intervals warm in the period 650-900 kya; in the high-latitudes glacial temperatures cool during this interval and other records of tropical temperature do not warm. Spectral analysis of the orbital-resolution records of tropical SST, benthic foraminiferal $\delta^{18}O$, insolation, and preliminary greenhouse gas concentrations reveals important forcing relationships for tropical SST. In particular, I show that eastern Pacific equatorial SST is not inversely correlated on precession timescales to equatorial insolation, as predicted from modeling studies of a semi-annual asymmetric ITCZ, but rather directly correlated, consistent with warming due to increased insolation. Additionally, Chapter 3 shows that at obliquity, where Site 846 SST is closely related to northern hemisphere insolation, Site 1239 SST may be

more related to ice sheet changes since peak benthic $\delta^{18}O$ maxima and minima are in phase with this record. This result is consistent with the theory that high ice volume may deflect atmospheric circulation bands. Where greenhouse gas records are available at orbital resolution (800-0 kya) tropical SST records are in phase with CO_2 concentrations at the 100-ky frequency band, suggesting that carbon cycle feedbacks are closely related to tropical SST at eccentricity. For the period from 1500-800 kya, atmospheric greenhouse gas records are still needed to test the hypothesis that CO_2 varied in phase with the dominant SST period of 41-kyr before the mid-Pleistocene transition. The next steps in this work should be to confirm the presence of 41-kyr atmospheric CO_2 cycles in the 1500-800 kya interval. Although ice cores may not be available from which to generate this data, new proxies for calculating past CO_2, such as the method that measures $\delta^{11}B$ in planktonic foraminifera, may be best suited to this endeavor.

The objective of Chapter 4 is two-fold: both to estimate the past tropical climate sensitivity to greenhouse gas forcing and to constrain the effect of preferential high-Mg-calcite dissolution for reconstructing SST. We calculate climate sensitivity using a new, well-dated record of SST from 500 kya to present from ODP Site 871 and the radiative forcing associated with published records of atmospheric CH_4 and CO_2. On long timescales, once climate feedbacks have been allowed to equilibrate, the tropics are at the high end of the sensitivity to greenhouse gas forcing than most current

models suggest. The location of Site 871 presents a unique advantage for this work; far from strong tropical temperature gradients, it represents an open ocean response that is not available from other records of tropical change. The final section of this chapter contains the methodology for a new formulation for Mg/Ca dissolution based on the notion that dissolution in this core may be approximated as a function of water depth. This new correction would benefit from additional core-top measurements of Mg/Ca so as to better constrain how much dissolution occurs in water shallower than 1.6 km depth. The dissolution correction and methodology presented in this chapter is critical for estimating the appropriate range of SST over glacial-interglacial cycles—one component of the climate sensitivity calculation. Other previously-used dissolution corrections tend to overestimate the glacial-interglacial range of SST and thus exacerbate the data-model mismatch in tropical climate sensitivity.

In Chapter 5 we present a comparison between a number of SST records from the western Pacific warm pool over the past 1.4 Ma to provide evidence for SST changes due to equatorial upwelling in the western Pacific. During glacial periods, SST is 1-2 C^{o} warmer at Site 871 (5^{o}N) than at Site 806 on the equator. Glacial SST patterns in the western Pacific therefore may have been more similar to the SST pattern that currently exists in the eastern Pacific. A cooler band of SST along the equator also has implications for the average glacial position of the ITCZ, which may have shifted to the north or bifurcated if a band of cooler temperature water existed along the

equator. Additional SST or subsurface temperature records from the western Pacific warm pool may confirm the strength of upwelling and position of the subsurface thermocline and atmospheric ITCZ during past glacial intervals.

This thesis displays a portion of the complex range of questions that remain regarding Pleistocene and Holocene climate variability, which can be explored using high-resolution records of sea-surface temperature. It also presents some of the caveats and considerations associated with each method of estimating past SST. Additional future work that could stem from the foundations presented here includes many possible avenues of research. First, the depth-correlated dissolution correction for Mg/Ca-based SST should be expanded to include a larger range of water depths and ocean basins. Second, the Site 871 temperature record (and corresponding age model) should be expanded to include the remainder of the Pleistocene timeperiod (2.6 to 1.5 Ma) and continue into the Pliocene. When compared with Site 806 in the center of the modern warm pool, these record offers clues into the nature of the western Pacific warm pool SST pattern. Yet a final promising avenue involves the construction of a high-resolution CO_2 record from the early Pleistocene to evaluate the tropical SST response to radiative greenhouse gas forcing from the timeperiod before ice-core records of atmospheric constituents are available. I look forward to the advancement of each of these opportunities of research in the future.